On dephasing and spin decay in open quantum dots

Björn Dieter Michaelis

ii

On dephasing and spin decay in open quantum dots

PROEFSCHRIFT

door

Björn Dieter Michaelis

GEBOREN TE SAARBRÜCKEN, DUITSLAND, OP 13 AUGUSTUS 1978

Promotiecommissie:

Prof. dr. C.W.J. Beenakker, promotor
Prof. dr. ir. W. van Saarloos, referent
Prof. dr. ir. G.E.W. Bauer (TU Delft)
Prof. dr. J.G.J. van den Brink
Prof. dr. P.H. Kes
Prof. dr. ir. L.P. Kouwenhoven (TU Delft)

Contents

Chapter 1

Introduction

The electron spin was discovered in 1925 by the Leiden physicists George Uhlenbeck and Samuel Goudsmit. Today, there is an entire field within electronics, called spintronics, that makes use of the electron spin to switch a current and control a logical device. For such applications it is important that the spin maintains its direction and that an initial polarization does not decay, for example due to a nuclear magnetic field. In this thesis we describe a method that we have developed to account for the decay of the spin polarization.

Since a few years a second class of applications of the electron spin is being developed, in which the spin is the carrier of quantum information. To transfer quantum information not only the direction of the electron spin should be preserved (up or down), but also superpositions of the two directions should be maintained. The degradation of a quantum mechanical superposition is called dephasing (or decoherence). The same mechanisms that cause decay of the polarization also cause dephasing, but there exist also mechanisms that cause only dephasing — without spin decay. The model for spin decay that we have developed can account for dephasing as well — because it is a fully quantum mechanical model.

Earlier models for spin decay and dephasing were mostly aimed at electrons in a small confined region in thermal equilibrium (a so-called quantum dot). Our model applies to an open system out of equilibrium, through which an electrical current can flow. The focus on nonequilibrium systems is a central theme of this thesis. The techniques that we use to describe these systems are introduced in this first chapter.

1.1   Transport and quantum mechanics

Text book quantum mechanics knows two qualitatively different ways how the wave function can behave in time. It can evolve according to the Schrödinger equation thus evolve according to a unitary operator. So the most general solution $|\Psi(t)\rangle$ of the time independent Schrödinger equation can be written in the basis of energy eigenstates $|\phi_k\rangle$ as

$$|\Psi(t)\rangle \;\;=\;\; \sum_k \rho_k \exp(-i\,E_k t/\hbar)|\phi_k\rangle, \tag{1.1}$$

where E_k are the energy eigenvalues of the Hamilton operator H, t is the time and the coefficients ρ_k are fixed by the initial conditions, e.g. the wave function at $t = 0$. Important is here the aspect, that the populations of the individual energy eigenstates ρ_k do not change under the unitary evolution.

But the wave function can also be measured. The measurement is a projection into a part of the hilbert space. But by the use of quantum formalism one can not predict when a measurement takes place. One does in general not even know what will be measured, thus in which type of states the projection takes place. The formalism provides only probabilities for measurement outcomes. These are the norm of the projection of the wave function into a part of the hilbert space. The measurement usually[1] doesn't have to conserve any property of the wavefunction except normalization. The populations ρ_k do especially not have to be preserved. I consider it as a transport process if

- one observes two distinct measurements and can explain them only by the fact that eigenstate populations were changing between,

- or one observes a statistic of pairs of measurements and can explain the statistic of outcomes only by the assumption that eigenstate populations were between the two paired measurements changing between.

How is that related to our understanding of wave function propagation? Can transport happen at all, if it is true what I wrote at the first place ? I distinguish three conceptionally different ways transport can at least be explained within quantum mechanics:

- The measurement was actually not probing the populations in the eigenbasis of the total hamiltonian. Instead was it referring only to a *local* eigenbasis of the hamiltonian. Scattering experiments are usually tried to be done

---

[1]This is only true for quantum mechanically complete measurements, quantum mechanically incomplete measurements preserve some structure of the wavefunctions [1].

in such a situation. The preparation (first measurement) and detection (second measurement) of the projectile particles happen far away from the area where they undergo the interesting collision.

- One or more unobserved measurements have been between the two observed ones. These intermediate measurements could have changed populations. As explained above, one can almost never exclude this possibility. But there are actually methods so that one can at least check if there was a certain type of unobserved measurement between by clever design of the experiments. To develop such methods are problems in the field "Quantum Cryptography", which has as a goal to find secure channels for information transfer. To the "measurement between" one refers there usually as an eavesdropper [2, 3].

- One just doesn't know what one is doing. Despite some theoretical effort to find a systematic approach [4], it is always necessary to postulate in which basis a measurement apparatus is projecting. Despite the fact, that in good experiments it seems to be just obvious how a detector acts - it probes e.g. the spatial separation of a particle wave function in the Stern Gerlach or the photon impact on the screen in a double slit experiment, there can be situations in which this separation is much more subtle. As an example of a dubious experiment, one may think of the spectroscopy of Rydberg states in atoms or a detection of the passage of individual electrons through quantum dots.
It is further necessary to postulate a hamiltonian for the unmeasured time evolution. This postulate can of course be checked by exactly these transport measurements. But especially in macroscopic disordered systems one will never be able to pin down all parameters of the hamiltonian by that. Thus this lack of knowledge about the evolution operator can lead to spurious transport effects.

I avoided in the aforementioned definition of transport especially any relation to locality. Common sense transport has of course to do with some changes in local behavior. But I hope that the general view stimulates to think more about the technical similarities which appear in the use of quantum theory to understand something like "transfer from point A to point B" as well as "changing the wavevector from k to q". One could consider e.g. in the broader sense as well the loss of magnetization of a sample of iron as a transport process even if the sample itself didn't move.

1.1.1 Scattering: the intuitive boundary conditions

What one calls usually a scattering experiment requires that the wave function of the particle to be scattered is prepared (at $t = -\infty$) and detected (at $t = \infty$) in an area, where its evolution operator U^0 is build up by the free hamiltonian H_0. If $|\Psi\rangle$ is the initial state at $t = -\infty$, then the actual state for all times is given by the full evolution operator $U(t, -\infty)|\Psi\rangle$ (see Fig. 1.1). Thus its knowledge provides of course also all information about the final state following from $|\Psi\rangle$. The following construction defines the scattering matrix S and describes as well the evolution between the limiting states. $|\Psi\rangle$ evolves until $t = 0$ only with the free evolution operator. This state is then multiplied by the scattering matrix and evolves further with the free evolution operator until $t = \infty$ to the right final state. Thus all the complications through the scattering process are put into the "instantaneous acting" operator S.

By just looking at its formal definition

$$\lim_{T \to \infty} U(T, -T) = \lim_{T \to \infty} U_0(T, 0) S U_0(0, -T) \qquad (1.2)$$

one finds first of all, that all population transfers in the eigenbasis of H_0 are taken care of by S. But further may one think that one can arbitrarily choose some part of H as H_0 and thus obtains just different matrix elements for S. Despite this is formally true, one wants to take H_0 in the aforementioned sense as the hamiltonian of the free particle because it makes S to be an object that can be calculated very well by perturbation theory in $H - H_0$.
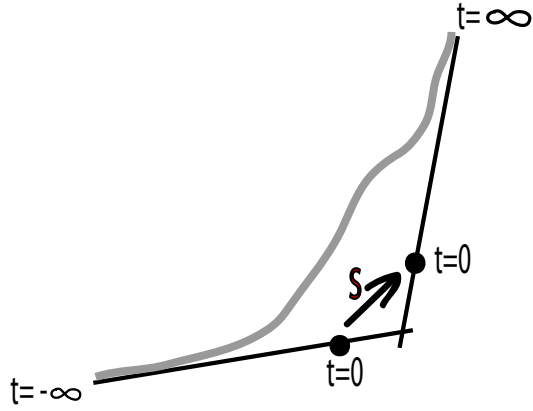
Figure 1.1: the grey line symbolizes the actual evolution in a scattering process. The black lines stand for the evolution of in- and outgoing scattering states. They evolve with a free hamiltonian but are at $t = 0$ connected by the scattering matrix S.

Landauer formula

An expression for the current through a little constriction between two big metals has been derived from that scattering point of view. The boundary conditions of the scattered particles have to be adjusted to the situation. Exactly this requires some intuition. And despite one understands very well pure metal, one could be worried about the back-effect of the little constriction to the big pure metal. This worry is supported by the Kondo problem [5], in which a single magnetic impurity is embedded in a pure metal and changes the thermodynamic properties of the whole system.

But here and throughout the whole thesis we stick to a free electron description of the metal. Thus carriers that approach the constriction are fully characterized by their occupation expectation value

$$\langle a^\dagger_{n,X}(E) a_{n',X'}(E') \rangle = \delta_{n,n'} \delta_{X,X'} \delta(E - E') f(E, \mu_X, T). \tag{1.3}$$

The operator $a^\dagger_{n,X}(E)$ creates an electron in the reservoir X with quantum number n, which labels spin and orbital degrees of freedom, and total energy E. T is the temperature and μ_X the chemical potential in the Xth reservoir. $f(E, \mu_X, T)$ is the fermi function. Because we will later study the relation to quantum information, it is convenient to state the same by writing the many particle density matrix of the reservoir

$$\hat{\rho}_{in} = \Pi_{E,X,n} \Big(f(E, \mu_X, T) a^\dagger_{n,X}(E) |0\rangle \langle 0| a_{n,X}(E) + [1 - f(E, \mu_X, T)]|0\rangle \langle 0| \Big). \tag{1.4}$$

Expectation values that involve electrons leaving the scatterer, created by $b^\dagger_{n,X}(E)$, can now be related to the in-going ones by use of the operator identity

$$b_{n,X}(E) = S(n, X, E; n', X', E') a_{n',X'}(E'), \tag{1.5}$$

in which one has to sum over repeated indices. The scattering matrix $S(..)$ is unitary, which ensures here the conservation of the number of particles in the scattering events. A first interesting expectation value is the average current. The operator for the current through the plane in lead X at position z is

$$\begin{aligned}
I(z, t, X) = {} & \frac{\hbar e}{2im} \int dn \Big[\Psi^\dagger(z, t, n, X) \frac{\partial}{\partial z} \Psi^\dagger(z, t, n, X) \\
& - \Big(\frac{\partial}{\partial z} \Psi^\dagger(z, t, n, X) \Big) \Psi(z, t, n, X) \Big],
\end{aligned} \tag{1.6}$$

where the integral over dn collects eventual spin and orbital degrees of freedom. The field operator Ψ is related to the second quantized creation and annihilation operators by

$$
\begin{aligned}
\Psi(z,t,n,L) &= \int dE \exp(-iEt/\hbar) \sum_{m=1} \frac{\chi_m(x_n,y_n)\Theta_n}{(2\pi\hbar^2 k_m/M)^{1/2}}, \\
&\times [a_{n,L}\exp(-ik_m z) + b_{n,L}\exp(ik_m z)]
\end{aligned}
\tag{1.7}
$$

and a corresponding expression for $X = R$, in which the directions of the momenta k_m are inverted. The χ_m are modes in the transversal direction, Θ_n is a spin 1/2 spinor and M the electron mass. We have introduced the wave vector k_m which can be expressed through $E = E_m + \hbar^2 k_m^2/2M$ by the total energy E and the energy of the modes E_m. If one inserts Eq. (1.7) into Eq. (1.6) and assumes, that $v_m(E)$ is a constant in the contributing energy range around the fermi surface, after some algebra, z drops out far away from the constriction and we obtain

$$
\begin{aligned}
I(z,t,X) = I(X,t) &= \frac{e}{2\pi\hbar} \sum_m \int dE dE' \exp(i(E-E')t/\hbar) \\
&\times \left[a^\dagger_{m,X}(E)a_{m,X}(E') - b^\dagger_{m,X}(E)b_{m,X}(E') \right],
\end{aligned}
\tag{1.8}
$$

from which one may eliminate the outgoing degrees by use of the scattering matrix in Eq. (1.5). The average current is then time independent and given by

$$
\langle I(L,t) \rangle = \frac{e}{2\pi\hbar} \int dE \, \mathrm{Tr}[t^\dagger(E)t(E)](f(E,\mu_L,T) - f(E,\mu_R,T)).
\tag{1.9}
$$

One sees, that the average current is given entirely by the sum of the eigenvalues $T_n(E)$ of the transmission matrix product $\sum_{n,n'} t^\dagger_{n,n'}(E)t_{n',n}(E)$ with $t_{n,n'}(E) = S(n,L,E;n',R,E)$. At zero temperature and if the voltage difference $V = (\mu_L - \mu_R)/e$ is small compared to the scale over which $T_n(E)$ varies, one writes Eq. (1.9) in the form

$$
\langle I(L,t) \rangle = G\,V, \qquad\qquad G = \frac{e^2}{2\pi\hbar} \sum_n T_n(E_F),
\tag{1.10}
$$

known as the Landauer Formula [6].

Voltage probe model

Suppose one believes to know the hamiltonian H, which describes the full time evolution. Then one can construct a matrix S to describe the scattering problem

in the sense above and predict transport characteristics.

But what shall one do, if experiments show that this description is wrong? One way to react on that would be to change the hamiltonian, renew the prediction and hope that this helps. Thus one can e.g. extend the hilbert space or change parameters of the hamiltonian. This process of including more and more but still not too complicate interactions is a well known procedure in traditional condensed matter physics. There one wants to describe properties of different type of materials and finds out e.g. that the electron phonon coupling is in some materials more important than in others.

But our formulation of transport in terms of S and the boundary conditions suggests an alternative strategy to design a theory which is not in contradiction to the experiment. Instead of the hamiltonian, one can manipulate the scattering matrix itself as well as the hilbert space of scattering states. Markus Büttiker was the first person who realized this and and got the idea of the *Voltage probe* concept (sometimes also called third lead model) [7]. It was used to include inelastic scattering events into the elastic scattering matrix description of the transport through little constrictions. He introduces despite the fact that there are only two real (man made) contacts of the constriction a third one, like depicted in Fig. 1.2. But Büttiker had now to postulate two parts of the extended model.

First he had to make use of the freedom to define the scattering matrix elements towards and away from that third lead. There is no detailed systematic way how one should choose all of these matrix elements. In practice one rather has to take care that there are no "anomalies" [8] induced by it. Model calculations have shown that at least the total weight of these scattering matrix elements from the fictitious lead to another lead, thus e.g.

$$T_{R,3}(E) = \sum_{n,n'} S(n,R,E;n',3,E)S^*(n,R,E;n',3,E), \qquad (1.11)$$

seem to have some general intuitive meaning. We come to an example in Chpt. 3 where we map the voltage probe model to a model with imaginary potential. There we also look only at statistical behavior of observables. We postulate these a priori unknown scattering matrix elements not only for one scattering matrix, but for a whole set of them. Thus we can even hope, that this averaging over many guessed scattering matrices can diminish individual anomalies.

Second, Büttiker had to postulate the in-going state in the fictitious voltage probe. Again - this seems to be a large reservoir of freedom. But led by the goal of simplicity and conservation laws he and others proposed several solutions for that, like e.g. the decoherence voltage probe model [9, 10]. What do we mean here by conservation laws? It is in quantum transport physics [11] (but also other
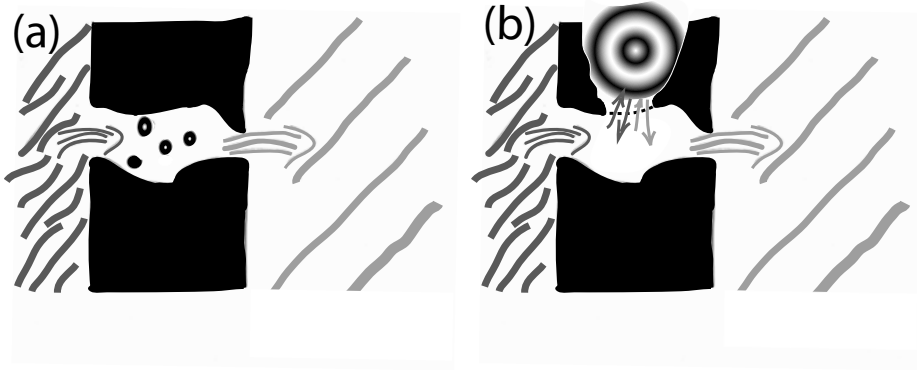
Figure 1.2: The voltage probe idea maps a scattering center allowing inelastic processes to a a purely elastic scattering problem in an extended hilbert space. *(a):* Sketches the transport from the left side with high to the right side with low electron density. The electrons have to pass a constriction containing some centers for inelastic collisions. *(b):* Corresponding scattering area with attached voltage probe, the stationary state in the voltage probe (symbolized by the rings) should not only allow a realistic mapping but also fulfill the condition of simplicity.

disciplines like hydrodynamics [12]) often necessary to be careful in defining a model, because one could violate widely accepted expectations on it. Such expectations concern conservation laws that follow from symmetries. One expects e.g. that the averaged number of electrons which enter a constriction from the right and left is the same as the number of particles that leave the constriction. Thus the constriction is on average no source or sink of electrons. It implies that the current inside the fictitious lead vanishes

$$\langle I(t,L)\rangle = -\langle I(t,R)\rangle \qquad \rightarrow \qquad \langle I(t,3)\rangle = 0. \tag{1.12}$$

Assuming that the incoming electrons in the voltage probe are distributed according to a fermi distribution at zero temperature, $f(E,\mu_3,0)$, Eq. (1.12) fixes its chemical potential μ_3.

One can impose more and more conservation laws and consequently has to design the state in the voltage probe more and more sophisticatedly. Again - Chpt. 3 exemplifies this, and we impose there that the particle number is even conserved for each energy.

1.1.2 System bath description: the intuitive border

We are going to discuss now a description for transport which is different from the scattering view. It complements it in the case of transport through a little constriction in a way which we will understand a bit later. Our goal is to find an equation describing the evolution of the state in a little part of a big system. Or to be more precise - it should describe the evolution of that object which is sufficient to calculate at all times the expectation value of every operator that acts only in that little part of the big system. This object is called reduced density matrix

$$\rho_{red}(t) \quad = \quad \text{Tr}_{par}\left(|\Psi(t)\rangle\langle\Psi(t)|\right). \tag{1.13}$$

It is obtained by performing the partial trace $\text{Tr}_{par}(..)$ over all the degrees which do not belong to the little part in the 'ket-bra' construction $|\Psi(t)\rangle\langle\Psi(t)|$ with $|\Psi(t)\rangle$ as the total wave function. In the following we call the little part "System" and the remaining part "bath". The total hamiltonian

$$H \quad = \quad H_{Sys} + H_{bath} + V \tag{1.14}$$

contains V as coupling between them. It seems here arbitrary to make this distinction between System and bath - after all, the predictions should in principle not depend on it. But exactly this changes if one uses the approximate time evolution of the System density matrix [13]

$$\frac{d\rho_{Sys}(t)}{dt} = -i\hbar^{-1}\left[H_{Sys}, \rho_{Sys}(t)\right]$$
$$-\hbar^{-2}e^{(-iH_{Sys}t/\hbar)}\int_0^t d\tau \, \text{Tr}_{bath}\left[\tilde{V}(t), \left[\tilde{V}(\tau), \rho_{Sys}(\tau) \times \rho_{bath}\right]\right]e^{(iH_{Sys}t/\hbar)},$$
$$\tag{1.15}$$

shorter written as

$$\frac{d\tilde{\rho}(t)}{dt} \quad = \quad -\hbar^{-2}\int_0^t d\tau \, \text{Tr}_{bath}\left(\left[\tilde{V}(t), [\tilde{V}(\tau), \tilde{\rho}_{Sys}(\tau) \times \rho_{bath}]\right]\right), \tag{1.16}$$

where operators with a tilde are given in the interaction picture, thus e.g. $\tilde{V}(t) = \exp(i(H_{Sys} + H_{bath})t)V\exp(-i(H_{Sys} + H_{bath})t/\hbar)$. [..,..] is the commutator. The approximation in Eq. (1.15) requires among others that the bath is for all times described by the equilibrium density matrix ρ_{bath}.[2] We apply this formula in two situations. The little constriction plays the role of the System and we write

$$H_{Sys} \quad = \quad \sum_n E(n)c_n^\dagger c_n \tag{1.17}$$

---

[2]To assume equilibrium means to enforce $[H_{bath}, \rho_{bath}] = 0$ for all times.

with $c_n^\dagger$ as fermionic creation operator in the n-th energy eigenstate. We ignore many body interactions because we will later only look at situations where we anyway don't have to treat them seriously.

We consider as a bath

- the two electron reservoirs of different chemical potential μ_L, μ_R. The reservoirs support electron tunneling into and out of the constriction.

  Thus we write micro canonically

$$H_{bath} = \sum_k \epsilon(k) \left(d_k^\dagger d_k + f_k^\dagger f_k \right), \tag{1.18}$$

  with d_k (f_k) referring to the electrons in the left (right) reservoir and k lumps together all their quantum numbers. Further is

$$V = \sum_{nk} T_{kn}^{(L)} c_n^\dagger d_k + T_{kn}^{(R)} c_n^\dagger f_k + h.c.. \tag{1.19}$$

  Appendix (1.A) derives then with help of Eq. (1.15) the master equation for the electron transport through the $\mathscr{S}$ystem in the Lindblad form

$$\hbar \frac{d\rho_{\mathscr{S}ys}(t)}{dt} = -i[H_{\mathscr{S}ys}, \rho_{\mathscr{S}ys}(t)] + \sum_{xn} L_{xn} \rho_{\mathscr{S}ys}(t) L_{xn}^\dagger$$
$$- \frac{1}{2} \left(L_{xn}^\dagger L_{xn} \rho_{\mathscr{S}ys}(t) + \rho_{\mathscr{S}ys}(t) L_{xn}^\dagger L_{xn} \right) \tag{1.20}$$

  with $L_{Ln} = \sqrt{\gamma_{Ln}} c_n^\dagger$, $L_{Rn} = \sqrt{\gamma_{Rn}} c_n$ and γ_{xn} as tunneling rates that depend especially on the $T_{kn}^{(x)}$'s. It is necessary to understand that the derivation relies very much on the fact, that the individual energies $E(n)$, or more correct the states to which their corresponding eigenstates hybridize to, are energetically several $k_B T$ inside the voltage window $[\mu_R, \mu_L]$. This stands in contrast to the derivation of the Landauer formula, because there we assumed the hybridization to be very homogeneous over the whole voltage window.

- a bosonic potential that couples to the position of the electrons inside the constriction. It resembles electron phonon interaction and it can e.g. lead to exchange of electronic energy and phononic energy.

  For simplicity we look here just at the situation in which we can identify quite individual dots inside the constriction and write the operators for these dot orbitals α_n in terms of the eigen modes of the $\mathscr{S}$ystem

$$\alpha_n = \sum_{n'} M_{n,n'} c_{n'}. \tag{1.21}$$

Distinct bunches of harmonic oscillators are coupled to each of the dot orbitals

$$H_{bath} = \sum_{ni} \Omega_{ni} h_{ni}^\dagger h_{ni} \qquad V = \sum_{ni} \mathcal{V}_{ni} \alpha_n^\dagger \alpha_n (h_{ni}^\dagger + h_{ni}) \quad (1.22)$$

Appendix (1.B) shows, that the time evolution has under reasonable assumptions again Lindblad form

$$\hbar \frac{d\rho_{sys}(t)}{dt} = -i[H_{sys}, \rho_{sys}(t)] + \sum_n L_n \rho_{sys}(t) L_n^\dagger$$

$$-\frac{1}{2}\left(L_n^\dagger L_n \rho_{sys}(t) + \rho_{sys}(t) L_n^\dagger L_n\right) \qquad (1.23)$$

but now with the jump operators $L_n = \sqrt{\gamma_{\phi,n}}\, \alpha_n^\dagger \alpha_n$ where the damping rates $\gamma_{\phi,n}$ depend on the coupling constants $\mathcal{V}_{ni}$.

1.2 Entanglement in quantum mechanics

1.2.1 Quantum computation

The wish that machines should support people in doing mathematical tasks is a quite old one and has driven the invention of abacus as much as that of nowadays computers. The computer technology had big impact on the life of many people also because the performance of processors has been increasing enormously. Thus one may think that we are close to the point where we don't need much more technological development in that respect. And it will probably be true, that the hardware requirements for writing and printing a letter in 2050 aren't much higher than today.

But for everyone who has ever tried to simulate on a computer the behavior of even a little quantum system it is clear, that our computers are very very limited in that respect. The basic reason for this is that the nowadays existing computers are classical whereas the evolution of the wave function is quantum. At this point one may be puzzled: Don't even todays computers follow the laws of quantum mechanics, because "classical" is just a special case of "quantum" ? Despite this is true, the events which correspond in a classical computer to the objects in the mathematical algorithms -intermediate results- are outcomes of measurements, thus real numbers. In the process of obtaining them one lost phase information. But to simulate a quantum system, one needs exactly such phase information "on the way" to obtain in the end a good real valued prediction. A quantum

computer tries to overcome this conceptual mismatch. In a quantum computer the intermediate information is contained in coefficients of the wave function. And it is not just that these are complex numbers what could make them so powerful, because a complex number is just twice as good as a real one. The qualitative difference to a classical computer is based on the fact, that there exist even in little quantum systems simultaneously very many of those coefficients - many more than even a quick repetition of measurements on such a system can generate real numbers in a reasonable time. A quantum computer should be able to use all of these complex coefficients of the wavefunction as mathematical objects - an enormous resource !

One needs for the realization of a quantum computer to find quantum algorithms - a sensible way to use its resources - and hardware which suits them. Unfortunately there are just a few quantum algorithms. There is the famous Shor algorithm for factorizing numbers [14], the Grover algorithm for searching in datas [15] and some other ones. A hardware, which allows to run e.g. the Shor program is believed to contain as information units the quantum generalization of a bit: the qubit. A qubit is a two dimensional hilbert space , lets say of basis $|1\rangle$ and $|0\rangle$, in which one can generate all superpositions $a|1\rangle + b|0\rangle$. It is important that a pair of locally distinct qubits, $a|10\rangle + b|01\rangle + c|11\rangle + d|00\rangle$, can become entangled into locally non-separable states, the so called Bell states

$$(|11\rangle + |00\rangle)/\sqrt{2} \tag{1.24}$$

$$(|00\rangle - |11\rangle)/\sqrt{2} \tag{1.25}$$

$$(|01\rangle + |10\rangle)/\sqrt{2} \tag{1.26}$$

$$(|10\rangle - |01\rangle)/\sqrt{2}. \tag{1.27}$$

Systems in which different particles have a many body interaction, e.g the Hubbard model, are known to have energy eigenstates which are very much non-separable. The simplest such system contains just two electrons at different positions. Their two spins $\vec{\sigma}_1, \vec{\sigma}_2$ can have an effective exchange interaction $|J|\vec{\sigma}_1\vec{\sigma}_2$, which leads e.g. to an entangled ground state $(|\uparrow\downarrow> + |\downarrow\uparrow>)/\sqrt{2}$.

But systems with many body interaction are unfortunately poorly understood. And especially to calculate or even design their evolution in superpositions of excited states is still a challenge. The main reason for this is already given above: the poor performance of classical computers[3] for such a task. Fortunately there could be a way around this - it is known under the name "free electron quantum computation". It is possible to combine charge and spin measurements to

---

[3]and maybe even of our minds

create a quantum algorithm without any interactions between the qubits [16]. If one only wants to entangle two qubits, then one can even do this without charge measurements, as discussed in the next subsection.

1.2.2 Entanglement production at a quantum dot

Interactions are not needed to entangle two particles, if one makes use of fermionic non-equilibrium states. The out of equilibrium condition can substitute for the entangling strength of many body interactions. In Refs. [17, 18] it was shown that the spin correlations in the current through biased tunnel junctions or quantum dots demonstrate the creation of spin-entanglement for non-interacting particles. Since this is the entangling mechanism that we will study in Chapter 3, we discuss it here in some detail. We consider a quantum dot with two point contacts of conductance $2e^2/h$. So each point contact transmits a single spin-degenerate electron mode. For an energy larger than the chemical potential on the right and smaller than that on the left side of the quantum dot, electrons approach the scattering area from the left and are in a separable state. They scatter and can so create superpositions of six outgoing states with equal energy,

$$|\uparrow,\downarrow\rangle = b_{R\uparrow}^\dagger(E)b_{L\downarrow}^\dagger(E)|GS\rangle \tag{1.28}$$

$$|\downarrow,\uparrow\rangle = b_{R\downarrow}^\dagger(E)b_{L\uparrow}^\dagger(E)|GS\rangle \tag{1.29}$$

$$|\uparrow,\uparrow\rangle = b_{R\uparrow}^\dagger(E)b_{L\uparrow}^\dagger(E)|GS\rangle \tag{1.30}$$

$$|\downarrow,\downarrow\rangle = b_{R\downarrow}^\dagger(E)b_{L\downarrow}^\dagger(E)|GS\rangle \tag{1.31}$$

$$|\uparrow\downarrow,0\rangle = b_{R\uparrow}^\dagger(E)b_{R\downarrow}^\dagger(E)|GS\rangle \tag{1.32}$$

$$|0,\uparrow\downarrow\rangle = b_{L\uparrow}^\dagger(E)b_{L\downarrow}^\dagger(E)|GS\rangle. \tag{1.33}$$

Here $|GS\rangle$ is the groundstate without outgoing particles. Coherences between states with different particle number on the left (and as well on the right) are suppressed , because the tunnel junction is fed by a constant voltage source. But even if one takes this into account, there remains among these six states still the superposition within the four dimensional subspace of one particle excitations on each side, Eqs. (1.28 - 1.31). In general a superposition of these states can contain some non-separability thus can be entangled.

1.2.3 Entanglement measure for electron pairs

From a quantum information point of view, the scattered electron pairs on the two sides of the quantum dot are shared between two locally distinct observers. Be-

cause these pairs are in general not exactly in superpositions of the form of the ideal Bell states, it is desirable to have a measure that tells the degree of usefulness for quantum computation. Degrees of usefulness are of course always dependent on the use. And despite the fact, that the development of further quantum algorithm will open new ways of use, we stick to some traditional measure. It is called bipartite entanglement entropy $\mathcal{E}$ and measures to how many Bell pairs one can convert a large number of copies of a single two electron state [19, 20]

$$\mathcal{E} = \frac{number\ of\ equivalent\ Bell\ pairs}{number\ of\ state\ copies}. \tag{1.34}$$

This conversion process has to fulfill the conditions that the two observers communicate only via classical channels and perform only local and reversible transformations. It is in that sense a unique measure [21] and can be calculated for pure states[4] as the von Neumann entropy of the partial density matrix seen by just one of the observers, ρ_L or ρ_R respectively,

$$\mathcal{E} \;\; = \;\; -\operatorname{Tr}\big(\rho_L \log_2(\rho_L)\big) = -\operatorname{Tr}\big(\rho_R \log_2(\rho_R)\big) \tag{1.35}$$

The number of equivalent Bell pairs is on the other hand a sensible measure, because the performance of such basic tasks like teleportation [22] or superdense coding [23] scales with it.

W.K. Wootters has found a generalization of Eq. (1.35) to mixed (total) density matrices ρ [24]. Because we make use of it in Chpt. 2 we state it here as

$$\mathcal{E} \;\; = \;\; \mathcal{F}\left(\frac{1+\sqrt{1-C^2}}{2}\right) \tag{1.36}$$

$$\mathcal{F}(x) \;\; = \;\; -x \log_2 x - (1-x)\log_2(1-x) \tag{1.37}$$

$$C \;\; = \;\; max\{0, \lambda_1 - \lambda_2 - \lambda_3 - \lambda_4\}, \tag{1.38}$$

where λ_i are the size ordered eigenvalues of $\sqrt{\sqrt{\rho}\hat{\rho}\sqrt{\rho}}$ with $\hat{\rho} = \big(\sigma_L^y \sigma_R^y\big)\rho^* \big(\sigma_L^y \sigma_R^y\big)$ containing the 2×2 pauli matrices σ_X^y in the subspace of the X-th observer.

1.2.4 Loss of entanglement

Interaction of the electron pairs with some bath degrees of freedom can lead to the situation, that the two observers share some wave function, but that this wave function is not a product state of a part just in their hilbert spaces and that of the bath. If the observers act then only locally on their part of the wave function, the

---

[4]The density matrix of a pure state ρ has the property $\rho = \rho^2$.

appropriate object to describe this is the reduced density matrix, which has the bath degrees traced out like in Eq. (1.13). It is common to distinguish two different types of decay of the spin degrees of freedom. Firstly, there is spin relaxation happening in a typical time T_1. This relaxation drives the spin-up and spin-down populations towards their equilibrium occupation $\propto \exp(-E/k_B T)$, thus changes the diagonal density matrix elements in the basis of energy eigenstates. Secondly, there can also be some unwanted change in the off-diagonal elements of the density matrix. If one looks e.g. on an ensemble of spins initially in phase and pointing along a direction parallel to an external magnetic field, one finds them to loose their phase relation due to fields that discriminate them in space or time. The time scale after which this happens is usually referred to as the coherence time T_2. In closed GaAs quantum dots, hyperfine interaction of the electron spins with fluctuating nuclear spins is the dominant source of spin decay, with $T_2 \simeq \mu s$ and T_1 increasing from μs to ms with increasing magnetic field [25–28]. In the open quantum dots considered in this Thesis, the decoherence of the orbital degrees of freedom also contributes to the loss of entanglement. Typically, orbital coherence is lost by electron-electron interactions on a time scale much smaller than the spin decoherence time in closed quantum dots, so that the total coherence time $\tau_\phi \ll T_1$. The voltage probe model for spin decay that we develop in Chapter 3 can treat decoherence and relaxation independently, with two different time scales. But we will analyze the model in that chapter only in the case of equal decoherence and relaxation times, respectively zero magnetic field. The model was however also extended to the case of more rapid decoherence than relaxation [29].

1.3 Transport in quantum dots

1.3.1 Open dots

This thesis addresses in Chpts. 2 and 3 open quantum dots. We call quantum dots open if their resistance is much smaller than e^2/h. This implies that the broadening $\hbar/\tau_{\text{dwell}}$ of the energy levels (due to the finite dwell time τ_{dwell} of an electron in the quantum dot) is large compared to the level spacing ΔE. The relatively small value of τ_{dwell} in an open quantum dot simplifies the study in two ways:

- We can use perturbation theory in the small parameter $\tau_{\text{dwell}}\Delta E/h$ to calculate the transport properties. This perturbation theory is essentially a semiclassical theory, because the effects of the finite level spacing are only included in first approximation.

- We can neglect the Coulomb repulsion of the electrons in the quantum dot, and use the single-electron scattering approximation to describe transport through the dot.

A common way to create quantum dots is to put metal electrodes on the surface of a doped semiconductor heterostructure, separated by an insulator. A voltage bias is then applied between these electrodes, called "gates", and the heterostructure. By adjusting these gate voltages one can deplete the two-dimensional electron gas underneath the electrodes. Fig. 1.3 shows two electron micrographs of such quantum dots. Both show areas of bright and dark color. The bright color represents the metal gates. These divide the two electron reservoirs and allow electrons only to move between them through two relatively narrow constrictions (= point contacts) and an intermediate wider region (= quantum dot). In an open quantum dot the width of the constrictions is large compared to the fermi wave length, so that its resistance is small compared to h/e^2.

The quantum dot is called ballistic if the mean free path for impurity scattering is large compared to its diameter. A ballistic quantum dot is also called an electron billiard, because the electron motion inside between the narrow constrictions is expected to be similar to a ball rolling over a billiard table. Of course the classical motion of a billiard ball does not show interference with itself thus it is an interesting task to search for quantum effects like weak localization in an electron billiard. Furthermore one already knows from real billiards, that the individual trajectories inside the billiard depend very sensitively on the exact shape of the boundaries and on the (initial) speed of the balls. Such sensitivity is called chaotic dynamics. This makes a detailed calculation for a particular electron billiard very difficult and the result maybe not very understandable.

To find anyhow some insight into electron billiards one turns to a statistical description. Rather than studying an individual billiard in a very detailed way, one studies the average properties of an ensemble of billiards with slightly different shapes. Random-matrix theory describes statistically well the distribution of scattering matrices of an ensemble of chaotic billiards. Experimentally, such an ensemble can be created and studied by varying the gate voltages to slightly change the shape of the quantum dot.

1.3.2   Closed dots

A quantum dot is called closed, if its resistance is larger than e^2/h. The level broadening is then small relative to the level spacing. One can then no longer use semiclassical perturbation theory, and one has to include the effects of Coulomb
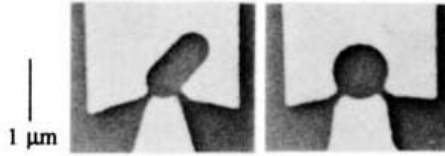
Figure 1.3: Electron micrographs of two open quantum dot devices. The bright area is the metal electrode (gate) underneath of which the electron gas is depleted. The two shapes have been fabricated to compare the difference of chaotic dynamics in the stadium billard (left) with nonchaotic (integrable) dynamics in the circular billiard (right). The conduction electron density is here $3800\,\mu m^{-2}$. These quantum dots are called "open" if the point contacts have resistances below h/e^2. The same device can be closed by increasing the gate voltage, so that the point contacts are pinched off to a resistance above h/e^2. Figures are taken from Ref. [30].

repulsion in a study of the transport properties. Closed quantum dots behave in many aspects like atoms. One can identify shell structures, Hund's rules can explain how electrons occupy them and structures with connected quantum dots behave in some sense like molecules [31].
Different to atoms is mainly the possibility to manipulate their electronic structure, because

- of their susceptibility to magnetic fields. Quantum dots can have sizes much larger than atoms in their groundstate - an external magnetic field can be more effective. The orbital energy inside a quantum dot is considerably changed if the magnetic field B can provide a full flux quantum $e/h = AB$, where A is the area of the orbital. Whereas in atoms one has to apply B-field strength of millions of Tesla, in quantum dots a few Tesla can be sufficient.

- the possibility to change the electron number in a given device. Electrons of a dot can come from the conduction band of a doped semiconductor thus an external potential can change their density.

- they can be connected to different electron reservoirs which allows transport through them.

1.3.3 Shot noise

Up to now we have only discussed the time-averaged current as a measurable transport quantity. The correlation function of the time-dependent current fluctuations $\Delta I(X,t) = I(X,t) - \langle I(X,t) \rangle$ is a further independent observable. It is defined as

$$S_{X,X'}(t-t') = \langle \Delta I(X,t) \Delta I(X',t') \rangle \tag{1.39}$$

and is the fourier transform of the so called noise power

$$S_{X,X'}(\omega) = \int_{-\infty}^{\infty} d\tau \, \exp(i\tau\omega) S_{X,X'}(\tau). \tag{1.40}$$

The labels X and X' indicate two different current-carrying contacts. We refer to Refs. [32] and [33] for, respectively, an introduction and a review.

The noise power $S(\omega)$ is called this way because it is proportional to the power spectrum of the electromagnetic radiation produced by the current fluctuations. One way to measure the noise power is to absorb this radiation in a bolometer (after passing it through a frequency filter), and measure the heat produced. In a theoretical description of the measurement process we deal with the outcome of actual current measurements $\mathcal{J}_X(t)$. These determine the average current and noise power through

$$\langle I(X,t) \rangle = \lim_{T \to \infty} \frac{1}{2T} \int_{-T}^{T} dt \, \mathcal{J}_X(t), \tag{1.41}$$

$$S_{X,X'}(\omega) = \lim_{T \to \infty} \frac{1}{T} \left| \int \int_{-T}^{T} dt dt' \, \exp[i\omega(t-t')] \mathcal{J}_X(t) \mathcal{J}_{X'}(t') \right|. \tag{1.42}$$

If there is no voltage applied to the constriction, the noise is called thermal or equilibrium noise S^{eq}. One can apply the scattering approximation and obtains

$$S_{L,R}^{eq}(\omega) = \frac{e^2 \omega}{\pi} \coth(\hbar\omega/2k_B T) \sum_n T_n(E_F), \tag{1.43}$$

which vanishes for zero temperature. [5]

---

[5]This is for zero frequency actually a special case of the more general Johnson-Nyquist relation to the conductivity G, $S_{L,R}^{eq}(0) = 4k_B T G$, which requires only the validity of the fluctuation dissipation theorem.

At finite voltage, there is also the shot noise contribution. The additional contribution appears because of the projective nature of the electronic reservoirs. They support unobserved measurements in the particle number basis and let the electrons seem to pass the constriction in discrete charges.[6] If the scattering approach is valid one obtains at zero temperature for the zero frequency component [36, 37]

$$S_{L,R}^{shot}(0) = \frac{e^3 V}{\pi \hbar} \sum_n T_n(E_F)[1 - T_n(E_F)]. \qquad (1.44)$$

In the Coulomb blockade regime where one has to use the master equation (1.20), one obtains for the zero frequency noise a much more complicated expression. But generally $S^{shot}(0)$ is proportional to the time averaged current $\langle I \rangle = \langle I(L,t) \rangle = \langle I(R,t) \rangle$. The voltage-independent ratio

$$F = \frac{S^{shot}(0)}{2e\langle I \rangle} \qquad (1.45)$$

is called the Fano factor. It is a numerical coefficient that contains information on the degree to which the electrons transferred through the conductor are independent. For independent electrons, the statistics of transferred charges is Poissonian, with $F = 1$ (since a Poisson distribution has variance equal to the mean). For anti-bunched electrons $F < 1$ and for bunched electrons $F > 1$. One speaks of sub-Poissonian and super-Poissonian noise, respectively. In Fig. 1.4 we show an experiment that measured the Fano factor in an open quantum dot in a two-dimensional electron gas [38]. The value 1/4 measured in the experiment is in agreement with the theoretical prediction using random-matrix theory [39] (see next subsection for more on this technique).

 Shot noise probes the particle nature of the electrons, and it is therefore not intrinsically a quantum mechanical effect. Indeed, shot noise was already understood by Schottky in 1918, before the development of quantum mechanics. Quantum corrections to the shot noise power exist, but they are smaller than the classical value by a factor $1/N$, with N the number of propagating modes in the point contacts. In the experiment of Fig. 1.4 one has $N = 5$, so the quantum interference corrections are not negligible, but still relatively small.

---

[6]Mathematically one can see this the best in the derivations of counting statistics [34, 35] by projection technique. One enforces that the density matrices for the reservoirs are almost diagonal in particle number.
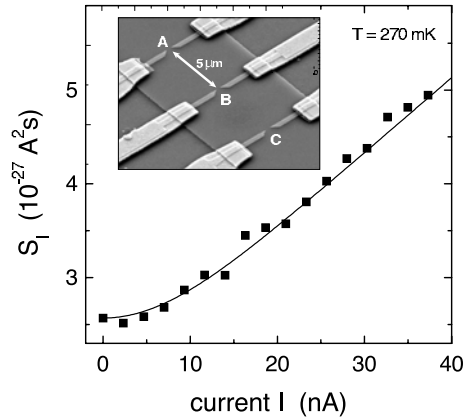
Figure 1.4: Low frequency noise power of the quantum dot shown in the inset. The current flows from point contact A to B, point contact C is inoperative. The solid line is the theoretical prediction which for large currents approaches the linear behavior $S = \frac{1}{4} \times 2eI$. At low currents the noise saturates at the thermal noise level. The figure is adapted from Ref. [38].

1.3.4   Weak localization

The resistivity of a metal is usually decreasing with temperature [40, 41], because the inelastic scattering gets frozen out and a Fermi liquid can stabilize. The residual resistivity at zero temperature is in semi-classical (Drude) approximation then just given by the carrier density and the mean free path for elastic impurity scattering. In thin films and narrow wires one finds a contrasting behavior — below a certain temperature the resistivity starts to rise again, see Fig. 1.5. It is a quantum mechanical peculiarity. Because the rise can be suppressed by an external magnetic field one surmises that time reversal symmetry plays some role. Indeed, theories which explain this weak localization correction to the (Drude) resistivity are based on the idea of constructive interference between time reversed paths [43–46], which is called coherent backscattering.

  The experiment shown in Fig. 1.5 is for a disordered conductor. In this thesis we consider ballistic conductors, without impurities, where all scattering is at the boundaries. A small ballistic conductor with two narrow openings (or point contacts) is called an open quantum dot. The semiclassical conductance of a quantum dot is just the series conductance of the two point contacts. If each point contact has the same conductance N in units of the conductance quantum $g_0 = 2e^2/h$, then the semiclassical conductance is just $G_{\text{class}} = (N/2)g_0$. The quantum me-
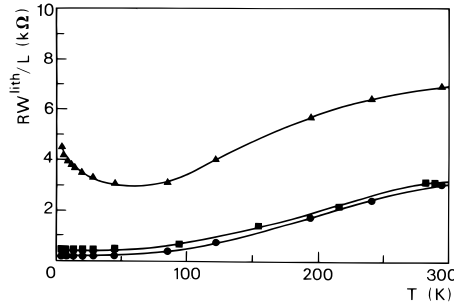
Figure 1.5: Temperature dependence of the resistivity of a two-dimensional electron gas in a GaAs-AlGaAs heterostructure. The upper set of data points is for a narrow wire ($0.5\,\mu$m wide), the lower sets are for wider wires (width $W > 1.5\,\mu$m). The wire length is $L = 10\,\mu$m. At low temperatures the resistivity rises because of the weak localization effect. Figure taken from Ref. [42].

chanical conductance is smaller than G_{class} because of coherent backscattering, just as in the case of a disordered system discussed above. Again, a magnetic field suppresses the weak localization correction and recovers G_{class}. An experimental observation of the weak localization effect in a quantum dot is shown in Fig. 1.6.

Theoretically, the weak localization correction $\delta g = G - G_{\text{class}}$ follows from Eq. (1.10), containing the N transmission eigenvalues of the quantum dot. To eliminate sample-to-sample fluctuations, one needs to average the conductance over an ensemble of quantum dots with small variations in shape. This can be done numerically, but if the shape of the quantum dot is such that the classical dynamics is chaotic, then an alternative analytical technique is possible. This is the technique of random-matrix theory [48], which is based on the fact that the scattering matrix of an ensemble of chaotic quantum dots is uniformly distributed in the group of unitary matrices. The ensemble averaged conductance $\langle G \rangle$ then follows directly from an integral over the unitary group, with the result [49]

$$\langle G \rangle = g_0 \frac{N^2}{1+2N} \Rightarrow \delta G = -g_0 \frac{N}{2+4N}. \tag{1.46}$$

The weak localization correction varies between $-g_0/6$ for $N = 1$ and $-g_0/4$ for $N \gg 1$.
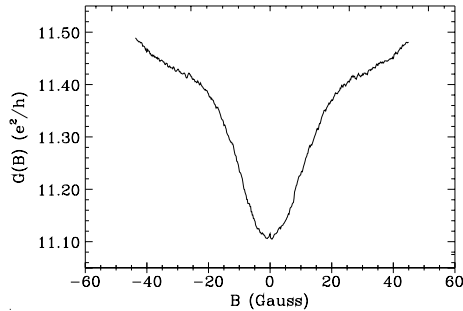
Figure 1.6: Magnetic field dependence of the conductance of a ballistic confined region (quantum dots) in the two-dimensional electron gas of a GaAs-AlGaAs heterostructure. The dots have the shape of a stadium, so the classical dynamics is chaotic. The conductance is averaged over 48 similar devices at 50 mK. The dip around zero magnetic field is due to the weak localization effect. Figure taken from Ref. [47].

1.4   This Thesis

Chapter 2: Stub model for dephasing in a quantum dot

Shot noise and weak localization are two effects that probe, respectively, the particle and wave nature of the electron — so they respond differently to decoherence. While shot noise seems to be much more insensitive to decoherence, weak localization is suppressed by it. The decoherence version of the voltage probe model discussed earlier in this introduction, indeed gives a suppression of weak localization while leaving the shot noise unaffected. The work in chapter 2 was driven by the search for a model of decoherence that does as well not have influence on shot noise but leads to a loss of the weak localization correction. In contrast to the voltage probe it should not have to deal with an artificially extended Hilbert space but it should rather make use of explicit time dependence in the hamiltonian. We have found that this can be realized if the Hilbert space of the scatterer is partitioned into two spaces. One of them doesn't decohere and the other decoheres because of weak time-dependent fields there - we call the latter space 'stub' [50]. The tunneling between these spaces is rare but once a part of the electronic wavefunction enters the stub it stays there very long. So it looses its phase relation with the part that didn't enter the stub even if the external field is so weak that no additional shot noise is produced. We reproduce the results for shot noise and weak localization that come out of the voltage probe model.
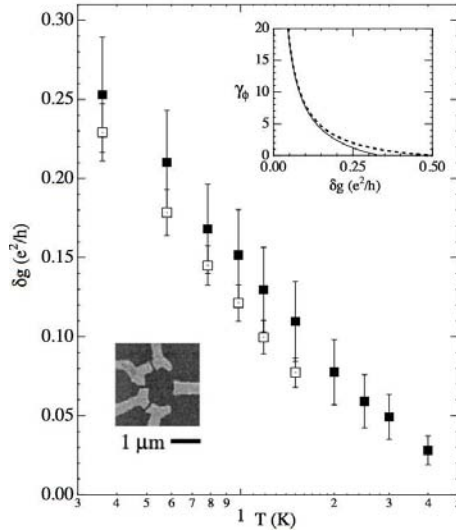
Figure 1.7: Temperature dependence of the weak localization correction δg in a quantum dot with two single channel point contacts. The two sets of data points correspond to two different samples (one of which is shown in the lower left inset). The upper right inset shows the dependence of δg on the decoherence rate γ_ϕ (scaled by the level spacing), as predicted by the voltage probe model. (The solid curve is for a voltage probe connected to the quantum dot by a tunnel barrier, the dashed curve is without a tunnel barrier.) Figure adapted from Ref. [51].

This is fortunate because the voltage probe model has been used extensively by experimentalists to extract the decoherence rate γ_ϕ from weak localization measurements. As a representative example, we show in Fig. 1.7 the experimental data of Huibers et al. [51]. Shown is the temperature T dependence of the weak localization correction δG in a quantum dot with two single channel point contacts. By comparing with the γ_ϕ dependence of δg predicted by the voltage probe model, they could determine the T dependence of γ_ϕ. In a further experiment they did not vary T but the intensity of microwave radiation which they were shining on the sample [52]. They found that it has the same influence as just increasing the temperature in the whole vacuum chamber. Their conclusion was that the fact that δg seems not to reach its theoretical $T = 0$ value of $1/3$ can not be explained by some fluctuating field that is just homogeneous over the whole sample. They argued that the delicate electron-electron interaction was the primary source of decoherence.

Chapter 3: Voltage probe model of spin decay in a chaotic quantum dot, with applications to spin-flip noise and entanglement production

We return to the voltage probe model. In this chapter we use this model to study the effect of spin-flip scattering on electrical conduction through a quantum dot with chaotic dynamics. The spin decay rate γ is quantified by the correlation of spin-up and spin-down current fluctuations (spin-flip noise). The resulting decoherence reduces the ability of the quantum dot to produce spin-entangled electron-hole pairs. For γ greater than a critical value γ_c, the entanglement production rate vanishes identically. The statistical distribution $P(\gamma_c)$ of the critical decay rate in an ensemble of chaotic quantum dots is calculated using the methods of random-matrix theory. For small γ_c this distribution is $\propto \gamma_c^{-1+\beta/2}$, depending on the presence ($\beta = 1$) or absence ($\beta = 2$) of time-reversal symmetry. To make contact with experimental observables, we derive a one-to-one relationship between the entanglement production rate and the spin-resolved shot noise, under the assumption that the density matrix is isotropic in the spin degrees of freedom. Unlike the Bell inequality, this relationship holds for both pure and mixed states. In the tunneling regime, the electron-hole pairs are entangled if and only if the correlator of parallel spin currents is at least twice larger than the correlator of anti parallel spin currents.

Chapter 4: All-electronic coherent population trapping in quantum dots

We present a fully electronic analogue of coherent population trapping in quantum optics, based on destructive interference of single-electron tunneling between three closed quantum dots. A large bias voltage plays the role of the laser illumination. The trapped state is a coherent superposition of the electronic charge in two of these quantum dots, so it is destabilized as a result of decoherence by coupling to external charges. The resulting current I through the device depends on the ratio of the decoherence rate Γ_ϕ and the tunneling rates. For $\Gamma_\phi \to 0$ one has simply $I = e\Gamma_\phi$. With increasing Γ_ϕ the current peaks at the inverse trapping time. The direct relation between I and Γ_ϕ can serve as a means of measuring the coherence time of a charge qubit in a transport experiment.

Recent experiments on a triple dot geometry have been performed by Vidan et al. [53]. We show their findings in Fig. 1.8 because they use a dot geometry that might be used to observe the effect predicted in this thesis. Their experiment, however, is done in an incoherent high temperature regime, so that it produces an incoherent trapping effect (rather than the coherent effect which we have predicted). It is due to carrier blocking because of Coulomb repulsion between an
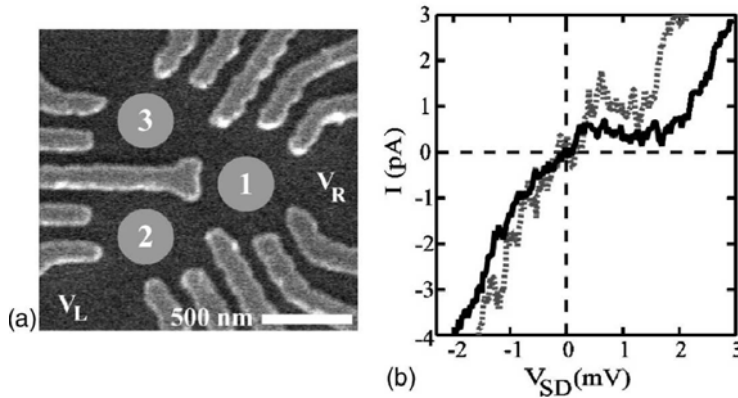
Figure 1.8: *figure (a):* Electron micrograph of a triple quantum dot. The light areas are gates used to define the quantum dots. The locations of the dots are highlighted by circles. This geometry allows for tunneling between dots 1 and 2, and between dots 1 and 3. Dots 2 and 3 are capacitively coupled, but no electrons may tunnel between these dots. A large voltage difference $V_{SD} = V_L - V_R$ between the current source and drain forces electrons to tunnel either from left to right (for $V_{SD} < 0$) or from right to left (for $V_{SD} > 0$). Dots 1 and 2 therefore act as "one way street dots". The current is blocked if $V_{SD} > 0$, because then an electron gets trapped in the "dead end dot" number 3, preventing other electrons to enter the device. This rectification behavior is shown in the current-voltage characteristic in (b). The dotted (solid) line corresponds to weaker (stronger) coupling between dots 2 and 3, which gives rise to weaker (stronger) current suppression for $V_{SD} > 0$. Figures are taken from Ref. [53].

electron that sits in a 'dead end dot' and electrons which want to move through the 'one way street dot'. The incoherent rectification mechanism of Ref. [53] (which happens for opposite voltage bias as our coherent effect) does not play a role in our structure because we do not have a 'dead end dot'.

Chapter 5: Counting statistics of coherent population trapping in quantum dots

In the previous chapter we considered the time averaged current through the triple quantum dot device. Here we consider higher moments of the time-dependent current fluctuations. The full distribution of the current, integrated over a cer-

tain detection time, represents the distribution of the number of charges transferred through the device in the detection time. This is the reason that one calls it "counting statistics". Our analysis was motivated by an experimental development, which we describe here. The experiment by Gustavsson et al. [54] showed that it is possible to detect the individual passage of electrons in time through nanoscopic constrictions. Their setup in Fig. 1.9 shows a quantum point contact capacitively coupled to an independently gated quantum dot device [55]. The time trace of the current through the point contact, Fig. 1.9, shows essentially two different current intensities. Each of them corresponds to a different occupation in the dot and allows by that to detect the individual tunneling events through it. Because the whole counting statistics is determined this way, also the Fano factor can be extracted. They find in consistency with a theory based on the master equation like Eq. (1.20) that it depends on the tunneling couplings of the dot to the reservoirs. Our calculations on the triple dot device predict, that analogous measurements on it should find Fano factors between 3 and 0.5 (in general sub- or super-Poissonian statistics) - depending on the tunneling constants and decoherence strengths.

Chapter 6: Transfer of entanglement from electrons to photons by optical selection rules

In designs of quantum computers one would like to use electron qubits to locally process the information and photon qubits to transport it over long distances. A first step on the way to realize this with solid state based devices was the transfer of the spin polarization of conduction band electrons of a GaAs/AlGaAs light-emitting diode to the circular polarization of the emitted photons [56]. The operation of this device, called a spin-LED, is illustrated in Fig. 1.10. It realizes a *classical* correlation transfer, which means, that one can see in the experiment only that diagonal elements of the density matrix in the energy eigenbasis are transferred between electron and photon degrees of freedom.

To transfer quantum information (in particular, to transfer entanglement), one needs to transfer all components of the density matrix. A method to do this with a spin-LED has been proposed by Vrijen and Yablonovitch [57]. Their proposal requires a strong magnetic field to break the spin degeneracy of the energy levels. In chapter 6 we examine alternative strategies that do not require a (strong) magnetic field.
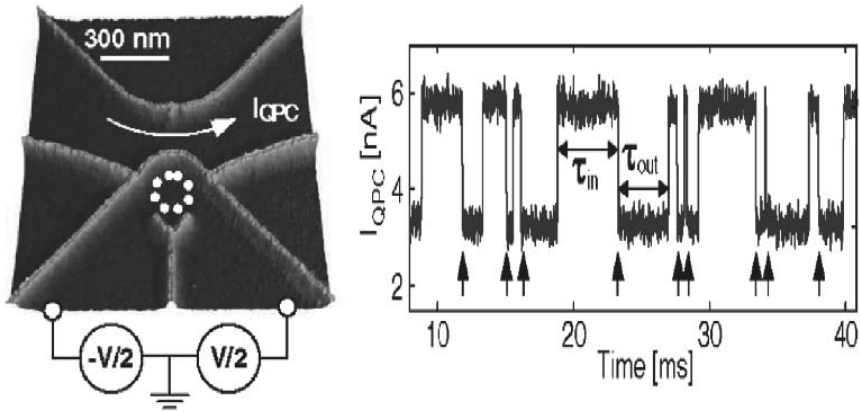
Figure 1.9: *Left panel:* AFM (atomic force microscope) micrograph of a device that capacitively couples a quantum dot (denoted by the ring of white points) and a quantum point contact. The current I_{QPC} through the quantum point contact depends on the charge in the quantum dot. *Right panel:* Example of the time dependent current through the quantum point contact. When it jumps downward an electron leaves the dot, when it jumps upward an electron enters the dot. In this way the full counting statistics of transferred charge can be measured. Figures adapted from Ref. [54].

1.A Derivation of Eq. (1.20) - electron tunneling to and from reservoirs

This appendix follows in some parts Ref. [58], but we generalise here to several orbitals. We write the density operator in the interaction picture but ignore its tilde sign

$$\frac{d\rho_s(t)}{dt} = -\hbar^{-2} \int_0^t d\tau \, \mathrm{Tr}_B \left([V(t), [V(\tau), \rho_s(\tau)\rho_B,]] \right) \qquad (1.47)$$
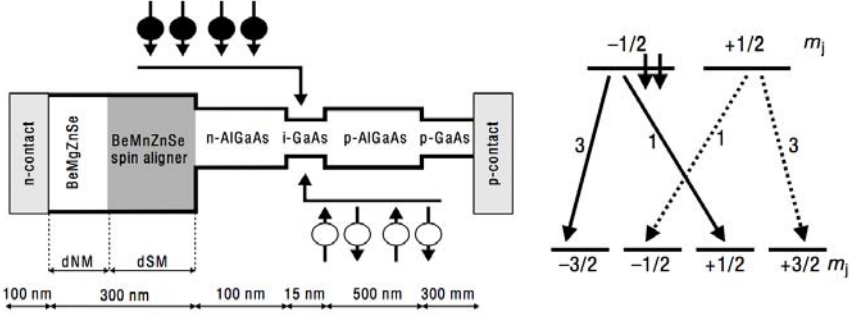
Figure 1.10: *Left panel:* Geometry of the spin-LED, a device that transfers elec-
tron spin polarization to photon polarization. Spin-polarised electrons are injected
from the left into the active GaAs layer, unpolarized holes are injected from the
right. Electron-hole recombination leads to to photons with a circular polariza-
tion determined by the electron spin. *Right panel:* energy level structure in GaAs.
The upper levels are states in the s-type conduction band, the lower ones states
in the p-type valence band. The total angular momentum quantum number m_j
is indicated. The transitions labeled 3 are a factor of three more probable than
those labeled 1. As a consequence, photons emitted by a spin down electron carry
predominantly angular momentum $+1$ (transition $-1/2 \to -3/2$), while photons
emitted by a spin up electron carry predominantly angular momentum -1 (tran-
sition $+1/2 \to +3/2$). Figures are taken from Ref. [56].

with V from Eq. (1.19) and the definition $\omega(n,k) = [E(n) - \epsilon(k)]/\hbar$ this gives

$$
\begin{aligned}
\frac{d\rho_s(t)}{dt} = -\hbar^{-2} \sum_{n,k,n'} \int_0^t d\tau \, & \Big\{ c_n^\dagger c_{n'}, \rho_s(\tau) \Big\} \Big(T_{kn}^{(L)} T_{kn'}^{(L)*} f(\epsilon(k), \mu_L, T) \\
& + T_{kn}^{(R)} T_{kn'}^{(R)*} f(\epsilon(k), \mu_R, T) \Big) \exp\big(i\omega(n,k)t - i\omega(n',k)\tau\big) \\
& + \Big\{ c_n c_{n'}^\dagger, \rho_s(\tau) \Big\} \Big(T_{kn}^{(L)*} T_{kn'}^{(L)} [1 - f(\epsilon(k), \mu_L, T)] \\
& + T_{kn}^{(R)*} T_{kn'}^{(R)} [1 - f(\epsilon(k), \mu_R, T)] \Big) \exp\big(-i\omega(n,k)t + i\omega(n',k)\tau\big) \\
& + c_n^\dagger \rho_s(\tau) c_{n'} \Big(T_{kn}^{(L)} T_{kn'}^{(L)*} f(\epsilon(k), \mu_L, T) + T_{kn}^{(R)} T_{kn'}^{(R)*} f(\epsilon(k), \mu_R, T) \Big) \\
& \cdot \big(\exp[i\omega(n,k)t - i\omega(n',k)\tau] + \exp[i\omega(n,k)\tau - i\omega(n',k)t] \big) \\
& + c_n \rho_s(\tau) c_{n'}^\dagger \Big(T_{kn}^{(L)*} T_{kn'}^{(L)} [1 - f(\epsilon(k), \mu_L, T)] + T_{kn}^{(R)*} T_{kn'}^{(R)} [1 - f(\epsilon(k), \mu_R, T)] \Big) \\
& \cdot \big(\exp[-i\omega(n,k)t + i\omega(n',k)\tau] + \exp[-i\omega(n,k)\tau + i\omega(n',k)t] \big)
\end{aligned}
$$

$$(1.48)$$

To simplify this expression one makes use of the fact that the reservoirs have a dense spectrum and substitutes the sum over k-points by the energy integral with the density of states $DOS(\epsilon(k))$. We encounter in Eq. (1.48) many integrals of the type

$$\int d\epsilon\, DOS(\epsilon) T^{(X)}_{k(\epsilon)n} T^{(X)*}_{k(\epsilon)n'} f(\epsilon, \mu_X, T) \exp[i\epsilon(t-\tau)]. \tag{1.49}$$

We consider the regime, where the hybridizations $T^{(X)}_{k(\epsilon)n}$ are several kT inside the voltage window set to $[\mu_R, \mu_L]$ and of a typical width δE. The $DOS(\epsilon)$ should not vary much on the scale of δE. We assume further out of notational simplicity, that $T^{(X)}_{k(\epsilon)n}$ and $T^{(X)}_{k(\epsilon)n'}$ do not overlap for $n \neq n'$. [7] Fig. (1.11) sketches the assumptions on the energy dependence of the functions. Thus one finds that the integral vanishes for $X = R$ and is in the case $X = L$ finite for $|t - \tau| < \hbar/\delta E$. Thus we write the integral as

$$2\hbar\gamma_{X,n}\delta_{n.n'}\delta_{\delta E}(t-\tau) \tag{1.49$'$}$$

where $\gamma_{X,n}$ contains the details of $DOS(\epsilon)$, the hybridizations and some further phase. The notation $\delta_{\delta E}(..)$ reminds to the finite width of the delta function through a finite δE. Thus all that follows should be used carefully if one makes statements about time differences or considers also different mechanisms acting on the time scale smaller than $\hbar/\delta E$. Making use of this simplification we find that Eq. (1.48) simplifies enormously to

$$
\begin{aligned}
\frac{d\rho_s(t)}{dt} &= \hbar^{-1}\sum_n \gamma_{L,n} c_n^\dagger \rho_s(t) c_n - \frac{\gamma_{L,n}}{2}\left\{c_n^\dagger c_n, \rho_s(t)\right\} \\
&\quad + \gamma_{R,n} c_n \rho_s(t) c_n^\dagger - \frac{\gamma_{R,n}}{2}\left\{c_n c_n^\dagger, \rho_s(t)\right\}.
\end{aligned} \tag{1.50}
$$

We remember now that we are still in the interaction representation of the density operator. But if one transforms now back to the Schrödinger picture, one encounters that (1.50) equals the Lindblad equation (1.20) with the there stated jump operators.

---

[7]This can in principle always be performed by unitary transformation of the inner orbitals inside the constriction. This is in Chpt. 3 and 4 used, where we take the hybridization functions of individual dots as non overlapping.
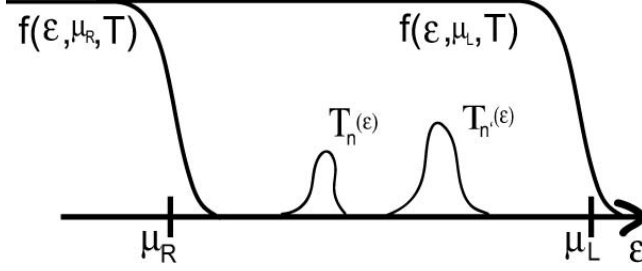
Figure 1.11: Unscaled plot for the conditions for the validity of the Master equation. The hybridization functions of the internal eigenfunctions inside the constriction (labled by n,n') have their main weight several $k_B T$ inside the voltage window from μ_R to μ_L.

1.B   Derivation of Eq. (1.20') - dynamical potential (phonons)

We write all operators in the interaction picture with a tilde, and find

$$\frac{d\tilde{\rho}_s(t)}{dt} = -\hbar^{-2} \int d\tau \sum_{ni,n'i'} \mathcal{V}_{ni}\mathcal{V}_{n'i'}$$

$$\left\{ \alpha_n^\dagger \alpha_n \alpha_{n'}^\dagger \alpha_{n'} \tilde{\rho}_s(\tau) \operatorname{Tr}_B\left[\left(\tilde{h}_{ni}^\dagger(t) + \tilde{h}_{ni}(t)\right) \left(\tilde{h}_{n'i'}^\dagger(\tau) + \tilde{h}_{n'i'}(\tau)\right) \rho_B \right] \right.$$

$$+ \tilde{\rho}_s(\tau) \alpha_n^\dagger \alpha_n \alpha_{n'}^\dagger \alpha_{n'} \operatorname{Tr}_B\left[\left(\tilde{h}_{ni}^\dagger(\tau) + \tilde{h}_{ni}(\tau)\right) \left(\tilde{h}_{n'i'}^\dagger(t) + \tilde{h}_{n'i'}(t)\right) \rho_B \right]$$

$$+ \alpha_n^\dagger \alpha_n \tilde{\rho}_s(\tau) \alpha_{n'}^\dagger \alpha_{n'} \operatorname{Tr}_B\left[\left(\tilde{h}_{ni}^\dagger(t) + \tilde{h}_{ni}(t)\right) \left(\tilde{h}_{n'i'}^\dagger(\tau) + \tilde{h}_{n'i'}(\tau)\right) \rho_B \right]$$

$$\left. + \alpha_n^\dagger \alpha_n \tilde{\rho}_s(\tau) \alpha_{n'}^\dagger \alpha_{n'} \operatorname{Tr}_B\left[\left(\tilde{h}_{ni}^\dagger(\tau) + \tilde{h}_{ni}(\tau)\right) \left(\tilde{h}_{n'i'}^\dagger(t) + \tilde{h}_{n'i'}(t)\right) \rho_B \right] \right\}$$

The bath is in equilibrium, thus only $n = n'$ and $i = i'$ contributes to the sum. We use further that there is a dense spectrum of oscillators, thus $\sum_{ni} \ldots \rightarrow \sum_n \int d\omega DOS_n(\omega)\ldots$. We use that $\tilde{h}_{ni}(t) = h_{ni}\exp(i\Omega_{ni}t)$ and find that like in the case of the electron reservoirs, the time integral 'shrinks' because of a regularized $\delta_{\delta_E}(t-\tau)$ function where δE is roughly given by the oscillator bandwidth. The integrals over the density of states, coupling constants and occupations of the oscillator levels are all pulled into the constant $\gamma_{\Phi,n}$ and one gets

$$\frac{d\tilde{\rho}_s(t)}{dt} = \hbar^{-1} \sum_n \gamma_{\Phi,n} \alpha_n^\dagger \alpha_n \tilde{\rho}_s(t) \alpha_n^\dagger \alpha_n - \frac{\gamma_{\Phi,n}}{2} \left(\alpha_n^\dagger \alpha_n \tilde{\rho}_s(t) + \tilde{\rho}_s(t) \alpha_n^\dagger \alpha_n \right),$$

$$(1.51)$$

which becomes with the appropriate jump operators Eq. (1.20').

Bibliography

[1] B. Michaelis, *cond-mat/0606608* (2006).

[2] C.H. Bennett and G. Brassard, *Proceedings of IEEE International Conference on Computer, Systems, and Signal Processing, Bangalore, India (IEEE, New York)*, 175, (1984).

[3] A.K. Ekert, *Phys. Rev. Lett.* **67**, 661 (1991).

[4] W.H. Zurek, *Rev. Mod. Phys.* **75**, 715 (2003).

[5] K.G. Wilson, *Phys. Rev. B* **4**, 3174 (1971).

[6] R. Landauer, *Z. Phys. B* **21**, 247, (1975); **86**, 217, (1987).

[7] M. Büttiker, *Phys. Rev. B* **33**, 3020 (1986); IBM J. Res. Dev. **32**, 63 (1988).

[8] A.A. Clark and D. Stone, *Phys. Rev. B* **69**, 245303 (2004).

[9] C.W.J. Beenakker and M. Büttiker, *Phys. Rev. B* **46**, 1889 (1992).

[10] M.J.M. de Jong and C.W.J. Beenakker, *Phys. Rev. B* **51**, 16867 (1995).

[11] G. Baym and L.P. Kadanoff, *Phys. Rev.* **124**, 287 (1961).

[12] L.D. Landau, *Course of Theoretical Physics, Vol.6: Fluid Mechanics* , Butterworth-Heinemann (1987).

[13] T. Brandes, *lecture notes on Quantum Information, Chpt.7 (quantum dissipation)*,
http://www.itp.physik.tu-berlin.de/brandes/public_html/publications/notes/.

[14] P.W. Shor, *SIAM J. Sci. Statist. Comput.* **26**, 1484 (1997).

[15] L.K. Grover, *Phys. Rev. Lett.* **79**, 325 (1997).

[16] C.W.J. Beenakker, D.P. DiVincenzo, C. Emary, and M. Kindermann, *Phys. Rev. Lett.* **93**, 020501 (2004).

[17] C.W.J. Beenakker, C. Emary, M. Kindermann, and J.L. van Velsen, *Phys. Rev. Lett.* **91**, 147901 (2003).

[18] C.W.J. Beenakker, M. Kindermann, C.M. Marcus, and A. Yacoby, *Fundamental Problems of Mesoscopic Physics*, eds. I.V. Lerner, B.L. Altshuler, and Y. Gefen, NATO Science Series II. Vol. 154 (2004).

[19] C.H. Bennett, G. Brassard, S. Popescu, B. Schumacher, J.A. Smolin, and W.K. Wootters, *Phys. Rev. Lett.* **76**, 722 (1996).

[20] C.H. Bennett, J. Bernstein, S. Popescu, and B. Schumacher, *Phys. Rev. A* **53**, 2046 (1996).

[21] S. Popescu and D. Rohrlich, *Phys. Rev. A* **56**, R3319 (1997).

[22] C.H. Bennett, G. Brassard, C Crépeau, R. Jozsa, A. Peres, and W.K. Wootters, *Phys. Rev. Lett.* **70**, 1895 (1993).

[23] C.H. Bennett and S.J. Wiesner, *Phys. Rev. Lett.* **69**, 2881 (1992).

[24] W.K. Wootters, *Phys. Rev. Lett.* **80**, 2245 (1998).

[25] H.-A. Engel, L.P. Kouwenhoven, D. Loss, and C.M. Marcus, Quantum Inf. Process. **3**, 115 (2004).

[26] J.M. Elzerman, R. Hanson, L.H. Willems van Beveren, B. Witkamp, L.M.K. Vandersypen, and L.P. Kouwenhoven, Nature **430**, 431 (2004).

[27] J.R. Petta, A.C. Johnson, J.M. Taylor, E.A. Laird, A. Yacoby, M.D. Lukin, C.M. Marcus, M.P. Hanson, and A.C. Gossard, Science **309**, 2180 (2005).

[28] D. Klauser, W.A. Coish, and D. Loss, *cond-mat/0604252* (2006).

[29] C.W.J. Beenakker, *Phys. Rev. B* **73**, 201304(R) (2006).

[30] C.M. Marcus, A.J. Rimberg, R.M. Westervelt, P.F. Hopkins, and A.C. Gossard, *Phys. Rev. Lett.* **69**, 506 (2006).

[31] W.G. van der Wiel, S. DeFranceschi, and J.M. Ezerman, *Rev. Mod. Phys.* **75**, 1 (2003).

[32] C.W.J. Beenakker and C. Schönenberger, *Physics Today*, May 2003, page 37

[33] Ya.M. Blanter and M. Büttiker, *Phys. Rep.* **336**, 1 (2000).

[34] A. Shelankov and J. Rammer, *Europhys. Lett.* **63**, 485, (2003).

[35] J. Rammer, A.L. Shelankov, and J. Wabnig, *Phys. Rev. B* **70**, 115327 (2004).

[36] G.B. Lesovik, *JETP Lett.* **49**, 592 (1989).

[37] M. Büttiker, *Phys. Rev. B* **65**, 2901 (1990).

[38] S. Oberholzer, E.V. Sukhorukov, C. Strunk, C. Schönenberger, T. Heinzel, and M. Holland, *Phys. Rev. Lett.* **86**, 2114 (2001).

[39] R.A. Jalabert, J.-L. Pichard, and C.W.J. Beenakker, *Europhys. Lett.* **27**, 255 (1994).

[40] A.F. Ioffe and A.R. Regel, *Prog. Semicond.* **4**, 237 (1970).

[41] N.F. Mott, *Metal Insulator Transitions*, Taylor and Francis, London (1974).

[42] H. van Houten, B.J. van Wees, M.G.J. Heijman, and J.P. André *Appl. Phys. Lett.* **49**, 1782 (1986).

[43] P.W. Anderson, E. Abrahams, and T.V. Ramakrishnan, *Phys. Rev. Lett.* **43**, 718 (1979).

[44] L.P. Go'rkov, A.I. Larkin, and D.E. Khmel'nitskii, *Pis'ma Zh. Eksp. Teor. Fiz.* **30**, 249, (1979).

[45] G. Bergmann, *Phys. Rev. B* **28**, 2914 (1983).

[46] S. Chakravarty and A. Schmid, *Phys. Rep.* **140**, 193 (1986).

[47] A.M. Chang, H.U. Baranger, L.N. Pfeiffer, and K.W. West, *Phys. Rev. Lett.* **76**, 1695 (1996).

[48] C.W.J. Beenakker, *Rev. Mod. Phys.* **69**, 731 (1997).

[49] H.U. Baranger and P.A. Mello, *Phys. Rev. Lett.* **73**, 142 (1994).

[50] M.L. Polianski and P.W. Brouwer, *J. Phys. A: Math. Gen.* **36**, 3215 (2003).

[51] A.G. Huibers, M. Switkes, C.M. Marcus, K. Campman, and A.C. Gossard, *Phys. Rev. Lett.* **81**, 200 (1998).

[52] A.G. Huibers, J.A. Folk, S.R. Patel, C.M. Marcus, C.I. Duruöz, and J.S. Harris, Jr., *Phys. Rev. Lett.* **83**, 5090 (1999).

[53] A. Vidan, R.M. Westervelt, M. Stopa, M. Hanson, and A.C. Gossard, *Appl. Phys. Lett.* **85**, 3602 (2004).

[54] S. Gustavsson, R. Leturcq, B. Simovic, R. Schleser, T. Ihn, P. Studerus, K. Ensslin, D.C. Driscoll, and A.C. Gossard, *Phys. Rev. Lett.* **96**, 076605 (2006).

[55] M. Field, C.G. Smith, M. Pepper, D.A. Ritchie, J.E.F. Frost, G.A.C. Jones, and D.G. Hasko, *Phys. Rev. Lett.* **70**, 1311 (1993).

[56] R. Fiederling, M. Keim, G. Reuscher, W. Ossau, G. Schmidt, A. Waag, and L.W. Molenkamp, *Nature* **402**, 787 (1999).

[57] R. Vrijen and E. Yablonovitch, *Physica E* **10**, 569 (2001).

[58] H.Bi Sun and G.J. Milburn, *Phys. Rev. B* **59**, 10748 (1999).

Chapter 2

Stub model for dephasing in a quantum dot

2.1 Introduction

The dephasing lead model was introduced by Büttiker in 1986 as a phenomeno-logical description of the loss of coherence in quantum electron transport [1]. A microscopic theory of dephasing by electron-electron interactions exists in disor-dered systems [2, 3], but not in (open) chaotic systems. For that reason, exper-iments on conduction through a chaotic quantum dot are routinely modeled by Büttiker's device — with considerable success [4–7].

An alternative phenomenogical approach, introduced by Vavilov and Aleiner in 1999, is to introduce dephasing by means of a fluctuating time-dependent elec-tric field [8]. This approach was reformulated as the dephasing stub model by Polianski and Brouwer [9]. The two models, dephasing lead and dephasing stub, are illustrated in Fig. 2.1. Polianski and Brouwer showed that the weak localiza-tion correction to the conductance is suppressed in the same way by dephasing in the two models.

The key difference between the dephasing lead and the dephasing stub is that the former system is open while the latter system is closed. Because the quantum dot is connected to an electron reservoir by the dephasing lead, only *expectation values* of the current can be forced to vanish at low frequencies; the outcome of an individual measurement is not so constrained. The quantum dot with the dephasing stub remains a closed system with a vanishing low-frequency current at each and every measurement. The difference is irrelevant for the time-averaged current (and therefore for the conductance), but not for the time-dependent current

37
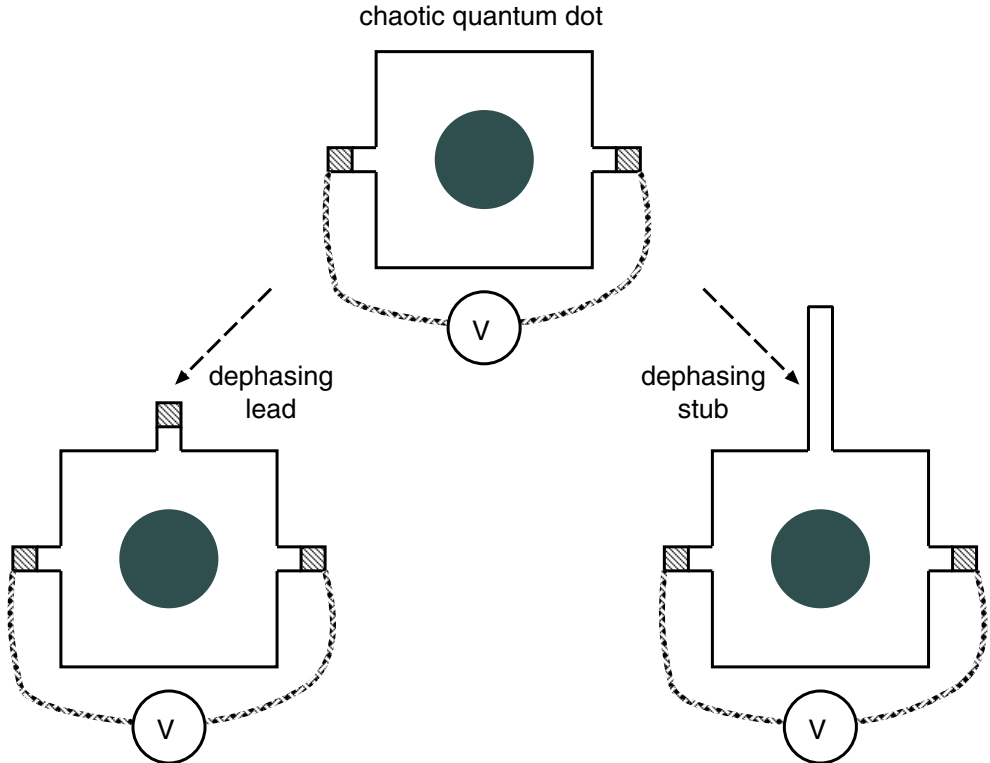
Figure 2.1: Illustration of two phenomenological ways to model dephasing in a quantum dot. The top panel shows the fully phase coherent system, while the two lower panels introduce dephasing either by means of a dephasing lead (left), or by means of a dephasing stub (right). The shaded rectangles indicate electron reservoirs and the encircled V indicates a voltage source. The voltage on the electron reservoir connected to the dephasing lead is adjusted such that it draws no current when averaged over many measurements. The dephasing stub, in contrast, draws no current at each measurement.

fluctuations. Indeed, recent studies of shot noise find differences between the two models of dephasing [6, 10, 11].

In the context of quantum information processing, the dephasing stub model seems a more natural starting point than the dephasing lead model. This is because quantum algorithms are based on the outcome of individual measurements rather than on expectation values, so the model for dephasing should conserve the particle number at each measurement — rather than only on average.

The existing dephasing stub model, however, has an undesired feature that prevents its use as a phenomenological model for dephasing. Ref. [9] considers a *short* dephasing stub, in which the mean dwell time of an electron is negligibly small compared to the mean dwell time in the quantum dot. The voltage fluctuations in a short stub drive the quantum dot out of equilibrium, as is manifested by a nonzero noise power at zero temperature and zero applied voltage [9, 13]. We need to avoid this, since true dephasing should have no effect in equilibrium. The original dephasing lead model had this property, that it preserved equilibrium. In this chapter we will remove this undesired feature of the dephasing stub model, by demonstrating that a *long* dephasing stub can be an effective dephaser without driving the quantum dot appreciably out of equilibrium. It therefore combines the two attractive features of the existing models for dephasing: (1) Current conservation for individual measurements and (2) preservation of equilibrium.

2.2 Formulation of the problem

The characteristic properties of quantum dot and stub are their level spacings $\delta_{\text{dot}}, \delta_{\text{stub}}$ and the contact conductances $g_{\text{dot}}, g_{\text{stub}}$ (in units of the conductance quantum e^2/h, ignoring spin). We assume that the dot is coupled to electron reservoirs by ballistic point contacts, with $g_{\text{dot}} = N_{\text{dot}}$ the total number of channels in these point contacts. The coupling between dot and stub is via a tunnel barrier with conductance $g_{\text{stub}} = N_{\text{stub}}\Gamma$ (where N_{stub} is the number of channels and Γ is the transmission probability per channel). The limit $N_{\text{stub}} \to \infty$, $\Gamma \to 0$ at fixed g_{stub} ensures spatial uniformity of the dephasing [26].

We assume that the dynamics in the quantum dot and in the stub is chaotic. We define the Heisenberg times $\tau_{\text{H,dot}} = h/\delta_{\text{dot}}$, $\tau_{\text{H,stub}} = h/\delta_{\text{stub}}$ and the dwell times $\tau_{\text{D,dot}} = \tau_{\text{H,dot}}/g_{\text{dot}}$, $\tau_{\text{D,stub}} = \tau_{\text{H,stub}}/g_{\text{stub}}$. The dwell time $\tau_{\text{D,dot}}$ refers to the original quantum dot, before it was coupled to the stub.

In the short-stub model of Polianski and Brouwer [9] the scattering by the stub is time dependent but instantaneous, described by an $N_{\text{stub}} \times N_{\text{stub}}$ scattering matrix $R(t)$ that depends on a single time argument only. We wish to introduce

a delay time in the stub, so we need a scattering matrix $R(t',t)$ that depends on an initial time t and a final time t'. The difference $t' - t > 0$ is the time delay introduced by the stub. The reflection by the tunnel barrier is incorporated in R, so that it also contains an instantaneous contribution $\delta(t - t')(1 - \Gamma)$ times the unit matrix.

The voltage fluctuations are introduced by a spatially random potential $V_{\text{stub}}(\mathbf{r}, t)$ of the stub, with Gaussian statistics characterized by a mean $v(t)$ and standard deviation $\sigma(t)$. Averages $\langle \cdots \rangle$ over sample-to-sample fluctuations are taken using the methods of random-matrix theory [22], in the metallic regime $g_{\text{stub}} \gg 1$, $g_{\text{dot}} \gg 1$.

2.3   Diffuson and cooperon

Quantum corrections to transport properties in the metallic regime are described by two propagators, the diffuson and the cooperon, each of which is determined by an integral equation (the Dyson equation). In disordered systems, the Dyson equation results from an average over random impurity configurations [16]. In the ensemble of chaotic quantum dots, it results from an average over the circular ensemble of scattering matrices [9].

The Dyson equation for the diffuson D has the form

$$\tau_{\text{D,dot}} D(t, t - \tau; s, s - \tau) = \theta(\tau) e^{-\tau/\tau_0} + \theta(\tau) \int_0^\tau d\tau_1 \, D(t, t - \tau_1; s, s - \tau_1)$$

$$\times \int_0^{\tau - \tau_1} d\tau_2 \, e^{-(\tau - \tau_1 - \tau_2)/\tau_0} N_{\text{stub}} D_{\text{stub}}(t - \tau_1, t - \tau_1 - \tau_2; s - \tau_1, s - \tau_1 - \tau_2),$$

$$(2.1)$$

where the kernel D_{stub} is the diffuson of the stub,

$$\langle \text{tr} \, R(t, t - \tau) R^\dagger(s, s - \tau') \rangle = \delta(\tau - \tau') N_{\text{stub}} D_{\text{stub}}(t, t - \tau; s, s - \tau), \qquad (2.2)$$

and we have defined $\tau_0 = \tau_{\text{H,dot}}/(N_{\text{dot}} + N_{\text{stub}})$. Eq. (2.1) reduces to the Dyson equation of Ref. [9] if the time delay in the stub is disregarded ($\tau_2 \to 0$).

In the presence of time-reversal symmetry we also need to consider the cooperon, determined by the Dyson equation

$$\tau_{\text{D,dot}} C(t, t - \tau; s + \tau, s) = \theta(\tau) e^{-\tau/\tau_0} + \theta(\tau) \int_0^\tau d\tau_1 \, C(t, t - \tau_1; s + \tau_1, s)$$

$$\times \int_0^{\tau - \tau_1} d\tau_2 \, e^{-(\tau - \tau_1 - \tau_2)/\tau_0} N_{\text{stub}} C_{\text{stub}}(t - \tau_1, t - \tau_1 - \tau_2; s + \tau_1 + \tau_2, s + \tau_1), (2.3)$$

where the cooperon of the stub is defined by

$$\langle \operatorname{tr} R(t,t-\tau)R^*(s+\tau',s)\rangle = \delta(\tau-\tau')N_{\text{stub}}C_{\text{stub}}(t,t-\tau;s+\tau,s). \qquad (2.4)$$

2.3.1 Without voltage fluctuations

Let us first consider the case of a stub without voltage fluctuations. Then only the time difference τ plays a role, and not the actual times t,s. We abbreviate $D(t,t-\tau;s,s-\tau) \equiv D(\tau)$. The cooperon need not be calculated separately, because $C(t,t-\tau;s+\tau,s) = D(\tau)$.

The diffuson of the stub is

$$D_{\text{stub}}(\tau) \;=\; (1-\Gamma)\delta(\tau)+\Gamma\tau_{\text{D,stub}}^{-1}\theta(\tau)e^{-\tau/\tau_{\text{D,stub}}}. \qquad (2.5)$$

Substitution in the Dyson equation (2.1) gives

$$\tau_{\text{D,dot}}D(\tau) \;=\; \theta(\tau)e^{-\tau/\tau_0}+\theta(\tau)\int_0^\tau d\tau'\,D(\tau')\Big[ae^{-(\tau-\tau')/\tau_0}+be^{-(\tau-\tau')/\tau_{\text{D,stub}}}\Big],$$

$$a = N_{\text{stub}}+\frac{N_{\text{stub}}\Gamma\tau_{\text{D,stub}}}{\tau_0-\tau_{\text{D,stub}}},\;\; b=\frac{N_{\text{stub}}\Gamma\tau_0}{\tau_{\text{D,stub}}-\tau_0}. \qquad (2.6)$$

This integral equation can be solved by Fourier transformation, or alternatively, by substituting the Ansatz $D(\tau)=\theta(\tau)(\alpha e^{-x\tau}+\beta e^{-y\tau})$ and solving for the coefficients α,β,x,y. The result is

$$\tau_{\text{D,dot}}D(\tau) \;=\; \theta(\tau)\frac{x_+ -1/\tau_{\text{D,stub}}}{x_+-x_-}e^{-x_+\tau}+\theta(\tau)\frac{x_- -1/\tau_{\text{D,stub}}}{x_- -x_+}e^{-x_-\tau}, \quad (2.7)$$

$$x_\pm \;=\; \frac{1}{2}\left(\frac{1}{\tau_{\text{D,stub}}}+\frac{1}{\tau_{\text{D,dot}}}+\frac{1}{\tau_\phi}\right)$$

$$\pm\frac{1}{2}\sqrt{\left(\frac{1}{\tau_{\text{D,stub}}}-\frac{1}{\tau_{\text{D,dot}}}-\frac{1}{\tau_\phi}\right)^2+\frac{4}{\tau_\phi\tau_{\text{D,stub}}}}. \qquad (2.8)$$

The time $\tau_\phi=\tau_{\text{H,dot}}/N_{\text{stub}}\Gamma$ corresponds to the dephasing time in the dephasing lead model. One can verify that the solution (2.7) satisfies the unitarity relation

$$\int_0^\infty D(\tau)\,d\tau = 1. \qquad (2.9)$$

Note that the two parameters N_{stub} and Γ always appear together as $N_{\text{stub}}\Gamma$. This is a simplying feature of the metallic regime $g_{\text{stub}} = N_{\text{stub}}\Gamma \gg 1$. Since in this regime the tunnel barrier in the stub only serves to renormalize the number of channels, we might as well have assumed a ballistic coupling of the quantum dot to the stub. To simplify the formulas, we will take $\Gamma = 1$ in what follows.

2.3.2   With voltage fluctuations

In the presence of a time dependent potential, the diffuson and cooperon of the stub are given by

$$D_{\text{stub}}(t, t-\tau; s, s-\tau) =$$

$$\tau_{\text{D,stub}}^{-1}\theta(\tau)e^{-\tau/\tau_{\text{D,stub}}} \exp\left(-i \int_{t-\tau}^{t} d\tau' \left[v(\tau') - v(s-t+\tau')\right]\right)$$

$$\times \exp\left(-2\tau_{\text{H,stub}} \int_{t-\tau}^{t} d\tau' \left[\sigma(\tau') - \sigma(s-t+\tau')\right]^2\right)$$

$$= C_{\text{stub}}(t, t-\tau; s, s-\tau). \tag{2.10}$$

(We have set $\hbar = 1$.)

To simplify the solution of the Dyson equation, we assume that the spatial average $v(t)$ of the potential $V_{\text{stub}}(\mathbf{r}, t)$ in the stub vanishes and that the standard deviation $\sigma(t)$ has Gaussian fluctuations in time with moments

$$\langle\sigma(t)\rangle = 0, \quad \langle\sigma(t)\sigma(t')\rangle = \frac{\gamma\tau_c}{4\tau_{\text{H,stub}}}\delta_{\tau_c}(t-t'). \tag{2.11}$$

The time τ_c is the correlation time of the fluctuating potential [setting the width of the regularized delta function $\delta_{\tau_c}(t)$] and the rate γ is a measure of its strength. The average of D_{stub} over the Gaussian white noise is

$$\langle D_{\text{stub}}(t, t-\tau; s, s-\tau)\rangle = \theta(\tau)\tau_{\text{D,stub}}^{-1} \exp\left[-\tau Q(s-t)\right], \tag{2.12}$$

$$Q(s-t) = \begin{cases} 1/\tau_{\text{D,stub}} + \gamma & \text{if } |s-t| \gg \tau_c, \\ 1/\tau_{\text{D,stub}} & \text{if } |s-t| \ll \tau_c. \end{cases} \tag{2.13}$$

For $\tau_{\text{D,stub}} \gg \tau_c$ the voltage fluctuations in the stub are self-averaging, which means that we may substitute the kernel D_{stub} in the Dyson equation (2.1) by its average $\langle D_{\text{stub}}\rangle$. The solution has the same form as the result (2.7) without voltage fluctuations, but with different coefficients:

$$\tau_{\text{D,dot}} D(t, t-\tau, s, s-\tau) = \theta(\tau)\frac{y_+ - Q(s-t)}{y_+ - y_-}e^{-y_+\tau} + \theta(\tau)\frac{y_- - Q(s-t)}{y_- - y_+}e^{-y_-\tau}, \tag{2.14}$$

$$y_\pm = \frac{1}{2}\left(Q(s-t) + \frac{1}{\tau_{\text{D,dot}}} + \frac{1}{\tau_\phi}\right) \pm \frac{1}{2}\sqrt{\left(Q(s-t) - \frac{1}{\tau_{\text{D,dot}}} - \frac{1}{\tau_\phi}\right)^2 + \frac{4}{\tau_\phi\tau_{\text{D,stub}}}}. \tag{2.15}$$

The cooperon is again given by the same expression, $C(t, t-\tau; s, s-\tau) = D(t, t-\tau; s, s-\tau)$.

2.4 Transport properties

A current is passed through the quantum dot by connecting $N_{\text{dot}}/2$ channels to one electron reservoir and $N_{\text{dot}}/2$ channels to another reservoir at a higher electrical potential V_{bias}. We calculate the conductance and the shot noise power of the quantum dot.

2.4.1 Weak localization

The weak localization correction δG to the classical conductance $G_0 = N_{\text{dot}}/2$ of the quantum dot is given by the time integral of the cooperon [9],

$$\delta G = -\frac{1}{4} \int_0^\infty d\tau\, C(0, -\tau; \tau, 0). \tag{2.16}$$

As before, the conductance is measured in units of the conductance quantum e^2/h (ignoring spin).

The function $C(0, -\tau; \tau, 0)$ is given by Eq. (2.14) with $Q(s-t) \to Q(\tau)$. For $\tau_{\text{D,stub}} \gg \tau_c$ we may substitute $Q = 1/\tau_{\text{D,stub}} + \gamma$, cf. Eq. (3.81). Carrying out the integration we obtain the expected algebraic suppression of the weak localization correction due to dephasing [9],

$$\delta G = -\tfrac{1}{4}(1 + \tau_{\text{D,dot}}/\tau^*)^{-1}, \quad \tau^* = \tau_\phi(1 + 1/\gamma\,\tau_{\text{D,stub}}). \tag{2.17}$$

For $\gamma\,\tau_{\text{D,stub}} \gg 1$ (strong dephasing in the stub) the dephasing time τ^* of the dephasing stub model becomes the same as the dephasing time τ_ϕ of the dephasing lead model [17, 18, 26].

2.4.2 Shot noise

In the absence of a fluctuating potential, the zero-temperature noise power is given by the shot noise formula [36]

$$S_{\text{shot}} = \tfrac{1}{4} e V_{\text{bias}} G_0. \tag{2.18}$$

The fluctuating potential drives the quantum dot out of equilibrium, adding a contribution ΔS to the total noise power $S = S_{\text{shot}} + \Delta S$. We would like to minimize this classical contribution, since it is unrelated to dephasing.

The general expression for ΔS contains a product of two diffusons [9],

$$\Delta S = \frac{N_{\text{dot}} e^2}{2} \int_0^\infty dt\, [1 - K(t)^2] \frac{1 - \sin^2(e V_{\text{bias}} t/2\hbar)}{2\pi^2 t^2}, \tag{2.19}$$

$$K(t) = \int_0^\infty d\tau\, D(0, -\tau, t, t-\tau). \tag{2.20}$$

Substitution of Eq. (2.14) gives

$$
\begin{aligned}
K(t) &= \left[1 + \frac{\tau_{\mathrm{D,dot}}}{\tau_\phi}\left(1 - \frac{1}{\tau_{\mathrm{D,stub}}Q(t)}\right)\right]^{-1} \\
&= \begin{cases} 1 & \text{if } t \ll \tau_c, \\ (1 + \tau_{\mathrm{D,dot}}/\tau^*)^{-1} & \text{if } t \gg \tau_c. \end{cases}
\end{aligned}
\tag{2.21}
$$

For strong dephasing ($\tau_{\mathrm{D,dot}}/\tau^* \gg 1$) the noise ΔS from the fluctuating potential saturates at a value of order $\Delta S_{\max} \simeq N_{\mathrm{dot}} e^2/\tau_c$. This is negligibly small relative to S_{shot} for sufficiently large bias voltages $V_{\mathrm{bias}} \gg \hbar/e\tau_c$. These are still small bias voltages on the scale of the Thouless energy $E_T = \hbar/\tau_{\mathrm{D,dot}}$, provided that $\tau_{\mathrm{D,dot}} \ll \tau_c$. Combined with our earlier requirement $\tau_c \ll \tau_{\mathrm{D,stub}}$ of rapid fluctuations, we conclude that the noise generated by the fluctuating potential can be neglected in the regime

$$
\tau_{\mathrm{D,dot}} \ll \hbar/V_{\mathrm{bias}} \ll \tau_c \ll \tau_{\mathrm{D,stub}}.
\tag{2.22}
$$

It is the separation of dwell times $\tau_{\mathrm{D,dot}} \ll \tau_{\mathrm{D,stub}}$, characteristic of the long-stub model, that makes it possible to enter this regime in which the fluctuating potential can be dephasing without being noisy. In contrast, in the short-stub model of Ref. [9] one is in the opposite regime $\tau_{\mathrm{D,stub}} \ll \tau_{\mathrm{D,dot}}$ in which the voltage fluctuations are either too weak to cause dephasing, or so strong that they dominate over the shot noise.

2.5   Conclusion

A fluctuating time-dependent potential in a conductor has both a quantum mechanical effect (destroying phase coherence) and a classical effect (driving the system out of equilibrium). The former effect shows up in the suppression of weak localization, while the latter effect manifests itself in the noise power. Both effects have been studied extensively in the literature [8,9,20,21], and both effects are important if one is describing a conductor in a real microwave field. However, if the voltage fluctuations are to serve as a phenomenological model of dephasing, e.g. by electron-electron interactions, then one needs to retain only the former effect — since shot noise should be insensitive to dephasing [22].

The key question we have addressed in this work, is whether a fluctuating potential can be dephasing without being noisy. We have found that this is indeed possible, provided that the potential fluctuates not in the conductor itself but in a spatially separated and weakly coupled region (the stub). The dephasing stub is a

fictitious device, much like the dephasing lead [1]. We expect that the dephasing stub model will be useful as a phenomenological description of decoherence in problems where one would rather not open up the system to an electron reservoir (as one needs to do in the dephasing lead model).

A recent paper by Sokolov [23] studies a similar geometry, a quantum dot connected to a long lead closed at one end, but in that work there are no voltage fluctuations in the stub. Energy averaging can still suppress certain quantum interference effects (such as the universal conductance fluctuations), but not others (such as weak localization).

Bibliography

[1] M. Büttiker, Phys. Rev. B **33**, 3020 (1986).

[2] B. L. Altshuler and A. G. Aronov, in *Electron-Electron Interactions in Disordered Systems*, edited by A. L. Efros and M. Pollak (North-Holland, Amsterdam, 1985).

[3] I. L. Aleiner, B. L. Altshuler, and M. E. Gershenson, Waves in Random Media **9**, 201 (1999).

[4] C. M. Marcus, A. J. Rimberg, R. M. Westervelt, P. F. Hopkins, and A. C. Gossard, Phys. Rev. Lett. **69**, 506 (1992).

[5] R. M. Clarke, I. H. Chan, C. M. Marcus, C. I. Duruöz, J. S. Harris, Jr., K. Campman, and A. C. Gossard, Phys. Rev. B **52**, 2656 (1995).

[6] A. G. Huibers, M. Switkes, C. M. Marcus, K. Campman, and A. C. Gossard, Phys. Rev. Lett. **81**, 200 (1998).

[7] A. G. Huibers, J. A. Folk, S. R. Patel, C. M. Marcus, C. I. Duruöz, and J. S. Harris, Jr., Phys. Rev. Lett. **83**, 5090 (1999).

[8] M. G. Vavilov and I. L. Aleiner, Phys. Rev. B **60**, 16311 (1999).

[9] M. L. Polianski and P. W. Brouwer, J. Phys. A **36**, 3215 (2003).

[10] F. Marquardt and C. Bruder, Phys. Rev. B **70**, 125305 (2004).

[11] F. Marquardt, cond-mat/0410333.

[12] A. A. Clerk and A. D. Stone, Phys. Rev. B **69**, 245303 (2004).

[13] M. L. Polianski, M. G. Vavilov, and P. W. Brouwer, Phys. Rev. B **65**, 245314 (2002).

[14] P. W. Brouwer and C. W. J. Beenakker, Phys. Rev. B **55**, 4695 (1997); **66**, 209901(E) (2002).

[15] C. W. J. Beenakker, Rev. Mod. Phys. **69**, 731 (1997).

[16] P. A. Lee and T. V. Ramakrishnan, Rev. Mod. Phys. **57**, 287 (1985).

[17] H. U. Baranger and P. A. Mello, Phys. Rev. B **51**, 4703 (1995).

[18] I. L. Aleiner and A. I. Larkin, Phys. Rev. B **54**, 14423 (1996).

[19] R. A. Jalabert, J.-L. Pichard, and C. W. J. Beenakker, Europhys. Lett. **27**, 255 (1994).

[20] G. Seelig, S. Pilgram, and M. Büttiker, Turk. J. Phys. **27**, 331 (2003).

[21] H. Forster, S. Pilgram, and M. Büttiker, cond-mat/0502400.

[22] M. J. M. de Jong and C. W. J. Beenakker, Physica A **230**, 219 (1996).

[23] V. V. Sokolov, cond-mat/0409690.

Chapter 3

Voltage probe model of spin decay in a chaotic quantum dot, with applications to spin-flip noise and entanglement production

3.1 Introduction

The voltage probe model, introduced by Büttiker in the early days of mesoscopic physics, [1] gives a phenomenological description of the loss of phase coherence in quantum transport. Electrons that enter the voltage probe are reinjected into the conductor with a random phase, so they can no longer contribute to quantum interference effects. Such a device is no substitute for a microscopic treatment of specific mechanisms of decoherence, but it serves a purpose in identifying model independent "universal" features of the transition from coherent to incoherent electrical conduction.

In this work we introduce and analyze a novel application of the voltage probe model, to spin-resolved conduction through a quantum dot. The voltage probe then serves a dual role: It randomizes the phase, as in the original spin-independent model, [1] but it also randomizes the spin. Two spin transport effects are examined: spin-flip noise and spin entanglement. The two effects are fundamentally connected, in the sense that the degree to which spin-up and spin-down current fluctuations are correlated provides a measure of the degree of spin entanglement of electron-hole pairs exiting the quantum dot. [2]
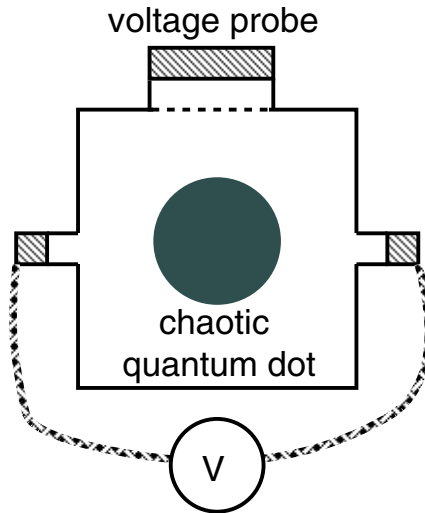
Figure 3.1: Illustration of the voltage probe model. A chaotic quantum dot is connected to a voltage source by two single-channel leads. Decoherence is introduced by means of a fictitious voltage probe, which conserves particle number within each energy range $\delta E \ll eV$, on time scales $\delta t = h/\delta E$. (The dashed line in the figure indicates the tunnel barrier that separates the voltage probe from the quantum dot.) The random spin flips introduced by the voltage probe give a nonzero correlator of spin-up and spin-down currents (= spin-flip noise). The voltage probe also reduces the entanglement production by transforming the pure spin-singlet state of electron-hole pairs into a mixed Werner state.

The geometry is sketched in Fig. 3.1. The coupling of the electron spin to other degrees of freedom (nuclear spins, magnetic impurities, other electrons ...) is replaced by an artificial reservoir connected to the quantum dot via a tunnel barrier. The reservoir draws neither particles nor energy from the quantum dot. [3] Both the time averaged current and the time dependent fluctuations vanish, enforced by a fluctuating distribution function of the artificial reservoir. [4,5] This phenomenological description of decoherence has found many applications in the context of (spin-independent) shot noise. (Recent references include [6–9].) For alternative models of decoherence in that context, see Refs. [6, 10–13].

In the context of spin-resolved conduction, the voltage probe introduces two altogether different decay processes: spin flip and decoherence. These are characterized in general by two independent decay times (denoted T_1 and $T_2 \le 2T_1$, respectively). In order to obtain two different time scales we could introduce, in addition to the spin-isotropic voltage probe, a pair of ferromagnetic voltage probes that randomize the phase without flipping the spin (pure dephasing). Here we will restrict ourselves to the simplest model of a single voltage probe, corresponding to the limit $T_2 = 2T_1$. This choice is motivated by the desire to have as few free parameters as possible in this exploratory study. The more general model will be needed to make contact with the existing microscopic theory for the spin decay times. [14–17]

The applications of the voltage probe model that we consider center around the concept of electron-hole entanglement. A voltage V applied over a single-channel conductor produces spin-entangled electron-hole pairs. [18] The entanglement production rate is maximally $eV/2h$ bits/second, for phase-coherent spin-independent scattering. Thermal fluctuations in the electron reservoirs [19] as well as dephasing voltage fluctuations in the electromagnetic environment [20,21] reduce the degree of entanglement of the electron-hole pairs. Unlike other quantum interference effects, which decay smoothly to zero, the entanglement production rate vanishes identically beyond a critical temperature or beyond a critical decoherence rate.

One goal of this investigation is to determine the probability distribution of the critical decoherence rate in an ensemble of quantum dots with chaotic scattering. The fluctuations in the artificial reservoir reduce the entanglement production by transforming the pure state of the electron-hole pair into a mixed state. For decoherence rates $\gamma \ge \gamma_c$ the density matrix of the electron-hole pairs becomes separable. The value of γ_c is sample specific, with a probability distribution $P(\gamma_c)$ that we calculate using the methods of random-matrix theory. [22]

The entanglement production is related to physical observables via the spin-

resolved shot noise. The correlator of spin-up and spin-down currents (spin-flip noise) is of particular interest, since it provides a direct measure of the spin relaxation time. [23] By assuming that the elastic scattering in the quantum dot is spin-independent (no spin-orbit interaction), we derive a one-to-one relation between the degree of entanglement (concurrence) of the electron-hole pairs and the spin-resolved shot noise. In the more general spin-dependent case such a relation exists for pure states, [24, 25] through a Bell inequality, but not for mixed states. [19] The expressions for the concurrence $\mathcal{C}$ take a particularly simple form in the tunneling regime, where we find that $\mathcal{C}$ is nonzero if and only if the correlator of spin current fluctuations is *at least twice larger for parallel spins than it is for antiparallel spins*.

We derive closed-form expressions for the ensemble averaged correlators in the regime of weak decoherence, both in the presence ($\beta = 1$) and absence ($\beta = 2$) of time-reversal symmetry. While the average spin-resolved current correlators are analytic in the decoherence rate γ around $\gamma = 0$, the average concurrence $\langle \mathcal{C} \rangle$ has a singularity at that point: a square-root singularity $1 - \langle \mathcal{C} \rangle \propto \sqrt{\gamma}$ for $\beta = 1$, and a logarithmic singularity $1 - \langle \mathcal{C} \rangle \propto \gamma |\ln \gamma|$ for $\beta = 2$. The singular effect of a small decoherence rate on the entanglement production also shows up in the probability distribution $P(\gamma_c)$ of the critical decoherence rate: It does not vanish for $\gamma_c \to 0$, but instead has a large weight $\propto \gamma_c^{-1+\beta/2}$.

The outline of this chapter is as follows. We start in Sec. 3.2 with a description of the system (quantum dot with voltage probe) and a formulation of the twofold question that we would like to answer (what is the entanglement production and how is it related to spin noise). A solution in general terms is presented in Sec. 3.3. We begin in Sec. 3.3.1 by simplifying the problem through the assumption of spin-independent scattering in the quantum dot. The concurrence of the electron-hole pairs is then given as a rational function of spin-resolved current correlators (Sec. 3.3.2). These correlators are expressed in terms of the scattering matrix elements of the quantum dot with voltage probe (Sec. 3.3.3). To evaluate these expressions an alternative formulation, in terms of a quantum dot without voltage probe but with an imaginary potential, is more convenient (Sec. 3.3.4). The connection to random-matrix theory is made in Sec. 3.4. By averaging over the random scattering matrices we obtain the nonanalytic γ-dependencies mentioned above (Secs. 3.5 and 3.6). We conclude in Sec. 3.7.

3.2 Formulation of the problem

We consider a quantum dot coupled to source and drain by single-channel point contacts. The voltage probe has N_ϕ channels, and is connected to the quantum dot by a barrier with a channel-independent tunnel probability Γ_ϕ. By taking the limit $\Gamma_\phi \to 0$, $N_\phi \to \infty$ at fixed (dimensionless) conductance $\gamma \equiv N_\phi \Gamma_\phi$, we model spatially homogeneous decoherence with coherence time [26]

$$\tau_{\text{coherence}} = \lim_{\Gamma_\phi \to 0} \lim_{N_\phi \to \infty} \frac{h}{\gamma \Delta}. \tag{3.1}$$

(We denote by Δ the mean spacing of spin-degenerate levels.) Since the mean dwell time in the quantum dot (without voltage probe) is $\tau_{\text{dwell}} = h/2\Delta$, one has

$$\gamma = 2\tau_{\text{dwell}}/\tau_{\text{coherence}}. \tag{3.2}$$

The scattering matrix S of the whole system has dimension $(N_\phi + 2) \times (N_\phi + 2)$. By convention the index $n = 1$ labels the source, the index $n = 2$ labels the drain, and the indices $3 \le n \le N_\phi + 2$ label the channels in the voltage probe. All of this refers to a single spin degree of freedom. Each channel is spin degenerate. As mentioned above, we assume that the scattering is spin independent. In particular, both the Zeeman energy and the spin-orbit coupling energy should be sufficiently small that spin rotation symmetry is not broken. The applied voltage V between source and drain is assumed to be large compared to the temperature, but sufficiently small that the energy dependence of the scattering can be neglected.

The energy range eV above the Fermi level is divided into small intervals $\delta E \ll eV$. The voltage probe conserves particle number and energy within each energy interval, on time scales $\delta t = h/\delta E$. We write this requirement as $I_\phi(E,t) = 0$, where $I_\phi(E,t)$ is the electrical current through the voltage probe in the energy interval $(E, E + \delta E)$, averaged over the time interval $(t, t + \delta t)$.

Because the voltage probe does not couple different energy intervals, we may consider the entanglement production in each interval separately and sum over the intervals at the end of the calculation. In what follows we will refer to a single energy interval (without writing the energy argument explicitly).

The density matrix ρ of the outgoing state in each energy interval, traced over the degrees of freedom of the voltage probe, contains combinations of 0, 1, or 2 excitations in the spin degenerate channel of the source lead and the drain lead. Only the projection ρ_{eh} onto a singly excited channel in the source as well as in the drain contributes to the entanglement production. [19] We denote by $w = \text{Tr}\,\mathscr{P}\rho$

the weight of the projection, with $\mathcal{P}$ the operator that projects onto singly excited channels (so that $w\rho_{eh} = \mathcal{P}\rho\mathcal{P}^\dagger$). The label "eh" stands for "electron-hole pair", where "electron" refers to the single excited channel in the drain and "hole" refers to the single nonexcited channel in the source.

In the absence of decoherence ρ_{eh} is pure ($\rho_{eh}^2 = \rho_{eh}$). The voltage probe transforms ρ_{eh} into a mixed state. Our aim is to calculate the loss of entanglement of ρ_{eh} as a function of γ and to relate it to the spin-resolved current correlators.

3.3 General solution

3.3.1 Simplification for spin-isotropic states

The assumption of spin-independent scattering implies that the 4×4 density matrix ρ_{eh} is invariant under the transformation $(U \otimes U)\rho_{eh}(U^\dagger \otimes U^\dagger) = \rho_{eh}$, for any 2×2 unitary matrix U. As a consequence, ρ_{eh} must be of the Werner form, [27]

$$\rho_{eh} = \tfrac{1}{4}(1-\xi)\mathbb{1} + \xi|\Psi_{Bell}\rangle\langle\Psi_{Bell}|, \quad -\tfrac{1}{3} \leq \xi \leq 1, \tag{3.3}$$

with $\mathbb{1}$ the unit matrix and

$$|\Psi_{Bell}\rangle = 2^{-1/2}\big(|\uparrow\downarrow\rangle - |\downarrow\uparrow\rangle\big) \tag{3.4}$$

the Bell state. [28] (The spin-up and spin-down arrows $\uparrow, \downarrow$ label the two eigenstates of the Pauli matrix σ_z.)

The concurrence [9] (degree of entanglement) of the Werner state is given by

$$\mathcal{C} = \frac{3}{2}\max\left\{0, \xi - \frac{1}{3}\right\}. \tag{3.5}$$

The Werner state is separable for $\xi \leq 1/3$. The entanglement production rate (bits per second) in the energy range δE under consideration is given by [19]

$$\mathcal{E} = \frac{\delta E}{h}w\mathcal{F}\left(\tfrac{1}{2} + \tfrac{1}{2}\sqrt{1-\mathcal{C}^2}\right), \tag{3.6}$$

$$\mathcal{F}(x) = -x\log_2 x - (1-x)\log_2(1-x). \tag{3.7}$$

The parameter ξ that defines the Werner state (3.3) can be obtained from the spin-spin correlator

$$\mathrm{Tr}\,\rho_{eh}\sigma_z \otimes \sigma_z = -\xi. \tag{3.8}$$

In order to make contact with the voltage probe model we now relate this correlator to a spin-resolved current correlator, along the lines of Refs. [2, 24, 25].

3.3.2 Solution in terms of current correlators

We define $N_{X,\alpha}^{\text{out}}(t)$ as the number of electrons going out of the quantum dot in a time interval $(t, t + \delta t)$ through the source lead ($X = S$) or through the drain lead ($X = D$) with spin up ($\alpha = \uparrow$) or with spin down ($\alpha = \downarrow$). In terms of the current $I_{X,\alpha}(t)$ one has $N_{D,\alpha}^{\text{out}}(t) = -I_{D,\alpha}(t)\delta t/e$, $N_{S,\alpha}^{\text{out}}(t) = 1 - I_{S,\alpha}(t)\delta t/e$, with the convention that the current is positive if electrons enter the quantum dot. The spin-spin correlator (3.8) is expressed by

$$
\begin{aligned}
\xi &= -\frac{\langle [N_{S,\uparrow}^{\text{out}}(t) - N_{S,\downarrow}^{\text{out}}(t)][N_{D,\uparrow}^{\text{out}}(t) - N_{D,\downarrow}^{\text{out}}(t)]\rangle}{\langle [N_{S,\uparrow}^{\text{out}}(t) + N_{S,\downarrow}^{\text{out}}(t)][N_{D,\uparrow}^{\text{out}}(t) + N_{D,\downarrow}^{\text{out}}(t)]\rangle} \\
&= -(\delta t/e)^2 \frac{1}{w} \langle [I_{S,\uparrow}(t) - I_{S,\downarrow}(t)][I_{D,\uparrow}(t) - I_{D,\downarrow}(t)]\rangle,
\end{aligned}
\tag{3.9}
$$

$$
w = (\delta t/e)^2 \langle [I_{S,\uparrow}(t) + I_{S,\downarrow}(t) - 2e/\delta t][I_{D,\uparrow}(t) + I_{D,\downarrow}(t)]\rangle,
\tag{3.10}
$$

where the brackets $\langle \cdots \rangle$ indicate an average over many measurements.

The time dependent current $I_{X,\alpha}(t) = \bar{I}_{X,\alpha} + \delta I_{X,\alpha}(t)$ has time average $\bar{I}_{X,\alpha}$. The current fluctuations $\delta I_{X,\alpha}(t)$ on the time scale $\delta t = h/\delta E$ have cross correlator $\langle \delta I_{S,\alpha}(t)\delta I_{D,\beta}(t)\rangle = (\delta E/h)P_{\alpha\beta}$, with spectral density [30]

$$
P_{\alpha\beta} = \int_{-\infty}^{\infty} dt \, \langle \delta I_{S,\alpha}(0)\delta I_{D,\beta}(t)\rangle.
\tag{3.11}
$$

The total spectral density of charge noise is given by

$$
P_{\text{charge}} = \sum_{\alpha,\beta} \int_{-\infty}^{\infty} dt \, \langle \delta I_{S,\alpha}(0)\delta I_{S,\beta}(t)\rangle = -\sum_{\alpha,\beta} P_{\alpha\beta}.
\tag{3.12}
$$

(The minus sign appears because $\sum_\beta \delta I_{S,\beta} = -\sum_\beta \delta I_{D,\beta}$, as a consequence of current conservation.)

Substitution into Eqs. (3.9) and (3.10) gives

$$
\begin{aligned}
\xi &= -\frac{h}{e^2\delta E}\frac{1}{w}\Big[(h/\delta E)(\bar{I}_{S,\uparrow} - \bar{I}_{S,\downarrow})(\bar{I}_{D,\uparrow} - \bar{I}_{D,\downarrow}) \\
&\quad + P_{\uparrow\uparrow} + P_{\downarrow\downarrow} - P_{\uparrow\downarrow} - P_{\downarrow\uparrow}\Big],
\end{aligned}
\tag{3.13}
$$

$$
\begin{aligned}
w &= \frac{h}{e^2\delta E}\Big[(h/\delta E)(\bar{I}_{S,\uparrow} + \bar{I}_{S,\downarrow} - 2e\delta E/h)(\bar{I}_{D,\uparrow} + \bar{I}_{D,\downarrow}) \\
&\quad + P_{\uparrow\uparrow} + P_{\downarrow\downarrow} + P_{\uparrow\downarrow} + P_{\downarrow\uparrow}\Big].
\end{aligned}
\tag{3.14}
$$

Because of the spin isotropy, $\bar{I}_{X,\uparrow} = \bar{I}_{X,\downarrow}$, $P_{\uparrow\uparrow} = P_{\downarrow\downarrow}$, and $P_{\uparrow\downarrow} = P_{\downarrow\uparrow}$. We denote by $\bar{I} > 0$ the total time averaged current from source to drain in the energy interval δE. Spin isotropy implies $\bar{I}_{S,\alpha} = \frac{1}{2}\bar{I}$ and $\bar{I}_{D,\alpha} = -\frac{1}{2}\bar{I}$. Eqs. (3.13) and (3.14) then simplify to

$$\xi = \frac{P_{\uparrow\downarrow} - P_{\uparrow\uparrow}}{e\bar{I} - \frac{1}{2}(h/\delta E)\bar{I}^2 - \frac{1}{2}P_{\text{charge}}}, \tag{3.15}$$

$$w = \frac{2h}{e^2\delta E}\left[e\bar{I} - \frac{1}{2}(h/\delta E)\bar{I}^2 - \frac{1}{2}P_{\text{charge}}\right]. \tag{3.16}$$

3.3.3   Solution in terms of scattering matrix elements

So far the analysis is general, not tied to a particular model of decoherence. Now we turn to the voltage probe model to express the average current and the current correlators in terms of the scattering matrix elements and the state of the reservoirs. For a recent exposition of this model we refer to Ref. [7]. The general expressions take the following form in the case of spin-independent scattering considered here:

$$\bar{I} = \frac{2e\delta E}{h}\left(T_{1\rightarrow 2} + \frac{T_{1\rightarrow\phi}T_{\phi\rightarrow 2}}{N_\phi - R_\phi}\right), \tag{3.17}$$

$$P_{\uparrow\downarrow} = \frac{e^2\delta E}{2h}\left(\frac{Q_{\phi\phi}T_{\phi\rightarrow 1}T_{\phi\rightarrow 2}}{(N_\phi - R_\phi)^2} + \frac{Q_{1\phi}T_{\phi\rightarrow 2} + Q_{2\phi}T_{\phi\rightarrow 1}}{N_\phi - R_\phi}\right), \tag{3.18}$$

$$P_{\uparrow\uparrow} = \frac{e^2\delta E}{h}Q_{12} + P_{\uparrow\downarrow}. \tag{3.19}$$

We have defined the transmission and reflection probabilities [1]

$$T_{n\rightarrow m} = |S_{mn}|^2, \quad R_\phi = \sum_{n,m=3}^{N_\phi+2}|S_{nm}|^2, \tag{3.20}$$

$$T_{\phi\rightarrow m} = \sum_{n=3}^{N_\phi+2}|S_{mn}|^2, \quad T_{n\rightarrow\phi} = \sum_{m=3}^{N_\phi+2}|S_{mn}|^2, \tag{3.21}$$

and the correlators of intrinsic current fluctuations [31]

$$Q_{nm} = \sum_{n',m'=1}^{N_\phi+2} \left(\delta_{nn'}\delta_{nm'} - S_{nn'}^* S_{nm'} \right)$$

$$\times \left(\delta_{mm'}\delta_{mn'} - S_{mm'}^* S_{mn'} \right) f_{n'}(1 - f_{m'}), \tag{3.22}$$

$$Q_{n\phi} = \sum_{m=3}^{N_\phi+2} Q_{nm}, \quad Q_{\phi\phi} = \sum_{n,m=3}^{N_\phi+2} Q_{nm}. \tag{3.23}$$

The state incident on the quantum dot from the reservoirs is fully characterized by the mean occupation number f_n, given by

$$f_n = \begin{cases} 1 & \text{if } n = 1, \\ 0 & \text{if } n = 2, \\ \dfrac{T_{1\to\phi}}{N_\phi - R_\phi} & \text{if } 3 \le n \le N_\phi + 2. \end{cases} \tag{3.24}$$

For the source and drain reservoirs this is a state of thermal equilibrium at zero temperature. For the fictitious reservoir this is the nonequilibrium state

$$\rho_\phi = \prod_{n=3}^{N_\phi+2} \left(f_n a_n^\dagger |0\rangle\langle 0| a_n + (1 - f_n)|0\rangle\langle 0| \right), \tag{3.25}$$

with $a_n^\dagger$ the operator that excites the n-th mode in the voltage probe. These are all Gaussian states, meaning that averages of powers of a_n and $a_n^\dagger$ can be constructed out of the second moment $\langle a_n^\dagger a_n \rangle = f_n$ by the rule of Gaussian averages.

3.3.4 Reformulation in terms of imaginary potential model

The model of a quantum dot with voltage probe can be reformulated in terms of a quantum dot without voltage probe but with an imaginary potential. [26] This reformulation simplifies the expressions for the entanglement production, so we will carry it out here.

The unitarity of S makes it possible to eliminate from the expressions in Sec. 3.3.3 all matrix elements that involve the voltage probe. Only the four matrix elements S_{nm}, $n,m \in \{1,2\}$, involving the source and drain remain. This sub-matrix of S forms the sub-unitary matrix

$$s = \begin{pmatrix} S_{11} & S_{12} \\ S_{21} & S_{22} \end{pmatrix} = \begin{pmatrix} r & t' \\ t & r' \end{pmatrix}. \tag{3.26}$$

As derived in Ref. [26], the matrix s corresponds to the scattering matrix of the quantum dot without the voltage probe, but with a spatially uniform imaginary potential $-i\gamma\Delta/4\pi$. The coefficients t,t',r,r' are the transmission and reflection amplitudes of the quantum dot with the imaginary potential.

After performing this elimination, the expressions (3.22–3.23) for the correlators Q_{nm} that we need take the form

$$Q_{12} = -|(1-f_\phi)S_{11}S_{21}^* - f_\phi S_{12}S_{22}^*|^2, \tag{3.27}$$

$$Q_{11} = Q_{22} = \big[f_\phi(1-|S_{12}|^2)+(1-f_\phi)|S_{11}|^2\big]$$
$$\times \big[(1-f_\phi)(1-|S_{11}|^2)+f_\phi|S_{12}|^2\big], \tag{3.28}$$

$$Q_{\phi\phi} = 2(Q_{12}+Q_{11}), \tag{3.29}$$

$$Q_{1\phi} = Q_{2\phi} = -\tfrac{1}{2}Q_{\phi\phi}, \tag{3.30}$$

with mean occupation number

$$f_\phi = \frac{T_{1\to\phi}}{N_\phi - R_\phi} = \frac{1-(s^\dagger s)_{11}}{2-\mathrm{Tr}\,ss^\dagger}. \tag{3.31}$$

We also define the quantity

$$\tilde{f}_\phi = \frac{T_{\phi\to 1}}{N_\phi - R_\phi} = \frac{1-(ss^\dagger)_{11}}{2-\mathrm{Tr}\,ss^\dagger}, \tag{3.32}$$

which equals f_ϕ in the presence of time-reversal symmetry (when $T_{n\to m} = T_{m\to n}$) — but is different in general.

The expressions (3.17–3.19) for the mean current $\bar{I}$ and the correlators $P_{\alpha\beta}$ simplify to

$$\bar{I} = \frac{2e\delta E}{h}\big[f_\phi(1-|S_{22}|^2)+(1-f_\phi)|S_{21}|^2)\big], \tag{3.33}$$

$$P_{\uparrow\downarrow} = P_{\uparrow\uparrow} - \frac{e^2\delta E}{h}Q_{12} = \frac{e^2\delta E}{2h}Q_{\phi\phi}\big[\tilde{f}_\phi(1-\tilde{f}_\phi)-\tfrac{1}{2}\big]. \tag{3.34}$$

Some more algebra shows that

$$e\bar{I} - \tfrac{1}{2}(h/\delta E)\bar{I}^2 = 2(e^2\delta E/h)Q_{11}, \tag{3.35a}$$

$$Q_{\phi\phi} = 2f_\phi(1-f_\phi)(1-\mathrm{Det}\,ss^\dagger). \tag{3.35b}$$

Substitution of Eqs. (3.34) and (3.35) into Eqs. (3.15) and (3.16) finally gives compact expressions for the Werner parameter ξ and the weight w of the electron-hole pair:

$$\xi = \frac{Y}{X+Y}, \tag{3.36}$$

$$w = 2(X+Y), \tag{3.37}$$

$$X = f_\phi(1-f_\phi)[2\tilde{f}_\phi(1-\tilde{f}_\phi)+1](1-\mathrm{Det}\,ss^\dagger), \tag{3.38}$$

$$Y = |rt^* - f_\phi(ss^\dagger)_{12}|^2. \tag{3.39}$$

The spin-resolved current correlators (3.34) are expressed similarly by

$$P_{\uparrow\downarrow} = P_{\uparrow\uparrow} + \frac{e^2\delta E}{h}Y = \frac{e^2\delta E}{h}(\tfrac{1}{2}X - Z), \tag{3.40}$$

$$Z = f_\phi(1-f_\phi)(1-\mathrm{Det}\,ss^\dagger). \tag{3.41}$$

Let us check that we recover the known result [2] for the entanglement production in the absence of decoherence. In that case s is a unitary matrix s_0, so $X, Z \to 0$ and $Y \to |r_0 t_0^*|^2$ — independent of f_ϕ. (The label 0 indicates zero decoherence rate.) Hence $\xi = 1$ (maximally entangled electron-hole pairs) and

$$w_0 = 2g_0(1-g_0), \tag{3.42}$$

with $g_0 = |t_0|^2$ the phase coherent conductance of the quantum dot in units of $2e^2/h$. The total entanglement production rate (integrated over all energies) becomes

$$\mathcal{E}_0 = (eV/h)w_0 = (2eV/h)g_0(1-g_0), \tag{3.43}$$

in agreement with Ref. [2]. Furthermore, we verify that in this case $P_{\uparrow\downarrow} = 0$ (no spin-flip scattering without the voltage probe), while $P_{\uparrow\uparrow} = -(e^2\delta E/h)g_0(1-g_0)$ is given by the shot noise formula for spin-independent scattering. [32, 33]

3.4 Random-matrix theory

3.4.1 Distribution of scattering matrices

The expressions of the previous section refer to a single quantum dot. We now consider an ensemble of quantum dots, generated by small variations in shape or Fermi energy. For chaotic scattering the ensemble of scattering matrices is described by random-matrix theory, characterized by the symmetry index $\beta = 1$

in the presence of time-reversal symmetry and $\beta = 2$ if time-reversal symmetry is broken by a magnetic field. [22] (The magnetic field should be sufficiently weak that the Zeeman energy does not lift the spin degeneracy.) Since we assume that spin-orbit coupling is not strong enough to break the spin rotation symmetry, the case $\beta = 4$ of symplectic symmetry does not appear. [34]

In the absence of decoherence, s is unitary and its distribution is the circular ensemble. With decoherence, s is sub-unitary. Its distribution $P(s)$ was calculated in Ref. [26]. It is given in terms of the polar decomposition

$$s = u \begin{pmatrix} \sqrt{1 - \tau_1} & 0 \\ 0 & \sqrt{1 - \tau_2} \end{pmatrix} u', \tag{3.44}$$

with unitary matrices $u' = u^T$ if $\beta = 1$ and u' independent of u if $\beta = 2$. These matrices are uniformly distributed in the unitary group. The real numbers $\tau_1, \tau_2 \in [0, 1]$ are the two eigenvalues of $\mathbb{1} - ss^\dagger$. Their distribution $P_\beta(\tau_1, \tau_2)$ is given as a function of γ by Eq. (17) of Ref. [26]. (It is a rather lengthy expression, so we do not repeat it here.)

We parameterize the 2×2 unitary matrix u by

$$u = e^{i\alpha_3} \begin{pmatrix} e^{i\alpha_1 + i\alpha_2} \cos\alpha & e^{i\alpha_1 - i\alpha_2} \sin\alpha \\ e^{i\alpha_2 - i\alpha_1} \sin\alpha & -e^{-i\alpha_1 - i\alpha_2} \cos\alpha \end{pmatrix}, \tag{3.45}$$

and similarly for u'. The angles $\alpha_1, \alpha_2, \alpha_3$ are uniformly distributed in the interval $(0, 2\pi)$, while the angle $\alpha \in (0, \pi/2)$ has distribution $P(\alpha) = \sin 2\alpha$.

In this parameterization the occupation numbers (3.31) and (3.32) are

$$f_\phi = \tfrac{1}{2} + \tfrac{1}{2} \cos 2\alpha' \frac{\tau_1 - \tau_2}{\tau_1 + \tau_2}, \tag{3.46}$$

$$\tilde{f}_\phi = \tfrac{1}{2} + \tfrac{1}{2} \cos 2\alpha \frac{\tau_1 - \tau_2}{\tau_1 + \tau_2}, \tag{3.47}$$

with $\alpha' = \alpha$ if $\beta = 1$. The quantities X, Y, Z that determine ξ, w, $P_{\uparrow\downarrow}$, $P_{\uparrow\uparrow}$ become

$$X = f_\phi(1 - f_\phi)[2\tilde{f}_\phi(1 - \tilde{f}_\phi) + 1](\tau_1 + \tau_2 - \tau_1\tau_2), \tag{3.48}$$

$$Y = \left| \left(e^{-i\Phi} \sqrt{1 - \tau_1} \sin\alpha \cos\alpha' - e^{i\Phi} \sqrt{1 - \tau_2} \cos\alpha \sin\alpha' \right) \right.$$

$$\left. \times \left(e^{i\Phi} \sqrt{1 - \tau_1} \cos\alpha \cos\alpha' + e^{-i\Phi} \sqrt{1 - \tau_2} \sin\alpha \sin\alpha' \right) + \tfrac{1}{2} f_\phi(\tau_1 - \tau_2) \sin 2\alpha \right|^2 \tag{3.49}$$

$$Z = f_\phi(1 - f_\phi)(\tau_1 + \tau_2 - \tau_1\tau_2). \tag{3.50}$$

The phase $\Phi = \alpha_2 + \alpha_1'$ is uniformly distributed in $(0, 2\pi)$, regardless of the value of β.

3.4.2 Weak decoherence

In the regime $\gamma \ll 1$ of weak decoherence the expressions simplify considerably. The distribution $P_\beta(\tau_1, \tau_2)$ is then given by the Laguerre ensemble [26, 35]

$$P_\beta(\tau_1, \tau_2) = c_\beta \gamma^{3\beta+2} \exp[-\tfrac{1}{2}\gamma\beta(\tau_1^{-1} + \tau_2^{-1})] \frac{|\tau_1 - \tau_2|^\beta}{(\tau_1\tau_2)^{2\beta+2}}, \tag{3.51}$$

with $c_1 = 1/48$ and $c_2 = 1/24$. Since $\tau_1, \tau_2 \lesssim \gamma \ll 1$, we may expand

$$X = f_\phi(1 - f_\phi)[2\tilde{f}_\phi(1 - \tilde{f}_\phi) + 1](\tau_1 + \tau_2) + \mathcal{O}(\tau_i^2), \tag{3.52}$$

$$\begin{aligned} Y &= g_0(1 - g_0)(1 - \tau_1 - \tau_2) + (\tau_1 - \tau_2)(f_\phi - \tfrac{1}{2}) \\ &\quad \times \left[(g_0 - \tfrac{1}{2})\cos 2\alpha + \tfrac{1}{2}\cos 2\alpha'\right] + \mathcal{O}(\tau_i^2), \end{aligned} \tag{3.53}$$

$$Z = f_\phi(1 - f_\phi)(\tau_1 + \tau_2) + \mathcal{O}(\tau_i^2). \tag{3.54}$$

The phase coherent conductance $g_0 = |t_0|^2$ is given in terms of the angles α, α', Φ by

$$g_0 = \tfrac{1}{2} - \tfrac{1}{2}\cos 2\alpha \cos 2\alpha' - \tfrac{1}{2}\sin 2\alpha \sin 2\alpha' \cos 2\Phi. \tag{3.55}$$

It is independent of τ_1 and τ_2, with distribution [36]

$$P(g_0) = \tfrac{1}{2}\beta g_0^{-1+\beta/2}, \ \ 0 \le g_0 \le 1. \tag{3.56}$$

3.5 Ensemble averages

Averages over the ensemble of chaotic cavities require a four-fold integration for $\beta = 1$ (when $\alpha' = \alpha$),

$$\langle \cdots \rangle_1 = \int_0^1 \int_0^1 d\tau_1 d\tau_2 P_1(\tau_1, \tau_2) \int_0^{2\pi} \frac{d\Phi}{2\pi} \int_0^{\pi/2} \sin 2\alpha \, d\alpha \cdots \tag{3.57}$$

and a five-fold integration for $\beta = 2$,

$$\langle \cdots \rangle_2 = \int_0^1 \int_0^1 d\tau_1 d\tau_2 P_2(\tau_1, \tau_2) \int_0^{2\pi} \frac{d\Phi}{2\pi} \int_0^{\pi/2} \int_0^{\pi/2} \sin 2\alpha \sin 2\alpha' \, d\alpha d\alpha' \cdots \tag{3.58}$$
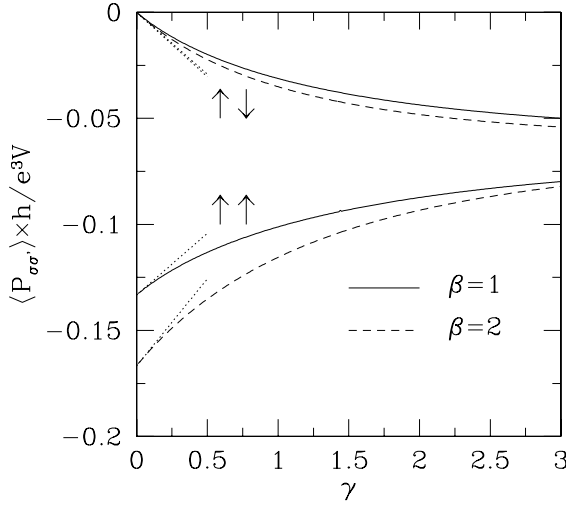
Figure 3.2: Dependence on the dimensionless decoherence rate $\gamma = 2\tau_{\text{dwell}}/\tau_{\text{coherence}}$ of the ensemble averaged spin-resolved current correlators $P_{\uparrow\downarrow}$ and $P_{\uparrow\uparrow}$, both in the presence ($\beta = 1$) and absence ($\beta = 2$) of time-reversal symmetry. The solid and dashed curves are computed by averaging Eq. (3.40) with the random-matrix distributions, according to Eqs. (3.57) and (3.58). The dotted lines are the weak-decoherence asymptotes (3.60–3.63). For strong decoherence all curves tend to the value $-\frac{1}{16} e^3 V / h$.

Results are plotted in Figs. 3.2 and 3.3. In Fig. 3.2 we see that the correlator $P_{\uparrow\uparrow}$ of parallel spin currents (lower curves) is reduced in absolute value by the voltage probe — in contrast to the spin-flip noise $P_{\uparrow\downarrow}$ (upper curves), which is increased in absolute value. For large γ all correlators tend to the same limit,

$$\lim_{\gamma \to \infty} P_{\sigma\sigma'} = -\frac{1}{16} \frac{e^3 V}{h}, \tag{3.59}$$

regardless of the presence or absence of time-reversal symmetry. In Fig. 3.3 we see how the decoherence introduced by the voltage probe reduces both the entanglement per electron-hole pair (quantified by the concurrence $\mathcal{C}$), as well as the total entanglement production rate $\mathcal{E}$.

In the limit of weak decoherence, the averages can be calculated in closed form using the formulas from Sec. 3.4.2. For the spin-resolved current correlators
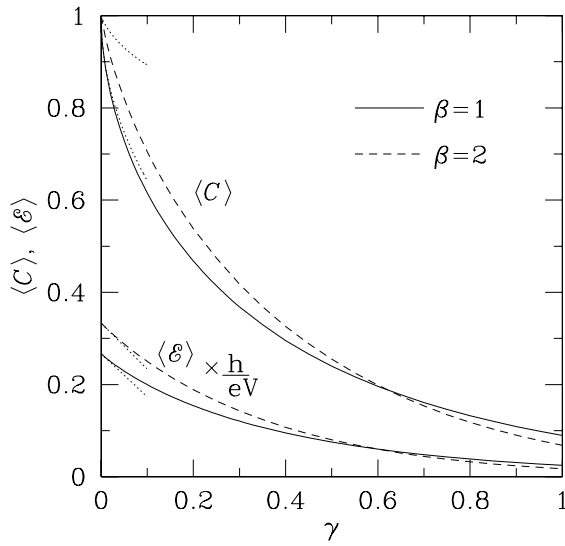
Figure 3.3: Dependence on γ of the average concurrence $\mathcal{C}$ and entanglement production rate $\mathcal{E}$. The solid and dashed curves are computed by averaging Eqs. (3.5–3.6) and (3.36–3.37). The dotted lines are the weak-decoherence asymptotes (3.65–3.69). The asymptote for $\langle\mathcal{C}\rangle_2$ converges poorly, because the next term of order γ in Eq. (3.66) is not much smaller than the term of order $\gamma\ln\gamma$.

we find, to order γ^2:

$$\langle P_{\uparrow\downarrow}\rangle_1 = -\frac{7}{120}\gamma\,\frac{e^3 V}{h}, \tag{3.60}$$

$$\langle P_{\uparrow\downarrow}\rangle_2 = -\frac{23}{378}\gamma\,\frac{e^3 V}{h}, \tag{3.61}$$

$$\langle P_{\uparrow\uparrow}\rangle_1 = \left(-\frac{2}{15}+\frac{7}{120}\gamma\right)\frac{e^3 V}{h}, \tag{3.62}$$

$$\langle P_{\uparrow\uparrow}\rangle_2 = \left(-\frac{1}{6}+\frac{31}{378}\gamma\right)\frac{e^3 V}{h}. \tag{3.63}$$

(We have replaced δE by eV, to obtain the total integrated contributions.)

The average Werner parameter,

$$\langle\xi\rangle_\beta = 1 - \left\langle\frac{X}{X+Y}\right\rangle_\beta, \tag{3.64}$$

is nonanalytic in γ around $\gamma = 0$, because $\langle X/g_0\rangle_\beta$ diverges. Since $P(g_0) \propto g_0^{-1+\beta/2}$, cf. Eq. (3.56), the average has a square-root singularity for $\beta = 1$ and a logarithmic singularity for $\beta = 2$. The average concurrence has the same singularity, in view of Eq. (3.5). To leading order in γ we find

$$\langle\xi\rangle_1 = 1 - 0.75\,\gamma^{1/2} \Rightarrow \langle\mathcal{C}\rangle_1 = 1 - 1.13\,\gamma^{1/2}, \tag{3.65}$$

$$\langle\xi\rangle_2 = 1 - \frac{13}{42}\gamma\ln\frac{1}{\gamma} \Rightarrow \langle\mathcal{C}\rangle_2 = 1 - \frac{13}{28}\gamma\ln\frac{1}{\gamma}. \tag{3.66}$$

The ensemble averaged weight $\langle w\rangle_\beta = 2\langle X+Y\rangle_\beta$ of the electron-hole pairs is analytic in γ,

$$\langle w\rangle_1 = \frac{4}{15}+\frac{11}{30}\gamma, \quad \langle w\rangle_2 = \frac{1}{3}+\frac{62}{189}\gamma. \tag{3.67}$$

The average entanglement production is given, to leading order in γ, by

$$\langle\mathcal{E}\rangle_\beta = \frac{eV}{h}\left(2\langle X+Y\rangle_\beta - \frac{3}{\ln 2}\langle X\rangle_\beta\right)_\beta \tag{3.68}$$

$$\Rightarrow \begin{cases} \langle\mathcal{E}\rangle_1 = \left(\frac{4}{15}+\frac{11}{30}\gamma-\frac{9}{10\ln 2}\gamma\right)\frac{eV}{h}, \\[2mm] \langle\mathcal{E}\rangle_2 = \left(\frac{1}{3}+\frac{62}{189}\gamma-\frac{58}{63\ln 2}\gamma\right)\frac{eV}{h}. \end{cases} \tag{3.69}$$

(We have again replaced δE by eV for the total entanglement production.)

3.6 Critical decoherence rate

For each quantum dot in the ensemble, the entanglement production rate $\mathcal{E}$ vanishes identically for γ greater than a certain value γ_c at which the Werner parameter ξ has dropped to 1/3. For γ slightly less than γ_c we may expand $\xi = 1/3 + \mathcal{O}(\gamma_c - \gamma)$. In view of Eqs. (3.5) and (3.6) the entanglement production rate has a logarithmic singularity at the critical point,

$$\mathcal{E} \propto (\gamma_c - \gamma)^2 \ln(\gamma_c - \gamma)^{-1}, \quad \text{if } \gamma \uparrow \gamma_c. \tag{3.70}$$

This is a generic feature of the loss of entanglement by the transition to a mixed state, cf. the logarithmic singularity in the temperature dependence of the entanglement production found in Ref. [19].

The statistical distribution $P_\beta(\gamma_c)$ of the critical decoherence rate in the ensemble of chaotic quantum dots is defined by

$$P_\beta(\gamma_c) = - \frac{d}{d\gamma} \langle \Theta(\xi - \tfrac{1}{3}) \rangle_\beta \Big|_{\gamma \to \gamma_c}, \tag{3.71}$$

with $\Theta(x)$ the unit step function ($\Theta(x) = 1$ if $x \geq 0$ and $\Theta(x) = 0$ if $x < 0$). The result of a numerical evaluation of Eq. (3.71) is plotted in Fig. 3.4. The ensemble average is

$$\langle \gamma_c \rangle_\beta = \begin{cases} 0.954 & \text{if } \beta = 1, \\ 0.957 & \text{if } \beta = 2. \end{cases} \tag{3.72}$$

Since $\gamma = 2\tau_{\text{dwell}}/\tau_{\text{coherence}}$, the critical decoherence rate of a typical sample in the ensemble of chaotic quantum dots is of the order of the inverse of the mean dwell time. Although the mean of the distributions for $\beta = 1$ and $\beta = 2$ is almost the same, their shape is entirely different, cf. Fig. 3.4.

The full probability distribution shows that sample-to-sample fluctuations are large, with a substantial weight for $\gamma_c \ll 1$. For small γ_c the distribution $P_\beta(\gamma_c)$ has the same limiting behavior $\propto \gamma_c^{-1+\beta/2}$ as the conductance g_0 [cf. Eq. (3.56)]. More precisely, as derived in App. 3.A,

$$\lim_{\gamma_c \to 0} P_\beta(\gamma_c) = \begin{cases} 0.085\,\gamma_c^{-1/2} & \text{if } \beta = 1, \\ 13/42 & \text{if } \beta = 2. \end{cases} \tag{3.73}$$

3.7 Discussion

3.7.1 Strength and weakness of the voltage probe model

We have shown how the voltage probe model of shot noise [1,4,5] can be used to study spin relaxation and decoherence in electrical conduction through a quantum
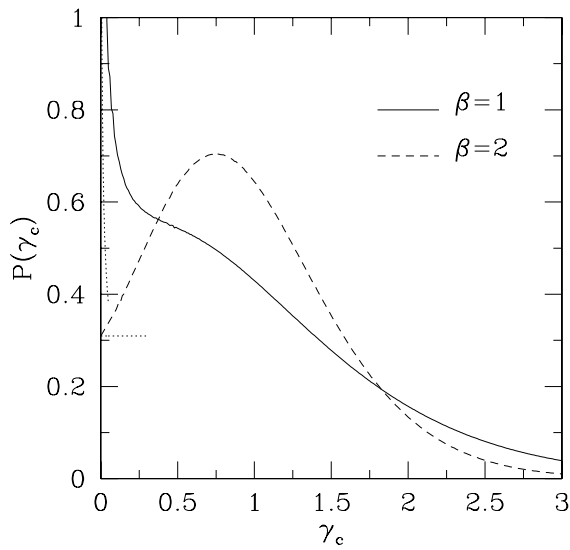
Figure 3.4: Probability distribution of the critical decoherence rate γ_c, beyond which the entanglement production vanishes. The solid and dashed curves are computed from Eq. (3.71). The dotted lines are the weak-decoherence asymptotes (3.73): $P(\gamma_c) \propto \gamma_c^{-1+\beta/2}$ for $\gamma_c \ll 1$.

dot. The strength of this approach to spin transport is that it is nonperturbative in the dimensionless conductance g_0, permitting a solution for g_0 of order unity using the methods of random-matrix theory. It is therefore complementary to existing semiclassical approaches to spin noise, [37] which require $g_0 \gg 1$.

The weakness of the voltage probe model is that it is phenomenological, not directly related to any specific mechanism for decoherence. We have examined here the simplest implementation with a single voltage probe, corresponding to a single decay rate γ. The dominant decoherence mechanism of electron spins in a quantum dot, hyperfine coupling to nuclear spins, [38] has a much shorter (ensemble averaged) decoherence time T_2 than the spin-flip time T_1. Pure dephasing (decoherence without spin flips) can be included into the model by means of ferromagnetic voltage probes. This is one extension that we leave for future investigation.

Another extension is to include spin-orbit scattering (symmetry index $\beta = 4$). We surmise that the result $P(\gamma_c) \propto \gamma_c^{-1+\beta/2}$ for the distribution of the critical decoherence rate in the weak decoherence regime, derived here for the case $\beta = 1, 2$ without spin-orbit scattering, holds for $\beta = 4$ as well — but this still needs to be demonstrated.

3.7.2 Entanglement detection for spin-isotropic states

By restricting ourselves to a system without a preferential basis in spin space, we have derived in Sec. 3.3.2 a one-to-one relation between the entanglement production and the spin-resolved shot noise. This relation goes beyond the voltage probe model, so we discuss it here in more general terms.

The basic assumption is that the conduction electrons have no preferential quantization axis for the spin. This socalled SU(2) invariance means that the full density matrix ρ is invariant under the simultaneous rotation of each electron spin by any 2×2 unitary matrix U:

$$U \otimes U \otimes U \cdots \otimes U \rho\, U^\dagger \otimes \cdots U^\dagger \otimes U^\dagger \otimes U^\dagger = \rho. \qquad (3.74)$$

The 4×4 matrix ρ_{eh}, obtained from ρ by projecting onto a single excited channel in the source as well as in the drain, has the same invariance property:

$$U \otimes U \rho_{\mathrm{eh}}\, U^\dagger \otimes U^\dagger = \rho_{\mathrm{eh}}. \qquad (3.75)$$

As explained in Sec. 3.3.1, the concurrence of the electron-hole pairs then follows directly from

$$\mathcal{C} = \frac{3}{2} \max \left\{ 0, -\mathrm{Tr}\, \rho_{\mathrm{eh}} \sigma_z \otimes \sigma_z - \frac{1}{3} \right\}. \qquad (3.76)$$

Here we have excluded a spontaneous breaking of the spin-rotation symmetry (no ferromagnetic order). The more general case has been considered in the context of the isotropic Heisenberg model. [39]

The concurrence in this spin-isotropic case is related to the spin-resolved shot noise by Eqs. (3.5) and (3.15). The entanglement production rate $\mathcal{E}$ follows according to Eq. (3.6) from $\mathcal{C}$ and a weight factor w, given in terms of the shot noise by Eq. (3.16). To detect the spin entanglement one thus needs to measure the correlator of parallel and anti-parallel spin currents. This is in essence a form of "quantum state tomography", simplified by the fact that an SU(2) invariant mixed state of two qubits is described by a single parameter (the Werner parameter ξ). The isotropy assumption does away with the need to compare correlators in different bases, as required for the Bell inequality, [24, 25] or for quantum state tomography of an arbitrary density matrix. [40]

In closing, we mention the remarkable simplification of the general expressions of Sec. 3.3.2 if the (dimensionless) conductance $g_0 \ll 1$ (tunneling regime). Then the shot noise is Poissonian, hence $P_{\text{charge}} = e\bar{I} = -2(P_{\uparrow\uparrow} + P_{\uparrow\downarrow})$. Moreover, the term quadratic in $\bar{I}$ is smaller than the term linear in $\bar{I}$ by a factor g_0, so it may be neglected. Instead of Eqs. (3.15) and (3.16) we thus have

$$\xi = \frac{P_{\uparrow\uparrow} - P_{\uparrow\downarrow}}{P_{\uparrow\uparrow} + P_{\uparrow\downarrow}}, \quad w = \frac{h}{e\delta E}\bar{I}. \tag{3.77}$$

The expressions (3.5) and (3.6) for the concurrence and entanglement production simplify to

$$\mathcal{C} = \frac{3}{2}\max\left\{0, \frac{P_{\uparrow\uparrow} - P_{\uparrow\downarrow}}{P_{\uparrow\uparrow} + P_{\uparrow\downarrow}} - \frac{1}{3}\right\} \tag{3.78}$$

$$= \frac{2}{e\bar{I}}\max\left\{0, |P_{\uparrow\uparrow}| - 2|P_{\uparrow\downarrow}|\right\}, \tag{3.79}$$

$$\mathcal{E} = \frac{\bar{I}}{e}\mathcal{F}\left(\tfrac{1}{2} + \tfrac{1}{2}\sqrt{1 - \mathcal{C}^2}\right). \tag{3.80}$$

We thus arrive at the conclusion that the electron-hole pairs produced by a tunnel barrier in a single-channel conductor with spin-independent scattering are entangled if and only if $|P_{\uparrow\uparrow}| > 2|P_{\uparrow\downarrow}|$, that is to say, if and only if the correlator of parallel spin currents is at least twice as large as the correlator of antiparallel spin currents. We hope that this simple entanglement criterion will motivate further experimental efforts in the detection of spin noise.

3.A   Derivation of Eq. (3.73)

We wish to evaluate the distribution $P_\beta(\gamma_c)$ of the critical decoherence rate in the limit $\gamma_c \to 0$. We can use the expressions of Sec. 3.4.2 for the weak decoherence regime.

If $\gamma \ll 1$ the criticality condition $\xi = 1/3$ is equivalent to $g_0(1 - g_0) = Q\gamma$, with the definition

$$
\begin{aligned}
Q = {} & (\tilde\tau_1 + \tilde\tau_2)\left[f_\phi(1 - f_\phi)(\tilde f_\phi(1 - \tilde f_\phi) + \tfrac{1}{2}) + g_0(1 - g_0)\right] \\
& - (\tilde\tau_1 - \tilde\tau_2)(f_\phi - \tfrac{1}{2})\left[(g_0 - \tfrac{1}{2})\cos 2\alpha + \tfrac{1}{2}\cos 2\alpha'\right].
\end{aligned}
$$

$$(3.81)$$

The Laguerre distribution (3.51) of the rescaled variables $\tilde\tau_i = \tau_i/\gamma$ is independent of γ in the limit $\gamma \to 0$ (when $\tilde\tau_i$ ranges from 0 to ∞). Substitution into Eq. (3.71) gives

$$
P_\beta(\gamma_c) = \left\langle \delta\left(\frac{g_0(1 - g_0)}{Q} - \gamma_c\right)\right\rangle_\beta.
$$

$$(3.82)$$

We first consider the case $\beta = 1$. Then $\alpha' = \alpha$, so g_0 and Q simplify to

$$
\begin{aligned}
g_0 = {} & (\sin 2\alpha \sin \Phi)^2, && (3.83) \\
Q = {} & (\tilde\tau_1 + \tilde\tau_2)\left[f_\phi^2(1 - f_\phi)^2 + \tfrac{1}{2}f_\phi(1 - f_\phi) + g_0(1 - g_0)\right] \\
& - (\tilde\tau_1 - \tilde\tau_2)(f_\phi - \tfrac{1}{2})g_0 \cos 2\alpha. && (3.84)
\end{aligned}
$$

The average over Φ contributes predominantly near $\Phi = 0$ and $\Phi = \pi$, with the result

$$
\lim_{\gamma_c \to 0} P_1(\gamma_c) = \frac{1}{2\pi}\sqrt{\frac{1}{\gamma_c}}\left\langle \frac{(\tilde\tau_1 + \tilde\tau_2)^{1/2}\left[f_\phi^2(1 - f_\phi)^2 + \tfrac{1}{2}f_\phi(1 - f_\phi)\right]^{1/2}}{\sin 2\alpha}\right\rangle_1.
$$

$$(3.85)$$

The remaining average over $\tilde\tau_i$ and α gives simply a numerical coefficient, resulting in Eq. (3.73).

Turning now to the case $\beta = 2$, we first observe that the limit $\gamma_c \to 0$ contains equal contributions from g_0 near 0 and 1. Hence Eq. (3.82) simplifies to

$$
\lim_{\gamma_c \to 0} P_2(\gamma_c) = 2\langle Q\delta(g_0)\rangle_2.
$$

$$(3.86)$$

To reach $g_0 = 0$ we need $\alpha = \alpha'$ and $\Phi = 0$ or π. Expanding around $\alpha = \alpha'$ and $\Phi = 0$, we have to second order $g_0 = \Phi^2 \sin^2 2\alpha + (\alpha - \alpha')^2$. There is a similar

expansion around $\Phi = \pi$. Using the identity $\delta(a^2 + b^2) = \pi\delta(a)\delta(b)$ we thus arrive at

$$\delta(g_0) = \frac{\pi}{\sin 2\alpha}\delta(\alpha - \alpha')\left[\delta(\Phi) + \delta(\Phi - \pi)\right]. \tag{3.87}$$

Substitution into Eq. (3.86) gives the limiting value

$$\lim_{\gamma_c \to 0} P_2(\gamma_c) = \left\langle(\tilde{\tau}_1 + \tilde{\tau}_2)\left[2f_\phi^2(1 - f_\phi)^2 + f_\phi(1 - f_\phi)\right]\right\rangle_2 = \frac{13}{42}, \tag{3.88}$$

as stated in Eq. (3.73).

Bibliography

[1] M. Büttiker, IBM J. Res. Dev. **32**, 63 (1988).

[2] C. W. J. Beenakker, M. Kindermann, C. M. Marcus, and A. Yacoby, in: *Fundamental Problems of Mesoscopic Physics: Interactions and Decoherence*, edited by I. V. Lerner, B. L. Altshuler, and Y. Gefen, NATO Science Series II. Vol. 154 (Kluwer, Dordrecht, 2004).

[3] The absence of energy exchange with the reservoir (energy conserving voltage probe) is appropriate for quasi-elastic scattering. Alternatively, one may require only that no particles are exchanged with the reservoir (dissipative voltage probe), in order to model inelastic scattering. The effect of inelastic scattering on entanglement has been studied by E. Prada, F. Taddei, and R. Fazio, Phys. Rev. B **72**, 125333 (2005).

[4] C. W. J. Beenakker and M. Büttiker, Phys. Rev. B **46**, R1889 (1992).

[5] M. J. M. de Jong and C. W. J. Beenakker, Physica A **230**, 219 (1996).

[6] A. A. Clerk and A. D. Stone, Phys. Rev. B **69**, 245303 (2004).

[7] V. S.-W. Chung, P. Samuelsson, and M. Büttiker, Phys. Rev. B **72**, 125320 (2005).

[8] M. L. Polianski, P. Samuelsson, and M. Büttiker, Phys. Rev. B **72**, 161302(R) (2005).

[9] S. Pilgram, P. Samuelsson, H. Förster, and M. Büttiker, cond-mat/0512276.

[10] G. Seelig and M. Büttiker, Phys. Rev. B **64**, 245313 (2001).

[11] F. Marquardt and C. Bruder, Phys. Rev. B **70**, 125305 (2004).

[12] F. Marquardt, cond-mat/0410333.

[13] C. W. J. Beenakker and B. Michaelis, J. Phys. A **38**, 10639 (2005).

[14] V. N. Golovach, A. Khaetskii, and D. Loss, Phys. Rev. Lett. **93**, 016601 (2004).

[15] W. A. Coish and D. Loss, Phys. Rev. B **72**, 125337 (2005).

[16] M. Borhani, V. N. Golovach, and D. Loss, cond-mat/0510758.

[17] W. M. Witzel and S. Das Sarma, cond-mat/0512323.

[18] C. W. J. Beenakker, C. Emary, M. Kindermann, and J. L. van Velsen, Phys. Rev. Lett. **91**, 147901 (2003).

[19] C. W. J. Beenakker, cond-mat/0508488.

[20] J. L. van Velsen, M. Kindermann, and C. W. J. Beenakker, Turk. J. Phys. **27**, 323 (2003).

[21] P. Samuelsson, E. Sukhorukov, and M. Büttiker, Turk. J. Phys. **27**, 481 (2003).

[22] C. W. J. Beenakker, Rev. Mod. Phys. **69**, 731 (1997).

[23] O. Sauret and D. Feinberg, Phys. Rev. Lett. **92**, 106601 (2004).

[24] N. M. Chtchelkatchev, G. Blatter, G. B. Lesovik, and T. Martin, Phys. Rev. B **66**, 161320(R) (2002).

[25] P. Samuelsson, E. V. Sukhorukov, and M. Büttiker, Phys. Rev. Lett. **92**, 026805 (2004).

[26] P. W. Brouwer and C. W. J. Beenakker, Phys. Rev. B **55**, 4695 (1997); **66**, 209901(E) (2002).

[27] R. F. Werner, Phys. Rev. A **40**, 4277 (1989).

[28] The Bell state (3.4) refers to the spin of the electron excitation at source and drain. An equivalent way to represent the same state (used in Ref. [18]) is $|\Psi_{\text{Bell}}\rangle = 2^{-1/2}(|\uparrow_h\uparrow_e\rangle + |\downarrow_h\downarrow_e\rangle)$, in terms of the hole spin (h) at the source and the electron spin (e) at the drain. We will not use the latter representation in this chapter (although we will on occasion speak of "entangled electron-hole pairs").

[29] W. K. Wootters, Phys. Rev. Lett. **80**, 2245 (1998).

[30] The definition (3.11) of the spectral density does not contain the extra factor of two that is sometimes included in the literature. In particular, with our definition full shot noise is $P_{\text{charge}} = e\bar{I}$ rather than $2e\bar{I}$.

[31] M. Büttiker, Phys. Rev. B **46**, 12485 (1992).

[32] G. B. Lesovik, JETP Lett. **49**, 592 (1989).

[33] M. Büttiker, Phys. Rev. Lett. **65**, 2901 (1990).

[34] For a study of entanglement production in a quantum dot with strong spin-orbit scattering, see D. Frustaglia, S. Montangero, and R. Fazio, cond-mat/0511555.

[35] C. W. J. Beenakker and P. W. Brouwer, Physica E **9**, 463 (2001).

[36] R. A. Jalabert, J.-L. Pichard, and C. W. J. Beenakker, Europhys. Lett. **27**, 255 (1994).

[37] E. G. Mishchenko, A. Brataas, and Y. Tserkovnyak, Phys. Rev. B **69**, 073305 (2004).

[38] J. R. Petta, A. C. Johnson, J. M. Taylor, E. A. Laird, A. Yacoby, M. D. Lukin, C. M. Marcus, M. P. Hanson, and A. C. Gossard, Science **309**, 2180 (2005).

[39] X. Wang and P. Zanardi, Phys. Lett. A **301**, 1 (2002).

[40] P. Samuelsson and M. Büttiker, cond-mat/0506446.

Chapter 4

All-electronic coherent population trapping in quantum dots

4.1 Introduction

Coherent population trapping is a quantum optical phenomenon in which the laser illumination of an atom drives an atomic electron into a coherent superposition of orbital states and traps it there [1–3]. Such superpositions can be "dark", in that they are further decoupled from the optical fields. Brandes and Renzoni have shown how such states can also be formed in artificial atoms (quantum dots) through the use of laser illumination [4, 5]. In this chapter we present an all-electronic analogue, i.e. without laser illumination, of coherent population trapping in quantum dots. (For an analogy in superconducting Josephson junctions, see Ref. [2, 6]; for an analogy in single benzene molecules, see Ref. [8].) We illustrate this effect by considering a system of three tunnel-coupled quantum dots and show that, under proper bias and resonance conditions, an electron can become trapped in a coherent superposition of states in different dots. This state is "dark" in the sense that, due to the Coulomb blockade, no further electrons can pass through the dots and current flow is blocked in the absence of decoherence.

The trapping effect provides a novel mechanism for current rectification, since the blocking is effective for one sign of the bias voltage only. This quantum mechanical mechanism is distinct from mechanisms discussed previously. In particular, the classical rectification mechanism of Stopa and collaborators [9, 10] traps the electron in a *single* quantum dot, rather than in a coherent superposition of spatially separated states. Experiments by Ono and collaborators [11] on rectification in double quantum dots likewise trap an electron in a single dot. The three-dot
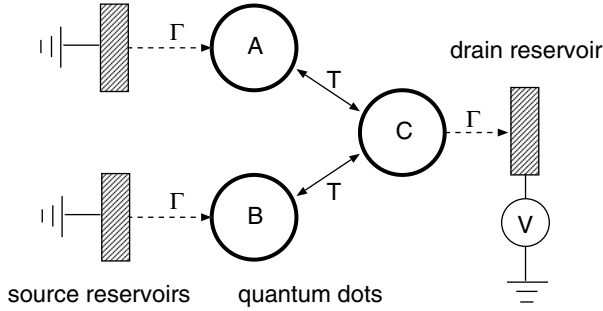
Figure 4.1: Schematic of the three-dot trap. The solid arrows indicate reversible transitions, described by the Hamiltonian (4.1). The dashed arrows indicate irreversible transitions, described by the quantum jump operator (4.3). Destructive interference of the two reversible transitions traps an electron in a coherent superposition $|\Phi_-\rangle = 2^{-1/2}(|A\rangle - |B\rangle)$ of the states on dots A and B. The trapped state has vanishing amplitude on dot C, so that it can not decay into the right reservoir. No trapping is possible if the bias is inverted, because the trapped state would then decay into the left reservoirs.

configuration requires no Aharonov-Bohm phase to trap an electron, in contrast to the two-dot configuration of Marquardt and Bruder [12]. Because of the phase coherent origin of the effect discussed here, the current that leaks through the device when it is blocked provides a method by which one can determine the coherence time of a charge qubit.

4.2 Coherent transport

The three-dot trap is shown schematically in Fig. 4.1. Three quantum dots and three electron reservoirs are connected by reversible or by irreversible transitions. Reversible transitions between the quantum dots are described by the tunnel Hamiltonian

$$H = T|C\rangle\langle A| + T|C\rangle\langle B| + \text{H.c.} = 2^{1/2}T|C\rangle\langle\Phi_+| + \text{H.c.} \qquad (4.1)$$

We have defined the states

$$|\Phi_\pm\rangle = 2^{-1/2}(|A\rangle \pm |B\rangle). \qquad (4.2)$$

We consider the case that the energies of the single-particle levels $|A\rangle$, $|B\rangle$, $|C\rangle$ in the three dots are all the same (set at zero), so that inelastic transitions between

these levels do not play a role. To minimize the number of free parameters, all tunnel rates are put equal to T. (The more general case of unequal tunnel rates will be considered at the end of the chapter.) We assume time-reversal symmetry, hence T is a real number. (Since results do not depend on the sign of T, we will take T positive for ease of notation.) We furthermore assume that the electrostatic charging energy of the combined three-dot system is sufficiently large that the total number of electrons does not exceed one. Many-electron states are projected out and hence we may ignore spin.

For a bias voltage $|V| \gg T/e$, and at zero temperature, the transitions from the source reservoirs into dots A and B and from dot C into the drain reservoir are irreversible. (Because of this restriction, the rectification provided by our device does not apply to the range $|V| \lesssim T/e$ around zero bias.) The tunnel rates between dots and reservoirs are all set equal to Γ. The quantum jump operators are

$$L_A = \sqrt{\Gamma}|A\rangle\langle 0|, \ L_B = \sqrt{\Gamma}|B\rangle\langle 0|, \ L_C = \sqrt{\Gamma}|0\rangle\langle C|, \tag{4.3}$$

where $|0\rangle$ is the state with all three dots empty.

We study the dynamics of this device by means of the master equation approach to single-electron tunneling [8, 14, 15], which describes not only the populations of the dot levels, but also accounts for quantum coherences between them. The master equation gives the time evolution of the three-dot density matrix $\rho(t)$ in the Lindblad form [16]

$$\frac{d\rho}{dt} = -i[H,\rho] + \sum_{X=A,B,C} \left(L_X \rho L_X^\dagger - \tfrac{1}{2} L_X^\dagger L_X \rho - \tfrac{1}{2} \rho L_X^\dagger L_X \right). \tag{4.4}$$

(We have set $\hbar \equiv 1$.) As initial condition we take $\rho(0) = |0\rangle\langle 0|$.

We use as a basis for the density matrix the four states

$$|e_1\rangle = |\Phi_+\rangle, \ |e_2\rangle = |\Phi_-\rangle, \ |e_3\rangle = |C\rangle, \ |e_4\rangle = |0\rangle. \tag{4.5}$$

This four-dimensional space may be reduced to a three-dimensional subspace by noting that the master equation (4.4) couples only ρ_{44} and ρ_{ij} with $i, j \leq 3$. The matrix elements ρ_{ij} with $i = 4, j \neq 4$ or $j = 4, i \neq 4$ remain zero. We may therefore seek a solution of the form

$$\rho(t) = \tilde{\rho}(t) + [1 - \mathrm{Tr}\,\tilde{\rho}(t)]\,|0\rangle\langle 0|, \tag{4.6}$$

where $\tilde{\rho}$ is restricted to the three-dimensional subspace spanned by the states $|e_i\rangle$

with $i \leq 3$. The evolution equation for $\tilde{\rho}$ reads

$$\frac{d\tilde{\rho}}{dt} = M\tilde{\rho} + \tilde{\rho}M^{\dagger} + Q, \quad \tilde{\rho}(0) = 0, \tag{4.7}$$

$$M = -\begin{pmatrix} 0 & 0 & 2^{1/2}iT \\ 0 & 0 & 0 \\ 2^{1/2}iT & 0 & \Gamma/2 \end{pmatrix}, \tag{4.8}$$

$$Q = \Gamma(1 - \mathrm{Tr}\,\tilde{\rho})\begin{pmatrix} 1 & 0 & 0 \\ 0 & 1 & 0 \\ 0 & 0 & 0 \end{pmatrix}. \tag{4.9}$$

All off-diagonal elements of $\tilde{\rho}$ vanish, except the purely imaginary $\tilde{\rho}_{13} = -\tilde{\rho}_{31}$. Four real independent variables remain, which we collect in a vector $v = (\mathrm{Tr}\,\tilde{\rho}, \tilde{\rho}_{11}, \tilde{\rho}_{33}, \mathrm{Im}\,\tilde{\rho}_{13})$ satisfying

$$\frac{dv}{dt} = X \cdot (v - v_{\infty}), \quad v(0) = 0, \tag{4.10}$$

$$X = \begin{pmatrix} -2\Gamma & 0 & -\Gamma & 0 \\ -\Gamma & 0 & 0 & -2^{3/2}T \\ 0 & 0 & -\Gamma & 2^{3/2}T \\ 0 & 2^{1/2}T & -2^{1/2}T & -\Gamma/2 \end{pmatrix}, \quad v_{\infty} = \begin{pmatrix} 1 \\ 0 \\ 0 \\ 0 \end{pmatrix}. \tag{4.11}$$

The solution is

$$v(t) = v_{\infty} - e^{Xt}v_{\infty}. \tag{4.12}$$

All four eigenvalues λ_n of X have a negative real part, so $v(t) \to v_{\infty}$ for $t \to \infty$ and hence

$$\lim_{t \to \infty} \rho(t) = |\Phi_-\rangle\langle\Phi_-|. \tag{4.13}$$

This is the trapped state: it does not decay because it is an eigenstate of H. For large times $|v(t) - v_{\infty}| \propto e^{-\alpha t}$, with trapping rate $\alpha = \min(|\mathrm{Re}\,\lambda_1|, |\mathrm{Re}\,\lambda_2|, |\mathrm{Re}\,\lambda_3|, |\mathrm{Re}\,\lambda_4|)$. The full expression for α is lengthy, but the two asymptotic limits have a compact form,

$$\alpha = \begin{cases} 4T^2/\Gamma & \text{if } T \ll \Gamma, \\ \frac{1}{4}(5 - \sqrt{17})\Gamma \approx 0.22\,\Gamma & \text{if } \Gamma \ll T. \end{cases} \tag{4.14}$$

If the coupling of the quantum dots to the reservoirs is weaker than between themselves, then the trapping time is of order $1/\Gamma$. One might have guessed the trapping time to be of order $1/T$ in the opposite regime $T \ll \Gamma$, but this guess underestimates the correct answer, which is larger by a factor Γ/T. The fact that $\alpha \to 0$
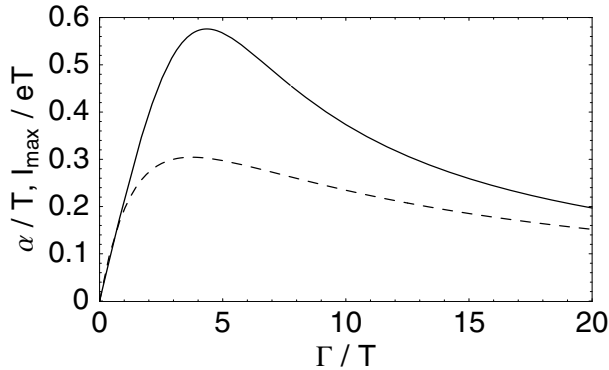
Figure 4.2: *Solid curve:* Dependence of the trapping rate α on the tunnel rate Γ between quantum dots and reservoirs. Both rates are normalized by the tunnel rate T between the quantum dots. The small and large-Γ limits are given by Eq. (4.14). *Dashed curve:* Maximal steady state current $I_{\max}$ in the presence of decoherence, according to Eq. (4.19). The two quantities $I_{\max}$ and $e\alpha$ differ by less than a factor of two over the whole range of tunnel rates.

when $\Gamma \to \infty$ can be understood as a decoherence of the inter-dot dynamics induced by a strong coupling to the electron reservoirs.

The full dependence of α on Γ and T is shown in Fig. 4.2. If Γ is increased at constant T, the trapping rate has a maximum of $\alpha_{\max} = 0.58\,T$ at $\Gamma = 4.35\,T$.

4.3 Decoherence beats interference trapping

The trapping effect requires the coherent superposition of spatially separated electronic states in quantum dots A and B. Such a charge qubit is sensitive to decoherence by coupling to other charges in the environment, which effectively project the qubit on one of the three localized states $|A\rangle$, $|B\rangle$, $|C\rangle$. We model this decoherence by including into the master equation the three quantum jump operators

$$L_{\phi_X} = \Gamma_\phi^{1/2}|X\rangle\langle X|, \quad X = A, B, C. \tag{4.15}$$

The decoherence rate Γ_ϕ parameterizes the strength of the charge noise and is taken to be dot independent. For a microscopic foundation of the charge noise model we refer to Ref. [17]. We also note that charge noise causes phase as well

as energy relaxation.[1]

The master equation reads

$$\frac{d\rho}{dt} = -i[H,\rho] + \sum_{X=A,B,C,\phi_A,\phi_B,\phi_C} \left(L_X \rho L_X^\dagger - \tfrac{1}{2} L_X^\dagger L_X \rho - \tfrac{1}{2} \rho L_X^\dagger L_X \right). \quad (4.16)$$

The steady-state current,

$$I = \lim_{t\to\infty} e\Gamma \langle C|\rho(t)|C\rangle, \quad (4.17)$$

is obtained by solving Eq. (4.16) with the left-hand-side set to zero. We find

$$
\begin{aligned}
I &= \frac{4e\Gamma T^2}{\Gamma^2 + 14T^2 + 2\Gamma\Gamma_\phi(1 + 2T^2/\Gamma_\phi^2)} \\
&\to \begin{cases} e\Gamma_\phi & \text{if } \Gamma_\phi \ll \Gamma, T, \\ 2eT^2/\Gamma_\phi & \text{if } \Gamma_\phi \gg \Gamma, T. \end{cases}
\end{aligned} \quad (4.18)
$$

As illustrated in Fig. 4.3, the current vanishes both in the limit $\Gamma_\phi \to 0$, because of the trapping effect, and in the limit $\Gamma_\phi \to \infty$, because of the quantum Zeno effect [18,19]. The maximal current is reached at $\Gamma_\phi = 2^{1/2} T$ and is equal to

$$
\begin{aligned}
I_{\max} &= \frac{4e\Gamma T^2}{\Gamma^2 + 14T^2 + 4\sqrt{2}\,\Gamma T} \\
&\to \begin{cases} 4eT^2/\Gamma & \text{if } T \ll \Gamma, \\ \tfrac{2}{7} e\Gamma \approx 0.29\, e\Gamma & \text{if } \Gamma \ll T. \end{cases}
\end{aligned} \quad (4.19)
$$

Comparison of Eqs. (4.14) and (4.19) shows that the maximal current $I_{\max}$ in the *presence* of decoherence is set by the trapping rate α in the *absence* of decoherence. For $T \ll \Gamma$ one has exactly $I_{\max} = e\alpha$, while for $\Gamma \ll T$ the two quantities differ by a numerical coefficient of order unity. In Fig. 4.2 both $I_{\max}/e$ and α are plotted together, and are seen to differ by less than a factor of two over the whole Γ, T range.

The trapping effect does not happen if the bias is inverted, so that the drain reservoir becomes the source and vice versa. In that case we find for the steady-state current the expression

$$
\begin{aligned}
I &= \frac{4e\Gamma T^2(2\Gamma + \Gamma_\phi)}{\Gamma(\Gamma + \Gamma_\phi)(\Gamma + 2\Gamma_\phi) + 4T^2(6\Gamma + 5\Gamma_\phi)} \\
&\to \begin{cases} 8e\Gamma T^2(\Gamma^2 + 24T^2)^{-1} & \text{if } \Gamma_\phi \ll \Gamma, T, \\ 2eT^2/\Gamma_\phi & \text{if } \Gamma_\phi \gg \Gamma, T. \end{cases}
\end{aligned} \quad (4.20)
$$

---

[1]To calculate the energy relaxation, we decouple the three quantum dots from the electron reservoirs (setting $\Gamma \equiv 0$) and calculate $dE/dt = (d/dt)\mathrm{Tr}\,\rho H$ from Eq. (4.16). One finds $dE/dt = -\Gamma_\phi E$, so the energy of the three-dot system relaxes to zero with rate Γ_ϕ.
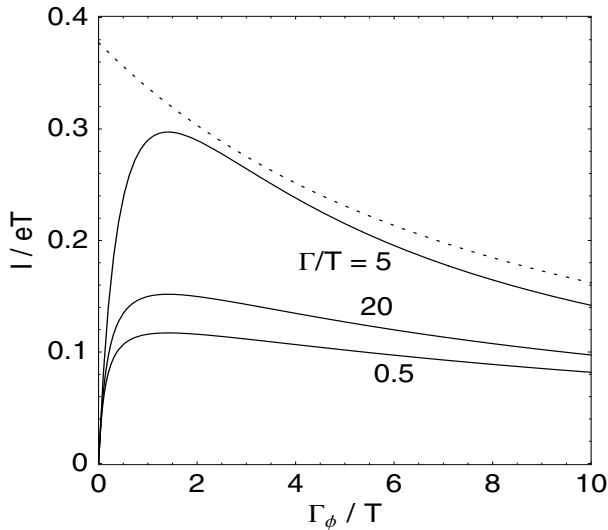
Figure 4.3: *Solid curves:* Dependence of the steady-state current I on the decoherence rate Γ_ϕ for three values of Γ/T, calculated from Eq. (4.18). The height of the maximum depends non-monotonically on Γ, first increasing $\propto \Gamma$ and then decreasing $\propto 1/\Gamma$, according to Eq. (4.19). *Dashed curve:* Steady-state current if source and drain reservoir are interchanged, calculated from Eq. (4.20) for $\Gamma/T = 20$.

For strong decoherence the current is the same in both bias directions, but for weak decoherence the current in the case of inverted bias does not drop to zero but saturates at a finite value. The two cases are compared in Fig. 4.3. We see that the appearance of a maximum current as a function of Γ_ϕ is characteristic for the trapping effect.

We have for simplicity assumed that all three dots have the same tunnel rates and decoherence rates, but this assumption may be easily relaxed. Let us consider first the case that the three-dot structure still has a reflection symmetry, so that dots A and B are equivalent, but that dot C has a different tunnel rate Γ' into the reservoir and a different decoherence rate Γ'_ϕ. We denote $\bar{\Gamma}_\phi = (\Gamma_\phi + \Gamma'_\phi)/2$. The result (4.18) for the steady-state current generalizes to

$$
\begin{aligned}
I &= \frac{4e\Gamma' T^2}{\Gamma'^2 + 2T^2(6 + \Gamma'/\Gamma) + 2\Gamma'\Gamma_\phi(\bar{\Gamma}_\phi/\Gamma_\phi + 2T^2/\Gamma_\phi^2)} \\
&\to \begin{cases} e\Gamma_\phi & \text{if } \Gamma_\phi \to 0, \\ 2eT^2/\bar{\Gamma}_\phi & \text{if } \Gamma_\phi \to \infty. \end{cases}
\end{aligned} \tag{4.21}
$$

The steady-state current still contains the desired information on the rates of decoherence, with the regimes of weak and strong decoherence governed by Γ_ϕ and $\bar{\Gamma}_\phi$, respectively.

In the most general case of arbitrarily different tunnel rates $T_A, T_B, \Gamma_A, \Gamma_B, \Gamma_C$ and decoherence rates $\Gamma_{\phi_A}, \Gamma_{\phi_B}, \Gamma_{\phi_C}$, the steady state current in the limit of weak and strong decoherence takes the form

$$I \quad \rightarrow \quad \frac{w_0 e (\Gamma_{\phi_A} + \Gamma_{\phi_B})}{w_A + w_B} \quad \text{if } \Gamma_\phi \rightarrow 0, \tag{4.22a}$$

$$I \quad \rightarrow \quad \frac{4 e T_A T_B}{w_A \Gamma_{\phi_A} + w_B \Gamma_{\phi,B} + (w_A + w_B) \Gamma_{\phi_C}} \quad \text{if } \Gamma_\phi \rightarrow \infty, \tag{4.22b}$$

with weight factors

$$w_0 = \frac{T_A T_B}{T_A^2 + T_B^2}, \quad w_A = \frac{\Gamma_A T_B / T_A}{\Gamma_A + \Gamma_B}, \quad w_B = \frac{\Gamma_B T_A / T_B}{\Gamma_A + \Gamma_B}, \tag{4.23}$$

that are functions of the tunnel rates — but independent of the decoherence rates. Notice that in this asymmetric case the trapped state $\sqrt{w_0 T_B / T_A} |A\rangle - \sqrt{w_0 T_A / T_B} |B\rangle$ has unequal weights on the two dots A and B.

4.4   Conclusion

In conclusion, we have demonstrated how the well known concept of coherent population trapping in atoms may be transferred to a purely electronic system. A large voltage bias plays the role of the laser illumination and single-electron tunneling between quantum dots plays the role of intra-atomic transitions. Because the quantum dots are charged, the trapped electronic state is sensitive to decoherence by coupling to charges in the environment. This decoherence destabilizes the trapped state, causing a leakage current I to flow through the quantum dots. We have found that the maximal I in the presence of decoherence is set by the trapping rate α, with $I_{\max} \approx e\alpha$ within a factor of two over the whole parameter range. For small decoherence rate Γ_ϕ we find $I = e\Gamma_\phi$, which provides a way to measure the coherence time of a charge qubit in a transport experiment. We finally note that extensions to many-electron trapping can serve as a source for the formation of entangled electron pairs [20].

Bibliography

[1] G. Alzetta, A. Gozzini, L. Moi, and G. Orriols, *Nuovo Cimento B*, **36** (1976) 5.

[2] E. Arimondo and G. Orriols, *Lett. Nuovo Cimento*, **17** (1976) 333.

[3] R. M. Whitley and C. R. Stroud, *Phys. Rev. A*, **14** (1976) 1498.

[4] T. Brandes and F. Renzoni, *Phys. Rev. Lett.*, **85** (2000) 4148.

[5] T. Brandes, *Phys. Rep.*, **408** (2005) 315.

[6] L. Faoro, J. Siewert, and R. Fazio, *Phys. Rev. Lett.*, **90**, 028301 (2003).

[7] J. Siewert and T. Brandes, *Adv. Solid State Phys.*, **44**, 181 (2004).

[8] M. H. Hettler, W. Wenzel, M. R. Wegewijs, and H. Schoeller, *Phys. Rev. Lett.*, **90**, 076805 (2003).

[9] M. Stopa, *Phys. Rev. Lett.*, **88** (2002) 146802.

[10] A. Vidan, R. M. Westervelt, M. Stopa, M. Hanson, and A. C. Gossard, *Appl. Phys. Lett.*, **85** (2004) 3602.

[11] K. Ono, D. G. Austing, Y. Tokura, and S. Tarucha, *Science*, **297** (2002) 1313.

[12] F. Marquardt and C. Bruder, *Phys. Rev. B*, **68** (2003) 195305.

[13] Yu. V. Nazarov, *Physica B*, **189**, 57 (1993).

[14] T. H. Stoof and Yu. V. Nazarov, *Phys. Rev. B*, **53** (1996) 1050.

[15] S. A. Gurvitz, *Phys. Rev. B*, **57** (1998) 6602.

[16] G. Lindblad, *Comm. Math. Phys.*, **48** (1976) 119.

[17] S. A. Gurvitz, *Phys. Rev. B*, **56** (1997) 15215.

[18] B. Misra and E. C. G. Sudarshan, *J. Math. Phys.*, **18** (1977) 756.

[19] W. M. Itano, D. J. Heinzen, J. J. Bollinger, and D. J. Wineland, *Phys. Rev. A*, **41** (1990) 2295.

[20] J. Fabian and U. Hohenester, cond-mat/0412229.

Chapter 5

Counting statistics of coherent population trapping in quantum dots

5.1 Introduction

The phenomenon of coherent population trapping, originating from quantum optics, has recently been recognized as a useful and interesting concept in the electronic context as well. [1, 2] An all-electronic implementation, proposed in Ref. [3], is based on destructive interference of single-electron tunneling between three quantum dots (see Fig. 5.1). The trapped state is a coherent superposition of the electronic charge in two of these quantum dots, so it is destabilized as a result of decoherence by coupling to external charges. In the limit of weak decoherence one electron is transferred *on average* through the device for each decoherence event.

In an experimental breakthrough, [4, 5] Gustavsson et al. have now reported real-time detection of single-electron tunneling, obtaining the full statistics of the number of transferred charges in a given time interval. The first two moments of the counting statistics give the mean current and the noise power, and higher moments further specify the correlations between the tunneling electrons. [6] This recent development provides a motivation to investigate the counting statistics of coherent population trapping, going beyond the first moment studied in Ref. [3].

Since the statistics of the decoherence events is Poissonian, one might surmise that the charge counting statistics would be Poissonian as well. In contrast, we find that charges are transferred in bunches instead of independently as in a Poisson process. The Fano factor (ratio of noise power and mean current) is three times the Poisson value in the limit of weak decoherence. We identify the
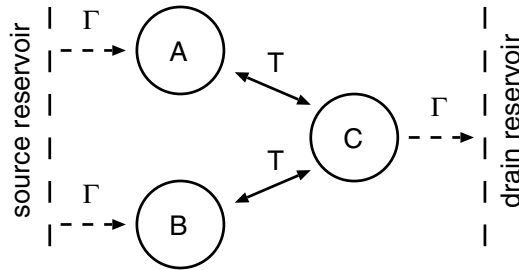
Figure 5.1: Three quantum dots connected to a source and a drain reservoir. Reversible transitions (rate T) and irreversible transitions (rate Γ) are indicated by arrows.

physical origin of this super-Poissonian noise in the alternation of two decay processes (tunnel events and decoherence events) with very different time scales—in accord with the general theory of Belzig. [7] For comparable tunnel and decoherence rates the noise becomes sub-Poissonian, while the Poisson distribution is approached for strong decoherence.

The analysis of Ref. [3] was based on the Lindblad master equation for electron transport, [8, 9] which determines only the average number of transferred charges. The full counting statistics can be obtained by an extension of the master equation due to Bagrets and Nazarov [10] (without phase coherence) and to Kießlich et al. [11] (with phase coherence). In spite of the added complexity, we have found analytical solutions for the second moment at any decoherence rate and for the full distribution in the limit of weak or strong decoherence.

5.2   Model

The system under consideration, studied in Ref. [3], is depicted schematically in Fig. 5.1. It consists of three tunnel-coupled quantum dots connected to two electron reservoirs. In the limit of large bias voltage, which we consider here, electron tunneling from the source reservoir into the dots and from the dots into the drain reservoir is irreversible. We assume that a single level in each dot lies within range of the bias voltage. We also assume that due to Coulomb blockade there can be at most one electron in total in the three dots. The basis states, therefore, consist of the state $|0\rangle$ in which all dots are empty, and the states $|A\rangle$, $|B\rangle$, and $|C\rangle$ in which one electron occupies one of the dots.

The time evolution of the density matrix ρ for the system is given by the

Lindblad-type master equation, [8,9]

$$\frac{\mathrm{d}\rho}{\mathrm{d}t} = -i[H,\rho] + \sum_{X=A,B,C,\phi_A,\phi_B,\phi_C} \left(L_X\rho L_X^\dagger - \tfrac{1}{2}L_X^\dagger L_X\rho - \tfrac{1}{2}\rho L_X^\dagger L_X\right). \quad (5.1)$$

The Hamiltonian

$$H = T|C\rangle\langle A| + T|C\rangle\langle B| + \text{H.c.} \quad (5.2)$$

is responsible for reversible tunneling between the dots, with tunnel rate T. For simplicity, we assume that the three energy levels in dots A, B, and C are degenerate and that the two tunnel rates from A to C and from B to C are the same. The quantum jump operators

$$L_A = \sqrt{\Gamma}|A\rangle\langle 0|, \quad L_B = \sqrt{\Gamma}|B\rangle\langle 0|, \quad L_C = \sqrt{\Gamma}|0\rangle\langle C|,$$

model irreversible tunneling out of and into the reservoirs, with a rate Γ (which we again take the same for each dot). Finally, the quantum jump operators

$$L_{\phi_X} = \sqrt{\Gamma_\phi}|X\rangle\langle X|, \quad X = A,B,C, \quad (5.3)$$

model decoherence due to charge noise with a rate Γ_ϕ.

As a basis for the the density matrix we use the four states

$$|e_0\rangle = 2^{-1/2}(|A\rangle - |B\rangle),$$
$$|e_1\rangle = 2^{-1/2}(|A\rangle + |B\rangle),$$
$$|e_2\rangle = |C\rangle, \quad |e_3\rangle = |0\rangle. \quad (5.4)$$

If the initial state is $|0\rangle\langle 0|$ most of the coefficients of ρ remain zero. We collect the five non-zero real variables in a vector

$$v = (\rho_{00}, \rho_{11}, \rho_{22}, \rho_{33}, \operatorname{Im}\rho_{02})^{\mathrm{T}}, \quad (5.5)$$

whose time evolution can be expressed as

$$\mathrm{d}v/\mathrm{d}t = Xv, \quad (5.6)$$

$$X = \begin{pmatrix} -\Gamma_\phi/2 & \Gamma_\phi/2 & 0 & \Gamma & -2^{3/2}T \\ \Gamma_\phi/2 & -\Gamma_\phi/2 & 0 & \Gamma & 0 \\ 0 & 0 & -\Gamma & 0 & 2^{3/2}T \\ 0 & 0 & \Gamma & -2\Gamma & 0 \\ 2^{1/2}T & 0 & -2^{1/2}T & 0 & -\Gamma/2-\Gamma_\phi \end{pmatrix}. \quad (5.7)$$

It is our goal to determine the full counting statistics, being the probability distribution $P(n)$ of the number of transferred charges in time t. Irrelevant transients are removed by taking the limit $t \to \infty$. The associated cumulant generating function $F(\chi)$ is related to $P(n)$ by

$$\exp[-F(\chi)] = \sum_{n=0}^{\infty} P(n) \exp(in\chi). \tag{5.8}$$

From the cumulants

$$C_k = -(-i\partial_\chi)^k F(\chi)|_{\chi=0} \tag{5.9}$$

we obtain the average current $I = eC_1/t$ and the zero-frequency noise $S = 2e^2 C_2/t$, both in the limit $t \to \infty$. The Fano factor is defined as $\alpha = C_2/C_1$.

As described in Refs. [10] and [11], in order to calculate $F(\chi)$ one multiplies coefficients of the rate matrix X which are associated with tunneling into one of the reservoirs (the right one in our case), by counting factors $e^{i\chi}$. This leads to the χ-dependent rate matrix

$$L(\chi) = \begin{pmatrix} -\Gamma_\phi/2 & \Gamma_\phi/2 & 0 & \Gamma & -2^{3/2}T \\ \Gamma_\phi/2 & -\Gamma_\phi/2 & 0 & \Gamma & 0 \\ 0 & 0 & -\Gamma & 0 & 2^{3/2}T \\ 0 & 0 & \Gamma e^{i\chi} & -2\Gamma & 0 \\ 2^{1/2}T & 0 & -2^{1/2}T & 0 & -\Gamma/2 - \Gamma_\phi \end{pmatrix}. \tag{5.10}$$

The cumulant generating function for $t \to \infty$ can then be obtained from the eigenvalue $\Lambda_{min}(\chi)$ of $L(\chi)$ with the smallest absolute real part, [10, 11]

$$F(\chi) = -t\Lambda_{min}^{(\chi)}. \tag{5.11}$$

5.3   Results

5.3.1   Fano factor

Low order cumulants can be calculated by perturbation theory in the counting parameter χ. The calculation in outlined in App. 5.A. For the average current we find

$$I = \frac{4e\Gamma T^2}{\Gamma^2 + 14T^2 + 2\Gamma\Gamma_\phi(1 + 2T^2/\Gamma_\phi^2)}, \tag{5.12}$$
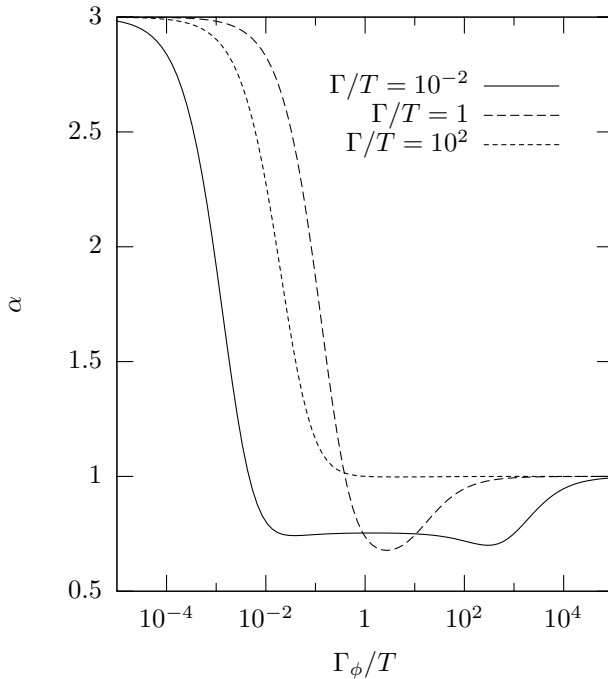
Figure 5.2: Dependence of the Fano factor α on the normalized decoherence rate Γ_ϕ/T for three values of Γ/T.

in agreement with Ref. [3]. By calculating the noise power and dividing by the mean current we obtain the Fano factor

$$
\begin{aligned}
\alpha &= \Big[\Gamma^4 + 148T^4 + 4\Gamma^2(\Gamma_\phi^2 + 4T^2 + 12T^4/\Gamma_\phi^2) + \\
&\quad (16T^2 + 2\Gamma^2)\beta\Big]\Big[\Gamma^2 + 14T^2 + \beta\Big]^{-2}, \\
\beta &= 2\Gamma\Gamma_\phi(1 + 2T^2/\Gamma_\phi^2).
\end{aligned}
$$

(5.13)

(5.14)

In Fig. 5.2 the Fano factor has been plotted as a function of Γ_Φ/T for three different values of Γ/T. The dependence of the Fano factor on the decoherence rate is nonmonotonic, crossing over from super-Poissonian ($\alpha > 1$) to Poissonian ($\alpha = 1$) via a region of sub-Poissonian noise ($\alpha < 1$). To obtain a better understanding of this behavior, we study separately the regions of weak and strong decoherence.

5.3.2   Weak decoherence

For decoherence rate $\Gamma_\phi \ll \Gamma, T$ we have the limiting behavior

$$I \to e\Gamma_\phi, \quad \alpha \to 3 - \Gamma_\phi \left(\frac{17}{\Gamma} + \frac{\Gamma}{T^2} \right). \tag{5.15}$$

Hence one charge is transferred on average per decoherence event, but the Fano factor is three times the value for independent charge transfers.

There exists a simple physical explanation for this behavior. For zero decoherence the system becomes trapped in the state $|e_0\rangle$. The system is untrapped by "decoherence events", which occur randomly at the rate Γ_ϕ according to Poisson statistics. If Γ_ϕ is sufficiently small there is enough time for the system to decay into the trapped state between two subsequent events, so they can be viewed as independent. The super-Poissonian statistics appears because a single decoherence event can trigger the transfer of more than a single charge.

The probability of n electrons being transferred in total as a consequence of one decoherence event is

$$R^1(n) = \frac{1}{2^{n+1}}, \tag{5.16}$$

since a decoherence event projects the trapped state $|e_0\rangle$ onto itself or onto $|e_1\rangle$ with equal probabilities $1/2$ and each electron subsequently entering the dots has a 50% chance of getting trapped in the state $|e_0\rangle$.

The number of electrons which have been transferred due to exactly k decoherence events has distribution $R^k(n)$, the $(k-1)$th convolution of $R^1(n)$ with itself. We get

$$\begin{aligned}
R^k(n) &= \frac{1}{2^{n+k}} \sum_{i_0=0}^{n} \sum_{i_1=0}^{i_0} \cdots \sum_{i_{k-2}=0}^{i_{k-3}} 1 \\
&= \frac{1}{2^{n+k}} \binom{n+k-1}{n}.
\end{aligned} \tag{5.17}$$

By definition,

$$R^0(n) = \delta_{n,0} = \begin{cases} 1 & n = 0 \\ 0 & n > 0 \end{cases} \text{ for } , \tag{5.18}$$

being the distribution of the transferred charges after no decoherence events have occurred.

The decoherence events in a time t have a Poisson distribution,

$$P_{\text{Poisson}}(k) = e^{-t\Gamma_\phi} (t\Gamma_\phi)^k / k!. \tag{5.19}$$

Combining with Eq. (5.17) we find the probability that n electrons have been transferred during a time t,

$$
\begin{aligned}
P(n) &= \sum_{k=0}^{\infty} P_{\mathrm{Poisson}}(k) R^k(n) \tag{5.20} \\
&= \sum_{k=1}^{\infty} \frac{e^{-t\Gamma_\phi}(t\Gamma_\phi)^k}{2^{n+k}k!} \binom{n+k-1}{n} + e^{-t\Gamma_\phi}\delta_{n,0}.
\end{aligned}
$$

The corresponding cumulant generating function is

$$
F(\chi) = t\Gamma_\phi - \frac{t\Gamma_\phi}{2 - e^{i\chi}}, \tag{5.21}
$$

which gives rise to the cumulants

$$
C_1 = t\Gamma_\phi, \quad C_2 = 3t\Gamma_\phi, \quad C_3 = 13t\Gamma_\phi, \tag{5.22}
$$

in agreement with Eq. (5.15).

The probability distribution (5.21) has been found by Belzig in a different model. [7] As shown in that paper, this superposition of Poisson distributions with Fano factor 3 arises generically whenever there are two transport channels with very different transport rates (in our case slow transport via the trapped state $|e_0\rangle$, and fast transport via the untrapped state $|e_1\rangle$).

5.3.3 Strong decoherence

We show that Poisson statistics of the transferred charges is obtained for strong decoherence. Consider the evolution equation (5.6) of the system. For $\Gamma_\phi \gg \Gamma, T$ the coefficients X_{00}, X_{01}, X_{10}, and X_{11} will ensure that v_0 is equal to v_1 after a time which is short compared to the other characteristic times of the system. The trapped and the non-trapped states will be equally populated. Let us therefore define

$$
v' = (\rho_{00} + \rho_{11}, \rho_{22}, \rho_{33}, \mathrm{Im}\,\rho_{02})^{\mathrm{T}} \tag{5.23}
$$

and use $\rho_{00} = \rho_{11} = v'_0/2$. The evolution of v' is governed by $dv'/dt = X'v'$, with

$$
X' = \begin{pmatrix}
0 & 0 & 2\Gamma & -2^{3/2}T \\
0 & -\Gamma & 0 & 2^{3/2}T \\
0 & \Gamma & -2\Gamma & 0 \\
2^{-1/2}T & -2^{1/2}T & 0 & -\Gamma/2 - \Gamma_\phi
\end{pmatrix}. \tag{5.24}
$$

The rate matrix $L'(\chi)$ is obtained by multiplying X'_{12} by the counting factor $e^{i\chi}$. An analytic expression can be found for the smallest eigenvalue $\Lambda'^{(\chi)}_{min}$ of $L'(\chi)$, leading to the cumulant generating function

$$F(\chi) = \frac{2T^2}{\Gamma_\phi} t \left(1 - e^{i\chi}\right) \tag{5.25}$$

of a Poisson distribution.

5.4   Conclusion

In conclusion, we have shown that coherent population trapping in a purely electronic system has a highly nontrivial statistics of transferred charges. Depending on the ratios of decoherence rate and tunnel rates, both super-Poissonian and sub-Poissonian statistics are possible. We have obtained exact analytical solutions for the crossover from sub- to super-Poissonian charge transfer, and have calculated the full distribution in the limits of weak and strong decoherence. We hope that the rich behavior of this simple device will motivate experimental work along the lines of Ref. [4] and [5].

5.A   Derivation of the Fano factor

To derive the result (5.13) for the Fano factor it is sufficient to know the cumulant generating function to second order in χ. The eigenvalues of the rate matrix $L(\chi)$ defined in Eq. (5.10) have the expansion

$$\lambda = \lambda_0 + \lambda_1 \chi + \lambda_2 \chi^2 + O(\chi^3). \tag{5.26}$$

We seek the eigenvalue with the smallest real part in absolute value. That eigenvalue has $\lambda_0 = 0$. We also express the eigenvector w corresponding to λ and the matrix itself in a power series in χ:

$$w = w_0 + w_1 \chi + w_2 \chi^2 + O(\chi^3), \tag{5.27}$$

$$L = L_0 + L_1 \chi + L_2 \chi^2 + O(\chi^3). \tag{5.28}$$

Inserting the above expansions into the eigenvalue equation $Lw = \lambda w$ yields the following relationships of respectively zeroth, first and second order:

$$L_0 w_0 = 0, \tag{5.29}$$

$$L_1 w_0 + L_0 w_1 = \lambda_1 w_0, \tag{5.30}$$

$$L_2 w_0 + L_1 w_1 + L_0 w_2 = \lambda_2 w_0 + \lambda_1 w_1. \tag{5.31}$$

The coefficients L_k are known, while w_k and λ_k remain to be found by solving these equations sequentially. The first two cumulants then follow from

$$C_1 = -it\lambda_1, \quad C_2 = -2t\lambda_2. \tag{5.32}$$

In an analogue way it is possible to calculate higher cumulants.

Bibliography

[1] T. Brandes, Phys. Rep. **408**, 315 (2005) .

[2] J. Siewert and T. Brandes, Adv. Solid State Phys. **44**, 181 (2004).

[3] B. Michaelis, C. Emary, and C. W. J. Beenakker, Europhys. Lett. **73**, 677 (2006).

[4] S. Gustavsson, R. Leturcq, B. Simovič, R. Schleser, T. Ihn, P. Studerus, K. Ensslin, D. C. Driscoll, and A. C. Gossard, Phys. Rev. Lett. **96**, 076605 (2006).

[5] S. Gustavsson, R. Leturcq, B. Simovič, R. Schleser, P. Studerus, T. Ihn, K. Ensslin, D. C. Driscoll, and A. C. Gossard, cond-mat/0605365.

[6] Ya. M. Blanter and M. Büttiker, Phys. Rep. **336**, 1 (2000).

[7] W. Belzig, Phys. Rev. B **71**, 161301(R) (2005).

[8] Yu. V. Nazarov, Physica B **189**, 57 (1993).

[9] S. A. Gurvitz, Phys. Rev. B **57**, 6602 (1998).

[10] D. A. Bagrets and Yu. V. Nazarov, Phys. Rev. B **67**, 085316 (2003).

[11] G. Kießlich, P. Samuelsson, A. Wacker, and E. Schöll, Phys. Rev. B **73**, 033312 (2006).

Chapter 6

Transfer of entanglement from electrons to photons by optical selection rules

6.1 Introduction

A key step in road maps for solid-state quantum information processing is the transfer of an entangled state from localized to flying qubits and vice versa. Several different schemes exist for the transfer of entanglement from squeezed radiation to localized qubits, e.g. distant atoms or superconducting quantum interference devices [1–4]. In another class of proposals, the entanglement is transferred from the localized qubits of electron spins to the flying qubits of photon polarizations [5]. *Classical* correlations between the spins can be transferred to the polarizations when conservation of angular momentum together with spin-orbit coupling imposes a one-to-one relation between the spin of the electron and the polarization of the photon that it produces in a radiative transition. Entanglement, however, is a quantum correlation which is easily lost in this process.

The obstacle to entanglement transfer is that the optical selection rules in the general case entangle the photons with the electrons — and then the entanglement of the photons among themselves is lost once one traces out the electronic degrees of freedom [6]. This "tracing out" is unavoidable when the photon state is measured independently of the electron state. After explaining this difficulty in some more detail, we will show that it can be circumvented by post-processing the photon state with the input of information obtained from a measurement on the electron state.

Our analysis has certain implications for a recent realistic proposal by Cerletti, Gywat, and Loss [5] to use electron-hole recombination in spin light-emitting diodes (spin-LEDs [7, 8]) as an efficient method for the transfer of entanglement from electron spins onto circular photon polarizations. We will argue, firstly, that the method of Ref. [5] transfers classical correlations but not quantum correlations; and, secondly, that the quantum entanglement transfer can be realized by measurement in a rotated basis of the hole angular momentum in each quantum dot after the photo-emission, followed by a single-photon operation conditioned on the outcome of that measurement.

In the concluding section we briefly discuss alternative schemes for quantum entanglement transfer, which do not require the subsequent measurements (post-processing) and might, therefore, be realized more easily in the laboratory.

6.2   General analysis

We consider two quantum dots A and B, each containing one qubit. The initial two-qubit electronic state has the generic form

$$|\Psi_{\text{in}}\rangle = \alpha|\downarrow\downarrow\rangle + \beta|\uparrow\uparrow\rangle, \ \ |\alpha|^2 + |\beta|^2 = 1. \tag{6.1}$$

The entanglement of formation of this state is quantified by the concurrence [9]

$$\mathcal{C}_{\text{in}} = 2|\alpha\beta|. \tag{6.2}$$

The two states $\downarrow$, $\uparrow$ of the qubits are eigenstates of the total (orbital + spin) angular momentum operator $\mathcal{L}_z$ in the z-direction, with eigenvalues $L_\downarrow$, $L_\uparrow$ (in units of $\hbar$). The first state in the ket $|\cdot\cdot\rangle$ refers to the qubit in quantum dot A and the second state refers to quantum dot B.

Photons with opposite circular polarizations $\sigma_\pm$ (angular momentum ± 1), emitted along the spin quantization axis, are produced according to the unitary evolution

$$|\downarrow\rangle|0\rangle \mapsto |\Phi_+\rangle|\sigma_+\rangle, \tag{6.3}$$

$$|\uparrow\rangle|0\rangle \mapsto |\Phi_-\rangle|\sigma_-\rangle, \tag{6.4}$$

where $|0\rangle$ denotes the photon vacuum and $|\Phi_\pm\rangle$ denotes the state of the quantum dot after the photo-emission of a $\sigma_\pm$ photon. Conservation of angular momentum requires that $|\Phi_+\rangle$ and $|\Phi_-\rangle$ are eigenstates of $\mathcal{L}_z$ with eigenvalues

$$L_+ = L_\downarrow - 1, \ \ L_- = L_\uparrow + 1, \tag{6.5}$$

respectively. In general, the two states $|\Phi_+\rangle$ and $|\Phi_-\rangle$ are orthogonal because they correspond to different eigenvalues $L_+ \neq L_-$. The exception is the special case $L_\downarrow - L_\uparrow = 2$, when $L_+ = L_-$ so that $|\Phi_+\rangle$ and $|\Phi_-\rangle$ may have a nonzero overlap.

The final state

$$|\Psi_{\text{final}}\rangle = \alpha|\Phi_+\Phi_+\rangle|\sigma_+\sigma_+\rangle + \beta|\Phi_-\Phi_-\rangle|\sigma_-\sigma_-\rangle \qquad (6.6)$$

represents an *encoding* rather than a *transfer* of the entanglement. Assuming that the photons are measured independently of the electrons, we trace out the electronic degrees of freedom to obtain the reduced density matrix ρ_{photon} of the photons by themselves:

$$
\begin{aligned}
\rho_{\text{photon}} &= \text{Tr}_{\text{electron}} |\Psi_{\text{final}}\rangle\langle\Psi_{\text{final}}| \\
&= |\alpha|^2|\sigma_+\sigma_+\rangle\langle\sigma_+\sigma_+| + |\beta|^2|\sigma_-\sigma_-\rangle\langle\sigma_-\sigma_-| + \gamma|\sigma_+\sigma_+\rangle\langle\sigma_-\sigma_-| + \\
&\quad \gamma^*|\sigma_-\sigma_-\rangle\langle\sigma_+\sigma_+|,
\end{aligned}
$$

$$(6.7)$$

where $\gamma = \alpha\beta^*\langle\Phi_-|\Phi_+\rangle_A\langle\Phi_-|\Phi_+\rangle_B$. The concurrence of the mixed state ρ_{photon} is

$$\mathcal{C}_{\text{final}} = 2|\gamma|. \qquad (6.8)$$

If $L_\downarrow - L_\uparrow \neq 2$, so that the final electronic states $|\Phi_+\rangle_X$ and $|\Phi_-\rangle_X$ in quantum dots $X = A, B$ are orthogonal, the polarizations of the photons have been correlated but not entangled ($\gamma = 0 \Rightarrow \mathcal{C}_{\text{final}} = 0$). Since unitary operations on the electronic degrees of freedom do not change ρ_{photon}, the entanglement can not be recovered by unitary evolution once the photons have left the quantum dots and their evolution has decoupled from the electrons.

While unitary evolution can not disentangle the electrons from the photons, a projective measurement of the quantum dots followed by post-processing of the photons can realize the entanglement transfer. Considering the generic case $L_\downarrow - L_\uparrow \neq 2$, so that $\langle\Phi_-|\Phi_+\rangle = 0$, we first perform the following local unitary operation on each of the two quantum dots:

$$|\Phi_+\rangle \mapsto (|\Phi_+\rangle + |\Phi_-\rangle)/\sqrt{2}, \qquad (6.9)$$

$$|\Phi_-\rangle \mapsto (|\Phi_+\rangle - |\Phi_-\rangle)/\sqrt{2}. \qquad (6.10)$$

We then measure $\mathcal{L}_z$. The outcome of the measurement on dot $X = A, B$ is denoted by L_X. The measurement leaves the photons in the state

$$|\Psi_{\text{photon}}\rangle = \alpha|\sigma_+\sigma_+\rangle + (-1)^x\beta|\sigma_-\sigma_-\rangle, \quad x = \frac{L_A - L_B}{L_+ - L_-}. \qquad (6.11)$$
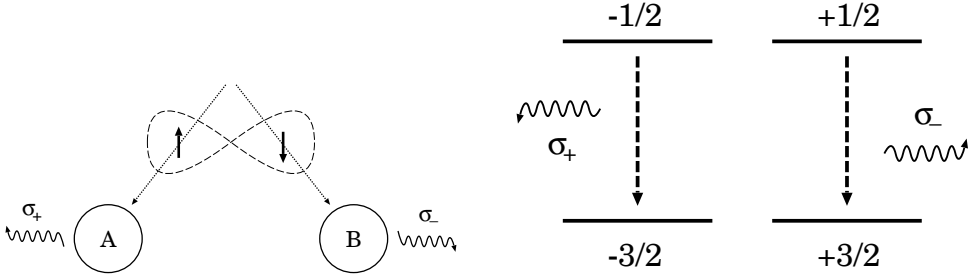
Figure 6.1: Left panel: A spin-entangled pair of electrons recombines with a hole in quantum dots A and B, to emit a pair of photons with anti-correlated circular polarizations $\sigma_\pm$. Right panel: The four lowest energy levels involved in the photo-emission of each quantum dot. The angular momentum quantum number is indicated. Initially both lower levels are filled by heavy holes. The recombination with a single electron in one of the two upper levels leaves the remaining hole entangled with the emitted photon. This prevents the transfer of the entanglement from the electrons to the photons.

If the measurement gives $L_A = L_B$ no post-processing is needed; otherwise, the conditional phase shift $|\sigma_\pm\rangle \mapsto \pm|\sigma_\pm\rangle$ performed on one of the two photons completes the entanglement transfer.

6.3 Application to spin-LEDs

The mechanism for entanglement transfer in spin-LEDs proposed in Ref. [5] is shown schematically in Fig. 6.1. Two spin-entangled electrons (spin $\pm 1/2$) are injected into the conduction band of two different quantum dots, each of which is charged with a pair of heavy holes in the valence band. The two heavy holes in each quantum dot have opposite angular momentum $\pm 3/2$, so that their total angular momentum along z vanishes. The initial state $|\Psi_{\text{in}}\rangle$ is of the form (6.1), with the identification $|\uparrow\rangle \equiv |+\frac{1}{2}, +\frac{3}{2}, -\frac{3}{2}\rangle$ and $|\downarrow\rangle \equiv |-\frac{1}{2}, +\frac{3}{2}, -\frac{3}{2}\rangle$. (The three fractions indicate the angular momentum quantum numbers of the electron and the two heavy holes.) Electron-hole recombination can proceed either from angular momentum $+1/2$ to $+3/2$ with emission of a σ_- photon or from $-1/2$ to $-3/2$ with emission of a σ_+ photon.

The remaining heavy holes become entangled with the photons, so that the final state $|\Psi_{\text{final}}\rangle$ is of the form (6.6) with the identification $|\Phi_+\rangle \equiv |+\frac{3}{2}\rangle$ and $|\Phi_-\rangle \equiv |-\frac{3}{2}\rangle$. These two states refer to two heavy holes with opposite angular

momentum, so they are definitely orthogonal. Hence the reduced density matrix of the photons ρ_{photon} is of the form (6.7) with $\gamma = 0$ and the concurrence $\mathcal{C}_{\text{final}} = 0$. The polarizations of the photons have become correlated but not entangled. No matter how the remaining holes evolve after the photons have decoupled, the degree of entanglement of ρ_{photon} remains zero.

As explained in the previous section, the holes can be disentangled from the photons by post-processing in a sequence of three steps:

1. Bring each heavy hole in a superposition of states with opposite angular momentum by means of the local unitary operation $|\pm\frac{3}{2}\rangle \mapsto \left(|+\frac{3}{2}\rangle \pm |-\frac{3}{2}\rangle\right)/\sqrt{2}$.

2. Measure the angular momentum of each hole in the z-direction, with outcome L_A, L_B.

3. Perform the conditional phase shift $|\sigma_\pm\rangle \mapsto \pm|\sigma_\pm\rangle$ on one of the two photons if $L_A \neq L_B$.

Step three is a routine linear optical operation. Step two might be achieved by detecting whether or not a spin-up heavy hole (angular momentum $+3/2$) can be injected separately into each of the two quantum dots. If both heavy holes enter their quantum dot, or if both do not enter, then $L_A = L_B$, while $L_A \neq L_B$ if one hole enters and the other does not. Step one might be achieved by an optical Raman transition [10, 11].

6.4 Conclusion

We have shown that the transfer of entanglement from localized electron spins to circular photon polarizations by means of optical selection rules can not be achieved solely by unitary evolution. Projective measurements and post-processing conditioned on the outcome of the measurements are required as well, to disentangle the final electronic state from the photons. This difficulty originates from the mismatch between the half-integer spin of fermions and the integer spin of bosons. It severely complicates the original spin-LED proposal of Cerletti, Gywat, and Loss [5], see Ref. [11]. In this concluding section we discuss several strategies that one might use to avoid the difficulty.

As proposed by Vrijen and Yablonovitch [6], entanglement transfer by unitary evolution to *linearly* polarized photons is possible if a strong magnetic field lifts the degeneracy between the up and down hole spins, so that the topmost hole state is nondegenerate. In the case of circular polarization considered here, it

is possible if the angular momentum difference of the initial electronic qubits satisfies $L_\downarrow - L_\uparrow = 2$. This might apply to a qubit formed from a $+3/2$ heavy hole and a $-1/2$ light hole. (The difference in mass might well prevent the formation of an entangled pair out of these qubits.) The spin-LEDs would then initially each contain a single $+1/2$ electron, which would recombine with the hole under emission of a $\sigma_\pm$ photon. The unique final state in this case is a pair of empty quantum dots.

Alternatively, one might construct a qubit solely out of orbital degrees of freedom (without spin-orbit coupling): An electron in a circularly symmetric quantum dot has degenerate eigenstates of orbital angular momentum $+1$ or -1, which would decay to the nondegenerate ground state (zero angular momentum) with emission of a $\sigma_\pm$ photon [12]. Since the final state of the quantum dot is unique, it is not entangled with the photons, in accord with the general condition $L_\downarrow - L_\uparrow = 2$ for the transfer of entanglement by unitary evolution.

An alltogether different way out of the constraints imposed by the optical selection rules is to let the spin-entangled electrons recombine with an *entangled* pair of holes. More specifically, if a pair of electrons in the state $\alpha|+\frac{1}{2}, -\frac{1}{2}\rangle + \beta|-\frac{1}{2}, +\frac{1}{2}\rangle)$ recombines with a pair of heavy holes in the singlet state $(|+\frac{3}{2}, -\frac{3}{2}\rangle - |-\frac{3}{2}, +\frac{3}{2}\rangle)/\sqrt{2}$, then the final photonic state (after tracing out the electronic degrees of freedom) becomes

$$\rho_{\text{photon}} = \frac{1}{2}|\Psi\rangle\langle\Psi| + \frac{1}{2}|0\rangle\langle0|, \ \ |\Psi\rangle = \alpha|\sigma_-\sigma_+\rangle - \beta|\sigma_+\sigma_-\rangle, \tag{6.12}$$

where $|0\rangle$ denotes the photon vacuum state. Detection of the photon pair projects onto the entangled state $|\Psi\rangle$. The efficiency of this entanglement transfer scheme is $1/2$ rather than unity, but it has the advantage that no measurement on the electronic state needs to be performed.

Bibliography

[1] B. Kraus and J. I. Cirac, Phys. Rev. Lett. **92**, 013602 (2004).

[2] M. Paternostro, W. Son, and M. S. Kim, Phys. Rev. Lett. **92**, 197901 (2004).

[3] M. Paternostro, W. Son, M. S. Kim, G. Falci, and G. M. Palma, Phys. Rev. A **70**, 022320 (2004).

[4] M. Paternostro, G. Falci, M. S. Kim, and G. M. Palma, Phys. Rev. B **69**, 214502 (2004).

[5] V. Cerletti, O. Gywat, and D. Loss, cond-mat/0411235, version 1.

[6] R. Vrijen and E. Yablonovitch, Physica E **10**, 569 (2001).

[7] R. Fiederling, M. Keim, G. Reuscher, W. Ossau, G. Schmidt, A. Waag, and L. W. Molenkamp, Nature **402**, 787 (1999).

[8] Y. Ohno, D. K. Young, B. Beschoten, F. Matsukura, H. Ohno, and D. D. Awschalom, Nature **402**, 790 (1999).

[9] W. K. Wootters, Phys. Rev. Lett. **80**, 2245 (1998).

[10] A. Imamoglu, D. D. Awschalom, G. Burkard, D. P. DiVincenzo, D. Loss, M. Sherwin, and A. Small, Phys. Rev. Lett. **83**, 4204 (1999).

[11] V. Cerletti, O. Gywat, and D. Loss, cond-mat/0411235, version 2.

[12] C. Emary, B. Trauzettel, and C. W. J. Beenakker, cond-mat/0502550.

Samenvatting

Met de *spin* van het elektron wordt de tollende beweging bedoelt die in 1925 door de Leidse natuurkundigen George Uhlenbeck en Samuel Goudsmit werd ontdekt. Tegenwoordig is er een vakgebied binnen de elektronica, de zogenaamde spintronica, die de spin van elektronen benut om een schakeling aan te sturen. Een linksomdraaiend elektron (spin omhoog) zet dan bijvoorbeeld de schakeling "uit" en een rechtsomdraaiend elektron (spin omlaag) zet de schakeling "aan". Voor deze toepassingen is het van belang dat de spin niet door onvoorziene invloeden van richting omkeert, bijvoorbeeld door het magnetische veld van atoomkernen. In dit proefschrift beschrijven we een methode die we ontwikkeld hebben om het verval van de spinrichting in rekening te brengen.

Zeer recent is er een tweede klasse van toepassingen van de elektronenspin ontwikkeld, waarbij de spin drager is van quantuminformatie. Bij een gewone "klassieke" schakeling wijst de spin omhoog óf omlaag, maar bij een quantumschakeling wijst de spin omhoog én omlaag. Men spreekt dan van een superpositie van omhoog en omlaag. Als zo'n superpositie vervalt, dan spreekt men van defasering (of decoherentie). Dezelfde mechanismen die het gewone, klassieke verval van de spinrichting veroorzaken, veroorzaken ook defasering, maar er zijn ook mechanismen die alleen defasering veroorzaken — zonder klassiek verval. In het algemeen heeft men dan ook twee verschillende tijden (gewoonlijk T_1 en T_2 genoemd), die respectievelijk de snelheid van spinverval en van defasering geven. Het model voor spinverval dat wij hebben ontwikkeld kan tevens de defasering in rekening brengen — het is dan ook een volledig quantummechanisch model.

Eerdere modellen voor spinverval en defasering waren vooral geschikt voor elektronen in een klein afgesloten gebied (een zogenaamde quantum dot). Ons model is toepasbaar op een open systeem, waar een elektrische stroom doorheen kan lopen. Die combinatie van elektrische geleiding en spin verval/defasering hebben wij hanteerbaar gemaakt door een oud model van Markus Büttiker uit te breiden, het zogenaamde "dephasing lead" model. In het oorspronkelijke model was de elektronenspin niet inbegrepen, alleen defasering van de ruimtelijke be-

weging werd behandeld. Behalve de uitbreiding naar de elektronenspin, hebben we ook een andere variant (de "dephasing stub") onderzocht.

Dit onderwerp uit de spintronica is het belangrijkste onderdeel van het proefschrift, behandeld in hoofdstukken 2 en 3 (na een inleiding in hoofdstuk 1). De elektronenspin staat ook centraal in hoofdstuk 6, waar we het probleem van de overdracht van een quantummechanische superpositie van de elektronenspin naar fotonpolarisaties onderzoeken. Deze overdracht is van belang voor de werking van een quantumcomputer. In hoofdstukken 4 en 5 speelt de elektronenspin zelf geen rol, maar wel het probleem van fasecoherente elektrische geleiding door quantum dots. We onderzoeken in deze hoofdstukken een systeem van drie quantum dots, waarin een elektron gevangen kan raken in een superpositie van toestanden op twee van de dots. Zulk een superpositie is een alternatieve manier om quantuminformatie op te slaan.

List of publications

- *Dynamical mean field theory for transition temperature and optics of CMR manganites*, B. Michaelis and A.J. Millis, Physical Review B **68**, 115111 (2003).

- *Stub model for dephasing in a quantum dot*, C.W.J. Beenakker and B. Michaelis, Journal of Physics A **38**, 10639 (2005) [Chapter 2].

- *Transfer of entanglement from electrons to photons by optical selection rules*, M. Titov, B. Trauzettel, B. Michaelis and C.W.J. Beenakker, New Journal of Physics **7**, 186 (2005) [Chapter 6].

- *Voltage probe model of spin decay in a chaotic quantum dot, with applications to spin-flip noise and entanglement production* , B. Michaelis and C.W.J. Beenakker, Physical Review B **73**, 115329 (2006) [Chapter 3].

- *All-electronic coherent population trapping in quantum dots*, B. Michaelis, C. Emary and C.W.J. Beenakker, Europhysics Letters **73**, 677 (2006) [Chapter 4].

- *Counting statistics of coherent population trapping in quantum dots*, C.W. Groth, B. Michaelis and C.W.J. Beenakker, Physical Review B **74**, 125315 (2006) [Chapter 5].

- *Measuring the squared magnetisation of a molecule*, B. Michaelis cond-mat/0606608

Curriculum Vitæ

Ik ben geboren op 13 augustus 1978 te Saarbrücken, Duitsland, en opgegroeid in het Saarland. Mijn eindexamen haalde ik in 1998 in St. Wendel op het Gymnasium Wendalinum. Ik twijfelde tussen de studies rechten en natuurkunde, maar koos uiteindelijk voor wiskundig geformuleerde wetten.

Halverwege mijn studie aan de Universiteit van Würzburg raakte ik geïnteresseerd in de fysica van de gecondenseerde materie. Gedurende enkele maanden deed ik een experimentele stage, waarin ik door middel van het optische Kerr-effect dunne magnetische lagen onderzocht. Tijdens een jaarlange buitenlandse stage aan de Rutgers Universiteit in de Verenigde Staten heb ik onder begeleiding van Prof. A.J. Millis aan de theorie van optische en elektronische verschijnselen in ferromagnetische overgangsmetaalverbindingen gewerkt. Terug in Würzburg behaalde ik in 2003 mijn "Diplom".

In de groep van Prof. W. Hanke ontwikkeld ik een programma dat op een supercomputer de elektronische eigenschappen van gedoteerde overgangsmetaal-oxiden berekent, gebruik makend van de eigenenergie-functionaalbenadering. Tijdens deelname aan de zomerschool "Frontiers in Magnetism 2003" in Boulder (V.S.) hebben verschilllende colleges mijn belangstelling voor nanostrukturen versterkt. Onder andere om deze reden heb ik in april 2004 mijn onderzoek omgebogen richting nanofysica, door over te stappen naar de groep van Prof. C.W.J. Beenakker aan de Universiteit Leiden.

Mijn onderzoek in Leiden, beschreven in dit proefschrift, deed ik in dienst van de Stichting voor Fundamenteel Onderzoek der Materie (FOM), als onderdeel van de Delft-Leidse concentratiegroep "Solid State Quantum Information Processing". Naast mijn onderzoek assisteerde ik bij de colleges "Fysica van de vaste Stof" en "Theory of Condensed Matter" en volgde zomerscholen in Les Houches (Frankrijk) en Varenna (Italië).

Stellingen

behorend bij het proefschrift
On dephasing and spin decay in open quantum dots

1. If you measure the energies in the excitations of two locally separate systems, let them collide, wait till they are separate again and measure then again these excitations, the sum of the energies does not have to be the same as before the collisions even if their relative velocity didn't change.

   cond-mat/0606608.

2. The average electron-hole entanglement production rate on a set of quantum dots decreases monotonously with the increasing decoherence strength of the voltage probe model and the latter increases with temperature.

   This thesis, Chapter 3, and Phys. Rev. Lett. **83**, *5090 (1999).*

3. The coherence time of a charge qubit can be measured in a transport experiment by an electronic analogue of the optical method of coherent population trapping.

   This thesis, Chapter 4.

4. There is no physical reality to the charge excitations with energies close to the middle of the gap in the insulating half-filled phase of the one-band Hubbard model, predicted by the self-energy functional approximation.

   Eur. Phys. J. B **32**, *429 (2003).*

5. Electron-hole pairs produced at a tunnel barrier are entangled if and only if the correlator of parallel spin currents is at least twice larger than the correlator of antiparallel spin currents.

   This thesis, Chapter 3.

6. A measurement of the squared magnetization on a many-particle spin system can be performed by guiding it through an antiferromagnetic tube.

   cond-mat/0606608.

7. Models in theoretical physics originate from intuition based on daily-life phenomena — thus a successful search for qualitatively new models should be preceded by extensions of that intuition.

8. Charge transfer in the regime of coherent population trapping occurs in bunches of three electrons on average.

   This thesis, Chapter 5.

9. In semiconductor electronics it is possible to measure the time dependence of a 10^{-19} A current very accurately with a 10^{-9} A current passing close by.

Björn Dieter Michaelis
16 November 2006